Title
The Role of O-GlcNAc in Adult Hippocampal Neurogenesis

Author
White, Charles Wellington

Publication Date
2020

Peer reviewed|Thesis/dissertation

The Role of O-GlcNAc in Adult Hippocampal Neurogenesis

by
Charles White

DISSERTATION
Submitted in partial satisfaction of the requirements for degree of
DOCTOR OF PHILOSOPHY

in

Developmental and Stem Cell Biology

in the

GRADUATE DIVISION
of the
UNIVERSITY OF CALIFORNIA, SAN FRANCISCO

Approved:

DocuSigned by:
Daniel Lim
FC7A2B6D45EF428...

Daniel Lim

Chair

DocuSigned by:
Barbara Panning
DocuSigned by:

Barbara Panning

DocuSigned by:
Alma L. Burlingame
DocuSigned by:

Alma L. Burlingame

DocuSigned by:
Saul Villeda
711626DA5837464...

Saul Villeda

Committee Members

To Dorothy Smith and Margaret White

ACKNOWLEDGEMENTS

First, I would like to thank my thesis advisor, PI, and mentor – Dr. Saul Villeda. Your patience has been invaluable in a long PhD full of wrong turns and dead ends. When I hit one of those inevitable dead ends however, you were there with the right guidance to turn this project around. Your optimism and caring nature gave me the support I needed to carry the project back to where it needed to be. I am grateful for having the chance to develop into the scientist I am today in your lab. The publication of this work in *PNAS* is an amazing capstone to a long journey and I am proud of everything we accomplished.

I would also like to thank my committee members. My thesis committee chair – Dr. Daniel Lim, my qualifying exam committee chair – Dr. Barbara Panning, and my mass spectrometry collaborator – Dr. Alma Burlingame. All of you have provided immeasurable insight for this project. I will always appreciate how you all took my career goals into account during my PhD Journey. Most of all, I am forever grateful for your guidance in trimming and refocusing my research efforts when my project started to become too unwieldy and wandering.

Beyond my committee, many faculty members have helped refine my project into what it is today. In particular I would like to thank the members of the Stem Cell Joint Lab Meeting – Dr. Diana Laird, Dr. Andrew Brack, Dr. Julie Sneddon, Dr. Emmanuelle Passegué, Dr. Tien Peng, and Dr. Alexander Pollen. Your feedback after my presentations was some of the most valuable and regular feedback I received during my time at UCSF. I owe my ability to communicate science to a broader audience to all of you.

Guidance and mentorship are essential, but a PhD happens on the ground, in a lab, day by day, for several years. I can't think of a better group of people to spend that time with than the Villeda Lab. To the students I overlapped with: Dr. Joe Udeochu, Dr. Karin Lin, Dr. Liz Wheatley, Dr. Lucas Smith, (soon to be Dr.) Alana Horowtiz, and Karishma Pratt; as well as the postdocs: Dr. Xuelai Fan, Dr. Geraldine Gontier, Dr. Jeremy Shea, Dr. Hank Garcia, Dr. Laura Remesal-Gomez, Dr. Adam Schroer, and Dr. Greg Bieri; and the technicians and managers: Dr.

Brit Ventura, Cedric Snethlage, Manasi Iyer, Cesar Sanchez-Diaz, Kirsten Chui; thank you all for making the lab a bright, positive, fun, and overall amazing place to come in to every day. I especially want to acknowledge those that have been here with me the whole time – Geraldine and Jeremy – whether it was sharing relevant papers with me, knowing the right protocols, or teaching me a surgery, I honestly could not have done my PhD without help from you two.

Outside of the lab, support from friends and family is essential. To my parents, mom and dad, and my sister Julia – thank you for you always being there. Being over 2,500 miles from family is hard, but your efforts have made it feel like you're all right down the street. Being able to visit you in New York and having you come to visit me has regularly provided a much need break from the lab. Your unconditional love and support have made this journey so much easier and I could not have gotten here without you.

My fiancé, Kaitlin Reynolds has been by my side for almost this entire journey. From my qualifying exam to the end, I can't thank you enough for all that you've done to support me. As hard as I've worked on my research, you have put in twice as much effort supporting me and keeping me afloat. This accomplishment is as much about my efforts as it is about your selflessness.

Finally, my inspiration every day has been my grandmothers, Grandma and Nana. I wish you both could have been here to see me complete this work. You sparked my passion for education and creativity at a young age and helped me develop the diligence that brought me to this point. I am proud of this body of work, and I know that both you would be too.

The Role of O-GlcNAc in Adult Hippocampal Neurogenesis

Charles White

ABSTRACT

The post-translational modification, O-linked N-Acetylglucosamine (O-GlcNAc) is a major regulator of aging, neurodegenerative disease, and stem cell function. Addition and removal of O-GlcNAc is tightly controlled by O-GlcNAc transferase (Ogt) and O-GlcNAcase (OGA), respectively. Reducing the expression of either of these enzymes has previously been shown to alter neurogenesis in the developing brain. Moreover, our lab has previously identified an age-related decrease in hippocampal O-GlcNAc levels underlying age-related impairments in cognitive function. Notwithstanding, whether O-GlcNAc plays a role in adult hippocampal neurogenesis has yet to be explored. Here we investigate the role of O-GlcNAc in regulating the decline of adult hippocampal neurogenesis. First, we identify an age-related loss of neural stem cell (NSC) O-GlcNAcylation concurrent with an increase in gliogenesis. Mechanistically, we demonstrate that loss of STAT3 O-GlcNAcylation in NSCs promotes gliogenesis at the expense of neurogenesis and NSC self-renewal. Next, we examine the role of the mitochondrial isoform of Ogt (mOGT). We identify an age-related increase in mOGT levels capable of driving NSC depletion by promoting aberrant neuronal differentiation. Finally, we explore the role of OGA in regulating age-related regenerative decline in the brain. While impairing OGA does not appear to alter neuronal differentiation, we identify a change in non-neuronal differentiation *in vivo*. Taken together, these data implicate O-GlcNAc as a major regulator of adult hippocampal neurogenesis and posit O-GlcNAc as a therapeutic target for combatting age-related regenerative decline in the brain.

TABLE OF CONTENTS

LIST OF FIGURES

Chapter 1

LIST OF ABBREVIATIONS

Abbreviation	Term
BrdU	5-bromo-2'-deoxyuridine
DAB	3,3'-Diaminobenzidine
DCX	Doublecortin
DG	Dentate Gyrus
EdU	5-Ethynyl-2´-deoxyuridine
EThcD	Electron-Transfer/Higher-Energy Collision Dissociation
GCL	Granule Cell Layer
GO	Gene Ontology
i.p.	Intraperitoneal
KEGG	Kyoto Encyclopedia of Genes and Genomes
LWAC	Lectin Weak Affinity Chromatography
mOGT	Mitochondrial Ogt
ncOgt	Nuclear Cytosolic Ogt
NOR	Novel Object Recognition
NSC	Neural Stem Cell
O-GlcNAc	O-linked N-Acetylglucosamine
OGA	O-GlcNAcase
Ogt	O-GlcNAc Transferase
qPCR	Quantitative PCR
RNAi	RNA interference
shRNA	Short Hairpin RNA
sOGT	Short Ogt

tdT	tdTomato
ThG	Thiamet-G
TMT	Tandem Mass Tag

CHAPTER 1:

Age-Related Loss of Neural Stem Cell O-GlcNAc Promotes a Glial Fate Switch Through Stat3 Activation

Charles W. White III[1,2], Xuelai Fan[1], Jason C. Maynard[3], Elizabeth G. Wheatley[1,2], Gregor Bieri[1], Julien Couthouis[4], Alma L. Burlingame[3] and Saul A. Villeda[1,2,5,6,#]

1. Department of Anatomy, University of California San Francisco, San Francisco, California 94143, USA
2. Developmental and Stem Cell Biology Graduate Program, University of California San Francisco, San Francisco, California 94143, USA
3. Mass Spectrometry Facility and Department of Pharmaceutical Chemistry, University of California, San Francisco, California 94158, USA
4. Department of Genetics, Stanford University School of Medicine, Stanford, California 94305, USA
5. Department of Physical Therapy and Rehabilitation Science, University of California San Francisco, San Francisco, California 94143, USA
6. The Eli and Edythe Broad Center for Regeneration Medicine and Stem Cell Research, San Francisco, California 94143, USA

AUTHOR CONTRIBUTIONS

C.W.W., X.F. and S.A.V. developed concept and designed experiments. C.W.W. and X.F. collected and analyzed data. C.W.W and X.F. performed RNA interference and genetic knockout studies. C.W.W performed pharmacological and lineage tracing studies. C.W.W and J.C.M performed and analyzed TMT-10plex and mass spectrometry studies. C.W.W, G.B. and J.C. performed and analyzed RNA-sequencing studies. E.G.W. and G.B. generated and validated viral constructs. A.L.B. provided scientific and technical expertise. C.W.W and S.A.V wrote the manuscript. S.A.V supervised all aspects of this project. All authors had the opportunity to discuss results and comment on manuscript.

ABSTRACT

Increased neural stem cell (NSC) quiescence is a major determinant of age-related regenerative decline in the adult hippocampus. However, a coextensive model has been proposed in which division-coupled conversion of NSCs into differentiated astrocytes restrict the stem cell pool with age. Here we report that age-related loss of the post-translational modification, O-linked N-Acetylglucosamine (O-GlcNAc), in NSCs promotes a glial fate switch. We detect an age-dependent decrease in NSC O-GlcNAc levels coincident with decreased neurogenesis and increased gliogenesis in the mature hippocampus. Mimicking an age-related loss of NSC O-GlcNAcylation in young mice reduces neurogenesis, increases astrocyte differentiation and impairs associated cognitive function. Using RNA-sequencing of primary NSCs following decreased O-GlcNAcylation, we detect changes in the STAT3 signaling pathway indicative of glial differentiation. Moreover, using O-GlcNAc-specific mass spectrometry analysis of the aging hippocampus, together with an *in vitro* site directed mutagenesis approach, we identify loss of STAT3 O-GlcNAc at Threonine 717 as a driver of astrocyte differentiation. Our data identify the post-translational modification, O-GlcNAc, as a key molecular regulator of regenerative decline underlying an age-related NSC fate switch.

INTRODUCTION

Within the dentate gyrus (DG) region of the adult mammalian hippocampus, NSCs undergo rounds of division and maturation, in a process termed adult neurogenesis, ultimately giving rise to functional neurons that integrate into existing hippocampal circuitry and regulate cognition (1, 2). While much less understood, adult NSCs can alternatively undertake a gliogenic program in which they terminally differentiate into astrocytes (3–6). During aging, neurogenesis precipitously declines in the adult hippocampus (7–11). While adult NSCs in the aging hippocampus remain somewhat controversial in humans (12), the most recent studies report adult hippocampal neurogenesis through the ninth decade of life, with age-related decline exacerbated in Alzheimer's disease patients (13) and correlating with cognitive dysfunction (14). It is therefore becoming evident that adult NSCs provide a significant source of cellular and cognitive plasticity in the adult brain. However, mechanisms governing age-related neurogenic decline remain to be fully elucidated.

The post-translational modification O-GlcNAc - a dynamic form of intracellular protein glycosylation - is quickly emerging as a potent regulator of brain aging (15–17). Recently, we identified age-related changes in O-GlcNAcylation associated with neuronal dysfunction in old mice (17). Moreover, the catalytic enzymes responsible for the addition and removal of O-GlcNAc, O-GlcNAc transferase (Ogt) and O-GlcNAcase (Oga), have been implicated in Alzheimer's disease (15, 18, 19), Parkinson's disease (20) and even lifespan regulation (21, 22). In the context of stem cell biology, previous studies have identified a critical role for O-GlcNAc in embryonic stem cell pluripotency (23) and proper organismal development (24). Additionally, aberrant neural development has been observed following abrogation of either Ogt or Oga (25, 26). Despite involvement in both aging and development, a role for O-GlcNAcylation in regulating age-related regenerative decline in any tissue, including the brain has yet to be explored.

In this study, we used pharmacological and RNAi *in vitro* approaches, in conjunction with RNA-sequencing, to demonstrate that decreasing NSC O-GlcNAcylation promotes a neuron to

glia fate switch. Functionally, we utilize genetic knock out models to demonstrate that decreasing NSC O-GlcNAcylation in young animals mirrors age-related changes in adult neurogenesis, cognitive function and gliogenesis. Mechanistically, we employ mass spectrometry to identify an age-related loss of STAT3 O-GlcNAcylation at Threonine 717 in the hippocampus that drives a gliogenic fate switch in NSCs.

RESULTS

NSC O-GlcNAC levels decline with age and are coincident with decreased neurogenesis and increased gliogenesis in the mature hippocampus.

We first compared age-related temporal kinetics of O-GlcNAc expression in adult NSCs with changes in adult neurogenesis and gliogenesis in the hippocampus of mice at young (2 months) and mature (6 months) ages by immunohistochemical analysis. We detected a sharp decrease in O-GlcNAc levels in Sox2/GFAP-positive NSCs in mature compared to young mice (**Figure 1.1A,B**). Concurrently, this decline was paralleled by a decrease in the number of Nestin-positive NSCs, Doublecortin (Dcx)/MCM2-positive neuroblasts and Dcx-positive/MCM2-negative newly born neurons in the mature hippocampus (**Figure 1.1C,D**), consistent with previous reports (7, 10). While glial differentiation has been reported at old age (3, 27), whether the decline in adult neurogenesis in the mature hippocampus is concurrent with an increase in gliogenesis is unknown. Therefore, we assessed astrocyte differentiation using a long-term 5-bromo-2'-deoxyuridine (BrdU) incorporation paradigm, in which differentiated astrocytes express both BrdU and the glial markers GFAP or S100ß. We observed an age-dependent increase in the number of long-term retaining BrdU/GFAP-positive and BrdU/S100ß-positive astrocytes in the mature compared to the young hippocampus (**Figure 1.1E,F**), in a timeframe consistent with decreased neurogenesis. These data raise the possibility that decreased NSC O-GlcNAcylation in the mature hippocampus is associated with age-related regenerative decline.

Decreased NSC O-GlcNAc levels impairs proliferation and promotes astrocyte differentiation i*n vitro*.

To gain insight into the functional consequence of reduced NSC O-GlcNAcylation we made use of a primary hippocampal NSC *in vitro* model. Using RNA-sequencing, we profiled gene expression in primary NSCs following either pharmacological inhibition of Ogt with OSMI-1 treatment (**Figure 1.2A**) or viral-mediated abrogation of Ogt by RNA interference (RNAi) (**Figure 1.3A**). We found 845 differentially expressed genes following Ogt inhibition (**Figure 1.3A**) and 741 differentially expressed genes after Ogt abrogation (**Figure 1.4A**). Gene ontology (GO) analysis of the most differentially downregulated genes identified biological processes including cell cycle, mitotic nuclear division, and cell division (**Figure 1.5B**; **Figure 1.4B**). Functionally, we assessed NSC proliferation *in vitro* following inhibition or abrogation of Ogt, and observed a significant decrease in the percentage of 5-Ethynyl-2´-deoxyuridine (EdU)-positive and Ki67-positive proliferating cells compared to control conditions (**Figure 1.5C; Figure 1.4C)**. No differences in cell death were detected by immunocytochemical analysis for cleaved caspase-3 (**Figure 1.6A**). These *in vitro* data indicate that reducing NSC O-GlcNAcylation negatively regulates NSC proliferation.

Given the relative low number of significantly upregulated genes following Ogt inhibition (**Figure 1.5A**), we performed gene list enrichment analysis using Enrichr for ChIP Enricher Analysis (ChEA) and ENCODE transcription factor targets datasets. We identified transcription factors previously associated with NSC function, including STAT3 (**Figure 1.5D; Figure 1.4D**) - a major initiator of astrocyte differentiation (28, 29). Correspondingly, we surveyed expression of known astrocyte genes in NSCs following Ogt inhibition using our RNA-sequencing dataset, and observed an upregulation of several astrocyte genes, including *S100ß*, *Aldh1l1* and *Sox9* (**Figure 1.5E**). Next, we examined whether reducing NSC O-GlcNAc levels impacted NSC differentiation *in vitro*. Primary hippocampal NSCs isolated from either postnatal or adult (2 month) mice were treated with the Ogt inhibitor OSMI-1 or vehicle control and cultured under differentiation

conditions. Ogt inhibition resulted in a concomitant decrease in neuronal (**Figure 1.5F**) and increase in astrocyte (**Figure 1.5G**) differentiation compared to vehicle control conditions. To ensure these changes in cell fate were not due to increased cell death during differentiation, we analyzed cytotoxicity (**Figure 1.6B**) and cell viability (**Figure 1.6C**) throughout the paradigm and observed no difference between Ogt inhibitor treated and control NSCs. These data suggest that the observed loss of proliferative capacity and neuronal differentiation following decreased NSC O-GlcNAcylation (**Figure 1.1**) may be the result of an altered neuron to glia fate switch.

Mimicking an age-related decline in NSC O-GlcNAcylation impairs adult neurogenesis and cognitive function and increases gliogenesis in the young hippocampus.

To understand the relationship between O-GlcNAc expression and adult neurogenesis *in vivo*, we asked whether mimicking an age-related decline in NSC O-GlcNAcylation within the adult hippocampus would impair neurogenesis. To resolve the role of O-GlcNAc in a temporally defined and cell type-specific manner in the adult brain, we generated male $Ogt^{flox/y}$ mice carrying an inducible *NestinCre-ERT*^{2} gene, in which the X-linked *Ogt* gene is excised specifically in adult NSCs (Ogt cKO) upon tamoxifen administration (**Figure 1.7A**). Young (2 months) mice were administered tamoxifen and changes in neurogenesis were assessed in young adult (3 months) Ogt cKO and littermate control ($Ogt^{flox/y}$) mice by immunohistochemical analysis. Loss of Ogt expression in adult NSCs resulted in a decrease in the number of Nestin-positive NSCs and Dcx/MCM2-positive neuroblasts in the hippocampus of Ogt cKO compared to littermate control animals (**Figure 1.7B,C**). We assessed neuronal differentiation and survival using a long-term BrdU incorporation paradigm, in which mature differentiated neurons express both BrdU and the neuronal marker NeuN. We observed a decrease in the number of long-term retaining BrdU/NeuN-positive mature differentiated neurons Ogt cKO compared to control animals (**Figure 1.7B,C**). To ensure these differences in neurogenesis were not due to increased cell death, we compared the number of cleaved caspase-3 positive cells and observed no difference in cell death

between Ogt cKO and littermate control mice (**Figure 1.8**). To corroborate our genetic studies, we abrogated hippocampal Ogt expression in wild type animals utilizing an *in vivo* viral-mediated RNAi approach. Young adult (3 months) animals were stereotaxically injected with high-titer lentivirus encoding Ogt or control shRNA sequences into the DG of contralateral hippocampi (**Figure 1.9A**). Decreased Ogt in the DG resulted in a significant decrease in the number of Dcx-positive/Edu-positive neuroblasts and long-term retaining BrdU/NeuN-positive neurons compared with the control contralateral DG (**Figure 1.9B**). Collectively, our genetic and *in vivo* RNAi data indicate that loss of NSC O-GlcNAcylation mirror an aging condition by negatively regulating neurogenesis in the adult hippocampus.

To investigate whether mimicking an age-related decline in NSC O-GlcNAcylation also impaired cognitive processes associated with adult neurogenesis, we assessed hippocampal-dependent object recognition and associative fear memory using novel object recognition (NOR) and contextual fear conditioning paradigms, respectively (**Figure 1.7A**). In the testing portion of the NOR task, control animals exhibited a significant preference for the novel object over the familiar object; however, this preference was lost in Ogt cKO mice (**Figure 1.7D**). During contextual fear conditioning testing, we observed decreased freezing in Ogt cKO mice compared to controls animals (**Figure 1.7E**). No differences were observed in baseline freezing during fear conditioning training (**Figure 1.10A**) or in cued fear conditioning testing between genotypes (**Figure 1.7E**). As a control, we profiled general health using an open field paradigm (**Figure 1.10B**) and observed no differences in overall activity, total distance traveled, or time spent in the periphery or center of the open field, indicative of normal motor and anxiety functions (**Figure 1.10C-E**). These behavioral data demonstrate that decreased adult NSC O-GlcNAcylation impairs hippocampal-dependent learning and memory.

Next, to examine the relationship between O-GlcNAcylation and gliogenesis, we asked whether mimicking an age-related decline in NSC O-GlcNAc levels would promote astrocyte differentiation using a genetic lineage tracing approach. We generated male Ogt cKO and control

mice carrying a loxP-flanked STOP cassette preventing transcription of a CAG-promoter driven tdTomato (tdT) reporter inserted into the Gt(Rosa)26Sor locus, in which tdT is expressed in adult NSCs upon tamoxifen administration. Young (2 months) mice were administered tamoxifen and changes in gliogenesis were assessed in young adult (3 months) Ogt cKO and littermate control mice by immunohistochemical analysis. Efficacy of our knockout model was confirmed by immunohistochemistry (**Figure 1.11**). Loss of Ogt expression in adult NSCs resulted in an increase in the number of tdT/GFAP-positive and tdT/S100ß-positive astrocytes in the hippocampus of Ogt cKO compared to control animals (**Figure 1.7F,G**). Our *in vivo* lineage tracing analysis identify an increase in adult gliogenesis in young mice following decreased NSC O-GlcNAcylation that reflect age-related changes in the mature hippocampus (**Figure 1.1E,F**).

O-GlcNAcylation of STAT3 at T717 is reduced in the aging hippocampus and promotes a glial fate switch in NSCs.

To gain mechanistic insight into site-specific changes in O-GlcNAcylation potentially regulating impaired NSC function during aging, we performed comparative O-GlcNAc-specific proteomics analysis of the hippocampus at ages before and after changes in adult neurogenesis and gliogenesis (**Figure 1.12A**). Due to technical limitations in the number of aged animals necessary to obtain sufficient amounts of primary NSCs to enrich for dynamic post-translational modifications, we opted to sub-dissect and pool hippocampi from young adult (3 months), middle aged (12 months) and old (24 months) mice. We isolated total hippocampal protein, trypsin digested, and labeled the resulting peptides with isobaric tandem mass tags (TMT) before enriching for O-GlcNAcylated peptides using lectin weak affinity chromatography (LWAC). Glycopeptides were analyzed by electron-transfer/higher-energy collision dissociation (EThcD) mass spectrometry. We detected 1344 O-GlcNAcylation sites across 474 unique proteins. We next examined mechanistic synergies between decreased sites of protein O-GlcNAcylation in the aging hippocampus (**Table**

1.1) and cell-type-specific molecular changes elicited in NSCs by decreased O-GlcNAc levels (**Figure 1.5; Figure 1.4**), and selectively identified STAT3. A representative EThcD spectrum used to resolve an unambiguous O-GlcNAcylation site on a peptide from the STAT3 protein (**Figure 1.12B**), as well as a schematic depicting an age-related decrease in STAT3 O-GlcNAcylation at Threonine 717 (T717) and Serine 719 (S719) (**Figure 1.12C**) are provided. Collectively, our proteomic analysis of the aging hippocampus, together with RNA-sequencing of primary NSCs, indicate changes in STAT3 signaling downstream of age-related decreased O-GlcNAcylation.

Currently, the functional consequences of STAT3 O-GlcNAcylation at S719 is unknown, however, increased STAT3 O-GlcNAcylation at T717 has been previously shown to inhibit STAT3 activation in immune cells by preventing STAT3 phosphorylation at Tyrosine 705 (Y705) (30). We therefore investigated whether decreasing O-GlcNAcylation in primary NSCs could conversely increase STAT3 activation. We assessed NSC STAT3 phosphorylation at Y705 following Ogt inhibition with OSMI-1 treatment *in vitro* by Western blot (**Figure 1.12D**). While STAT3 expression was not altered, pharmacological inhibition of Ogt significantly increased phosphorylation levels of STAT3 in NSCs (**Figure 1.12D**). Additionally, we made use of our RNA-sequencing dataset to survey expression of known STAT3 target genes in NSCs following Ogt inhibition, and likewise observed an upregulation of several genes associated with STAT3 activation (31), including *p21*, *Zeb1* and *Ccnd1* (**Figure 1.12E**).

To investigate whether blocking STAT3 activation would mitigate the effects of decreasing O-GlcNAcylation on differentiation in postnatal and adult NSCs, we generated viral expression constructs encoding a non-phosphorylatable STAT3 by converting Tyrosine into Phenylalanine at position 705 (Y705F STAT3). As a control, primary NSCs were infected with a virus encoding a wildtype STAT3. When treated with OSMI-1, control NSCs exhibited decreased neuronal (**Figure 1.12F**) and increased astrocyte (**Figure 1.12G**) differentiation, corroborating our previous findings (**Figure 1.5F,G**). Expression of Y705F STAT3 increased neuronal (**Figure 1.12F**) and decreased astrocyte differentiation (**Figure 1.12G**), consistent with previous reports (28, 29). Moreover, the

effects of decreasing NSC O-GlcNAcylation on STAT3 activation (**Figure 1.13A**) and neuronal differentiation (**Figure 1.12F**) were mitigated by expression of the Y705F STAT3 mutant. Next, we investigated whether mimicking an age-related decline in STAT3 O-GlcNAcylation at T717 altered NSC differentiation. It should be noted that the T717 site is only present on the predominant, full length STAT3 □ isoform, and not on the shorter □ isoform. We generated viral expression constructs encoding STAT3 with site-directed mutations converting Threonine to Alanine at position 717 (T717A STAT3). Expression of O-GlcNAcylation-deficient T717A STAT3 in NSCs resulted in increased activation of the STAT3 □ isoform (**Figure 1.13B**), along with decreased neuronal (**Figure 1.12H**) and increased astrocyte (**Figure 1.12I**) differentiation compared to wildtype STAT3 control conditions. These *in vitro* data indicate that increased STAT3 activity, stemming from reduced NSC O-GlcNAcylation, promotes an astrocyte differentiation program in NSCs.

Increased NSC O-GlcNAc levels promote neuronal and inhibit astrocyte differentiation *in vitro*.

Given the pro-gliogenic effects of reducing NSC O-GlcNAc levels, we next investigated whether increasing NSC O-GlcNAc levels would conversely promote neuronal differentiation. We generated a viral expression construct encoding Ogt under the control of the Nestin promoter and primary postnatal and adult NSCs were infected with this virus or a control encoding GFP. Ogt overexpression in NSCs resulted in a significant increase in Ogt and O-GlcNAc levels (**Figure 1.14**). Additionally, we observed an increase in neuronal differentiation (**Figure 1.12J**) and a corresponding decrease in astrocyte differentiation (**Figure 1.12K**) in NSCs overexpressing Ogt compared to a GFP control. These data indicate that increased O-GlcNAcylation is sufficient to promote a neuronal differentiation program and inhibit astrocyte differentiation in NSCs.

DISCUSSION

Cumulatively, our data indicate that age-related loss of NSC protein O-GlcNAcylation regulates a STAT3-mediated neuron to glia fate switch that contributes to a decline in adult hippocampal neurogenesis. While increased NSC quiescence has been highlighted as a major determinant of age-related neurogenic decline in the hippocampus (7, 32), a complementary model has been proposed in which division-coupled conversion of NSCs into mature astrocytes restrict the stem cell pool with age (3). Our data identifying an O-GlcNAc-mediated glial fate switch in the mature hippocampus provide evidence for this coextensive cellular mechanism, in which age-related increased gliogenesis contributes to regenerative decline and associated cognitive impairments.

Previous reports have observed that the absolute number of newly generated astrocytes in the adult brain remains relatively constant with age (3, 33, 34). Given the well documented age-related decline of total NSC number, it has been suggested that maintaining this constant level of gliogenesis from a shrinking adult NSC pool requires that an increasing proportion of NSCs adopt a gliogenic fate (3, 33), a phenomenon that we demonstrate in the mature hippocampus. While adult neurogenesis has been shown to be a division-coupled process capable of maintaining the NSC pool (3, 5), gliogenesis is indicative of a terminal cell cycle exit and leads to a reduction in total NSC number (3). This shift towards terminal astrocyte differentiation with age further exacerbates the age-related decline of the NSC pool. In fact, mathematical modeling of NSC differentiation estimates that maintaining constant levels of gliogenesis accounts for nearly half of the NSCs lost during aging (34). In our study, we demonstrate that this shift in NSC cell fate occurs alongside a decrease in NSC O-GlcNAc. Moreover, we find that O-GlcNAcylation of STAT3 T717 declines in the hippocampus with age, and that loss of this posttranslational modification is sufficient to promote astrocyte differentiation in NSCs. Ultimately the shrinking of the adult NSC pool - which stems in part from terminal astrocyte differentiation - results in

decreased neurogenesis during aging, with major functional implications for age-related decreased regenerative capacity and neurodegenerative disease. Indeed, in elderly humans, maintaining higher levels of hippocampal neurogenesis is thought to be neuroprotective, as they are associated with increased cognitive scores and slower disease progression in the context of Alzheimer's disease (13, 14).

The ability to utilize the neurogenic capacity of adult NSCs is predicated on understanding underlying molecular mechanisms that can be targeted to reverse the effects of aging in the brain. Although post-translational modification of proteins represents a fundamental mechanism by which information is transmitted, its role in regulating adult NSC function with age has been largely overlooked. Previous work has suggested a role for O-GlcNAc in mediating proper brain development. Specifically, genetic ablation of the O-GlcNAc cleaving enzyme, Oga, in NSCs during development has been shown to increase NSC proliferation and lead to an accumulation of progenitors and immature neurons in the olfactory bulb (26). In our study, we identify O-GlcNAc as a novel post-translational regulator of regenerative decline in the adult brain and posit site-specific changes in O-GlcNAcylation as potential targets to counter age-related regenerative dysfunction. In particular, age-related loss of STAT3 O-GlcNAcylation at T717 provides a mechanistic link between increased NSC STAT3 signaling and an aberrant astrocyte differentiation program - pointing to STAT3 activation as a driver of age-related neurogenic decline. Interestingly, inhibition of STAT3 signaling in aged muscle stem cells restores regeneration at old age (35). Moreover, we demonstrate that increasing O-GlcNAcylation in NSCs by overexpressing Ogt is sufficient to promote neuronal differentiation. These data raise the exciting possibility of rejuvenating regenerative capacity in the aging brain by inhibiting STAT3 signaling through an increase in NSC O-GlcNAcylation. Ultimately, our data frame O-GlcNAc as a pro-neurogenic post-translational modification, with functional implications for cognitive processes.

From a therapeutic perspective, while decreased O-GlcNAcylation has been implicated in Alzheimer's disease pathology and neurodegeneration (18, 19), we recently demonstrated that increasing neuronal O-GlcNAcylation ameliorates age-related cognitive decline (17). Similarly, others have shown that inhibiting STAT3 signaling ameliorates cognitive deficits in mouse models of Alzheimer's disease, in part by preventing astrogliosis (36). This growing body of work positions O-GlcNAcylation, STAT3 signaling and the balance between newly generated neurons and astrocytes as a focal point in combating age-related functional decline in the aging and diseased brain. Of note, the benefits of interventions that ameliorate cognitive-decline during aging and Alzheimer's disease, such as exercise, have been shown to involve increased adult neurogenesis (37, 38). Given recent observations of the persistence of adult neurogenesis in the aged human brain (13, 14), the promise of restoring cellular and cognitive plasticity in the elderly by targeting adult NSCs is increasingly evident. Here we identify both an age-related NSC fate switch, and the post-translational modification governing it, as potential cellular and molecular targets by which to maintain regenerative capacity at old age, restore adult neurogenesis and ameliorate cognitive decline.

METHOD DETAILS

Animal Models. All mouse handling and use was in accordance with institutional and ethical guidelines approved by the University of California San Francisco IACUC. The following mouse lines were used: C57BL/6J young mice (Jackson Laboratory), B6.129-Ogt^{tm1Gwh}/J (The Jackson Laboratory line 004860), C57BL/6-Tg(Nes-cre/ERT2)KEisc/J (Jackson Laboratory line 016261), and B6.Cg-Gt(ROSA)26Sor$^{tm14(CAG-tdTomato)Hze/}$J mice (Jackson Laboratory line 007914). All studies were done in male mice. The numbers of mice used to result in statistically significant differences were calculated using standard power calculations with $\alpha = 0.05$ and a power of 0.8. We used an online tool (http://www.stat.uiowa.edu/~rlenth/Power/index.html) to calculate power and samples size based on experience with the respective tests, variability of the assays and inter-individual

differences within groups. Mice were housed under specific pathogen-free conditions under a 12h light-dark cycle. All experiments were randomized and blinded by an independent researcher. Researchers remained blinded throughout histological, molecular, and behavioral assessments. Groups were un-blinded at the end of each experiment upon statistical analysis.

Immunohistochemistry. Tissue processing and immunohistochemistry was performed on free-floating sections following standard published techniques (39). Briefly, mice were anesthetized with a ketamine (100mg/kg)-xylazine (10mg/kg) cocktail (Patterson Veterinary, Henry Schein) and transcardially perfused with cold PBS. Brains were removed, fixed in phosphate-buffered 4% paraformaldehyde, pH 7.4, at 4°C for 48h followed by cryoprotection in 30% sucrose, and coronally sectioned at 40µm with a cryomicrotome (Leica SM2010 R). Sections were washed three times in tris-buffered saline with 0.1% Tween 20 (TBST) and incubated in 3% normal donkey serum (Thermo Fisher Scientific) for 1h. After overnight incubation in primary antibody (Mouse anti-O-GlcNAc (RL2) [1:500], Mouse anti-Nestin (clone rat-401)[1:200], Goat anti-Doublecortin (C-18) [1:7500], Mouse anti-BM28 (MCM2) [1:250], Goat anti-Sox2 (Y-17) [1:200], Rabbit anti-GFAP[1:1000], Mouse anti-NeuN (clone A60) [1:1000], Rat anti-BrdU [BU1/75 (ICR1)] [1:1000], Mouse anti-Ki67 (clone B56) [1:500], Mouse anti-MAP2[1:500], Rabbit anti-s100ß[1:500]) at 4°C, staining was revealed using fluorescence conjugated secondary Alexa antibodies (Donkey anti-Rabbit: Alexa-488 conjugated secondary antibody, Donkey anti-Rabbit: Alexa-555 conjugated secondary antibody, Donkey anti-Rat: Alexa-488 conjugated secondary antibody, Donkey anti-Goat: Alexa-555 conjugated secondary antibody, Donkey anti-Mouse: Alexa-488 conjugated secondary antibody, Donkey anti-Mouse: Alexa-555 conjugated secondary antibody, Donkey anti-Mouse: Alexa-647 conjugated secondary antibody [1:500]). Antigen retrieval for BrdU labeling required incubation in 3M HCl at 37°C for 30min before incubation with primary antibody; Nestin labeling required incubation in Citrate Buffer (Sigma-Aldrich) at 95°C (3 times 5 minutes) prior to incubation with primary antibody. To estimate the total number of immunopositive cells

per DG, confocal stacks of coronal sections of the DG (3-6 sections per mouse, 40μm thick, 360μm apart) were acquired on a Zeiss LSM 800.

***In vivo* O-GlcNAc Quantification in Neural Stem Cells.** Immunohistochemistry and imaging were performed as previously described. To quantify O-GlcNAc levels, neural stem cells were identified based on GFAP/Sox2-positive staining, localization within the SGZ, and radial morphology. As O-GlcNAc staining is nuclear, DAPI was used to identify the nucleus of the analyzed cells. To quantify O-GlcNAc levels in a single cell, intensity in the O-GlcNAc channel was measured within the region defined by DAPI, and normalized to the area of that region in a single z-plane. This measurement was repeated over every plane in which that nucleus appeared in order to quantify the entirety of the cell. These values were then summed and normalized to the number of planes quantified for that cell. This process was repeated for every neural stem cell which was fully included within the section (i.e. not within terminal z-plane). For each animal, neural stem cells were analyzed in all sections and averaged to determine a value per animal. 4 animals were quantified per group. Fiji was used for quantification.

Isolation of Primary Neural Stem Cells from the Mouse Hippocampus. Primary neural stem cell isolation and culture were preformed following previously published techniques (40). Hippocampi were dissected from male postnatal day 1 (P1) or adult (2 month old) Wildtype C57/BL6 mice and pooled by age for NSC isolation. After removing superficial blood vessels, hippocampi were mechanically dissociated by fine mincing and enzymatically digested for 30 minutes at 37ºC in DMEM media containing 2.5U/ml Papain (Worthington Biochemicals), 1U/ml Dispase II (Boeringher Mannheim), and 250U/ml DNase I (Worthington Biochemicals). NSCs were purified using a 65% Percoll gradient and cultured (Neurobasal A medium supplemented with 2% B27 without Vitamin A, 1% Glutamax, 1% Penicillin Streptomycin, 10ng/ml EGF, 10ng/ml bFGF) as a monolayer on poly-D-lysine and laminin-coated plates at a density of 10^5 cells/cm^2.

Viral Plasmids and Viruses. We generated lentiviruses (LVs) encoding shRNAs targeting Ogt or luciferase using a lentiviral shRNA expression system (pGreenPuro shRNA, System Biosciences) according to the manufacturer's instructions. The targeted sequences were cloned into the pGreenPuro vector (Ogt, 5′-AGGGAACTAGATAACATGCTT-3′; Luciferase, 5'-GCCATTCTATCCTCTAGAGGA -3'). Ovreexpression sequences were generated as follows. The Ogt coding sequence (CDS) and partial 3' and 5' untranslated regions (UTRs) were PCR amplified form mouse hippocampal cDNA (Ogt forward primer: CACCGTTCAGTATTCTGTGCCGCC; Ogt reverse primer: TAGGGCAATTCTCCTGTGCG) and cloned into the pENTR D-TOPO vector (Thermo Fisher Scientific). The coding sequence was further amplified and cloned into a lentiviral expression plasmid containing a mouse Nestin promoter using the restriction sites NheI and BamHI. The STAT3 CDS was obtained from the ORFeome 5.1 collection and sequence verified using Sanger sequencing. STAT3 mutant constructs were generated using the QuikChange Lightning Site-directed Mutagenesis kit (Agilent) in combination with the following primers: GTAGCGCTGCCCCATTCCTGAAGACCAAG (Y705F Forward), CTTGGTCTTCAGGAATGGGGCAGCGCTAC (Y705F Reverse), CTGTGTGACACCAACGGCCTGCAGCAATACCAT (T717A Forward), ATGGTATTGCTGCAGGCCGTTGGTGTCACACAG (T717A Reverse). The lentiviral Nestin-promoter plasmid was linearized using the restriction enzymes NheI and SalI and the wildtype and mutant STAT3 expression constructs were generated using Gibson assembly (NEB). All coding plasmid sequences were verified using Sanger sequencing. Endotoxin free plasmid maxiprep kits were used for viral plasmid preparation. Lentivirus was generated according to UCSF viracore protocols. Briefly Lenti-X 293T cells were transfected with the lentiviral expression plasmid along with Pax2 and VSV-G packaging and envelope plasmids respectively. 24 hours later, media was supplemented with ViralBoost (Alstem) according to manufacturer's instructions. 24 hours later, media was removed and filtered through a 0.45μm filter. The filtered virus-

containing media was then concentrated via ultracentrifugation at 24,000 x g. The resulting pellet was resuspended in 100µL PBS. Viral titer was determined using Lenti-X Go Stix Plus (Takara) according to manufacturer's instructions.

NSC Proliferation Assay. NSCs were seeded in 500 µL growth medium (Neurobasal A medium supplemented with 2% B27 without Vitamin A, 1% Glutamax, 1% Penicillin Streptomycin, 10ng/ml EGF, 10ng/ml bFGF) at a density of 10,000 cells/well on PDL/laminin-coated glass coverslips in a 24-well tissue culture plate. 24h later, cells were treated with either DMSO or 12.5µM OSMI-1 (Sigma-Aldrich). 16h later, cells were treated with 20µM EdU for 8h prior to fixing with 4% PFA. Acute knockdown of Ogt was induced by treating plated NSCs with shRNA -encoding lentiviruses (10 viral particles per cell) for three days prior to EdU treatment as described. Cells were washed 3 times with PBS after fixation, blocked in 3% donkey serum, and incubated in primary antibody at 4ºC for 16h. After 3 washes with PBS, EdU incorporation was revealed using a Click-iT EdU Alexa Fluor Imaging Kit (Thermo Fisher Scientific) and nuclei were counterstained with Hoechst 33342 (1:10000; Thermo Fisher Scientific). EdU-positive cells were counted per field of view at three randomly determined locations per coverslip. *In vitro* experiments were conducted in triplicates for each condition and repeated to ensure reproducibility.

NSC Differentiation Assay. NSCs were seeded in 500µL growth medium and treated with OMSI-1 or infected with lentivirus at a ratio of 10 viral particles per cell. 24h (OSMI-1) or 72h (knockdown and overexpression) after treatment, media was replaced with differentiation medium (Neurobasal A medium supplemented with 2% B27 without Vitamin A, 1% Glutamax, 1% Penicillin Streptomycin). Cells were maintained in differentiation medium for 7 days, with half the media replaced every other day. Cells were fixed with 4% PFA as previously described. Cells were washed 3 times with PBS after fixation, blocked in 3% donkey serum, and incubated in primary antibody at 4ºC for 16h. staining was revealed using fluorescence conjugated secondary Alexa

antibodies (1:500). MAP2- or GFAP-positive cells were counted per field of view at three randomly determined locations per coverslip. *In vitro* experiments were conducted in 3-6 replicates for each condition and repeated to ensure reproducibility.

Lactate Dehydrogenase Assay. Primary NSCs were seeded at 3000 cells per well in a 96-well plate and were treated with OSMI-1 or a vehicle control and differentiated as previously described. At 0, 1, 3, 5, and 7 days after removal of growth factors, cytotoxicity was assessed using the Pierce LDH Cytotoxicity Assay Kit (Thermo Fisher Scientific) according to the manufacturer's instructions. Measurements were performed on 6 individual replicates to ensure reproducibility.

Trypan Blue Assay. Primary NSCs were treated with OSMI-1 or a vehicle control and differentiated as previously described. At 1, 3, 5, and 7 days after removal of growth factors, cell viability was assessed using trypan blue. All cells and media were removed from the plate and centrifuged at 400 x g for 5 minutes. The pellet was resuspended in fresh media and diluted with an equal volume of trypan blue. Total cells, live cells (trypan blue excluding), and dead cells (trypan blue including) were counted using a hemocytometer. Cell viability was determined by dividing the number of lives cells by the total number of cells. Counts were performed on 6 replicates to ensure reproducibility.

Western Blot Analysis. Primary NSCs were lysed in RIPA lysis buffer (500 mM Tris, pH 7.4, 150 mM NaCl, 0.5% Na deoxycholate, 1% NP40, 0.1% SDS, complete protease inhibitors; Roche, Halt Phosphatase Inhibitor Cocktail; Thermo Fisher, and PUGNAc; Sigma-Aldrich). Protein lysates were mixed with 4x NuPage LDS loading buffer (Invitrogen) and loaded on a 4-12% SDS polyacrylamide gradient gel (Invitrogen) and subsequently transferred onto a nitrocellulose membrane. The blots were blocked in 5% milk in Tris-Buffered Saline with Tween (TBST) and incubated with primary antibody (Mouse anti-O-GlcNAc (RL2) [1:500] (Abcam, ab2739), Rabbit

anti-Ogt [1:500] (Novus, NBP1-32791), Rabbit anti-Histone H3 [1:1000] (Thermo Fisher Scientific, PA5-16183), Rabbit anti-STAT3 [1:1000] (Cell Signaling 12640), Rabbit anti-pSTAT3 (Y705) [1:1000] (Cell Signaling, 9131) at 4°C for 16h. Horseradish peroxidase-conjugated secondary antibodies and an ECL kit (GE Healthcare/BioRad) were used to detect protein signals. Blots were imaged with a ChemiDoc (BioRad) and quantified using ImageJ software (Version 1.8.0_91). Actin or HH3 bands were used for normalization.

PCR Genotyping . Ogt floxed, Nestin-CreERT2, and TdTomato alleles were genotyped from skin biopsies using PCR. Primers specific for the beta-globin gene were included in the reaction as a control. Ogt floxed forward primer: CATCTCTCCAGCCCCACAAACTG. Ogt floxed reverse primer: GACGAAGCAGGAGGGGAGAGCAC. Primer Cre forward: CACCCTGTTACGTATAGCCG. Primer Cre reverse: GAGTCATCCTTAGCGCCGTA. TdTomato mutant forward primer: CTGTTCCTGTACGGCATGG. TdTomato mutant reverse primer: GGCATTAAAGCAGCGTATCC. TdTomato wildtype forward primer: AAGGGAGCTGCAGTGGAGTA. TdTomato wildtype reverse primer: CCGAAAATCTGTGGGAAGTC. Beta-globin forward primer: CCAATCTGCTCACACAGGATAGAGAGGGCAGG. Beta-globin reverse primer: CCTTGAGGCTGTCCAAGTGATTCAGGCCATCG.

Tamoxifen injections. Animals were injected via intraperitoneal injection with 75mg/kg of tamoxifen or vehicle once every 24 hours for a total of 5 injections per animal. Animals were monitored after recovery and four weeks allowed to pass after the final injection before any analyses were performed.

BrdU administration and Quantification. For short-term proliferation studies, mice were intraperitoneally injected with EdU (50mg/kg body weight, Sigma-Aldrich) daily for six days prior

to euthanasia. For study of newborn neuron survival and astrocyte formation, mice were injected with BrdU (50mg/kg) for six days and animals were euthanized 28 days after administration. To estimate the total number of BrdU-positive cells in the brain, we performed fluorescence staining for BrdU on 3-6 hemibrain sections per mouse (40μm thick, 360μm apart). To quantify neuronal fate and maturation of dividing cells, BrdU-positive cells across 3-6 sections per mouse were analyzed by confocal microscopy for co-expression with NeuN. To quantify astrocyte formation, BrdU-positive cells across 3-6 sections per mouse were analyzed by confocal microscopy for co-expression with either GFAP or s100ß.

Contextual Fear Conditioning. Paradigm follows previously published techniques (10). Mice learned to associate the environmental context (fear conditioning chamber) with an aversive stimulus (mild foot shock; unconditioned stimulus, US) enabling testing for hippocampal-dependent contextual fear conditioning. The mild foot shock was paired with a light and tone cue (conditioned stimulus, CS) in order to also assess amygdala- dependent cued fear conditioning. Conditioned fear was displayed as freezing behavior. Specific training parameters are as follows: tone duration is 30 seconds; level is 70dB, 2kHz; shock duration is 2 seconds; intensity is 0.6mA. On day 1 each mouse was placed in a fear-conditioning chamber and allowed to explore for 2 minutes before delivery of a 30-second tone (70dB) ending with a 2-second foot shock (0.6mA). Two minutes later, a second CS-US pair was delivered. On day 2 each mouse was first place in the fear- conditioning chamber containing the same exact context, but with no administration of a CS or foot shock. Freezing was analyzed for 1-3 minutes. One hour later, the mice were placed in a new context containing a different odor, cleaning solution, floor texture, chamber walls and shape. Animals were allowed to explore for 2 minutes before being re-exposed to the CS. Freezing was analyzed for 1-3 minutes. Freezing was measured using a FreezeScan video tracking system and software (Clever Sys, Inc). All behavior is performed double blinded.

Novel Object Recognition. The novel object recognition task was adapted from a previously described protocol (41). During the habituation phase (day 1), mice could freely explore an empty arena for 10 minutes. During the training phase (day 2), two identical objects were placed in the habituated arena, and mice could explore the objects for 5 minutes. For the testing phase (day 3), one object was replaced with a novel object, and mice could explore the objects for 5 minutes. Time spent exploring each object was quantified using the Smart Video Tracking Software (Panlab; Harvard Apparatus). Two different sets of objects are used. To control for any inherent object preference, half of the mice are exposed to object A as their novel object and half to object B. To control for any potential object-independent location preference, the location of the novel object relative to the trained object is also varied. The objects were chosen based on their ability to capture the animal's interest, independent of genetic background or age. To determine percent time with novel object, we calculate (Time with novel object)/(Time with Trained Object + Time with Novel Object) * 100. In this preference index, 100% indicates full preference for the novel object, and 0% indicates full preference for the trained object. A mouse with a value of 50% would have spent equal time exploring both objects. Mice that did not explore both objects during the training phase were excluded from analysis.

Open Field. Mice were placed in the center of an open 40cm x 40cm square chamber (Kinder Scientific) with no cues or stimuli and allowed to move freely for 10 minutes. Infrared photobeam breaks were recorded and movement metrics analyzed by MotorMonitor software (Kinder Scientific).

Stereotaxic injections. Animals were placed in a stereotaxic frame and anesthetized with 2% isoflurane (2 liters/min oxygen flow rate) delivered through an anesthesia nose cone. Ophthalmic eye ointment was applied to the cornea to prevent desiccation during surgery. The area around the incision was trimmed. Solutions were injected bilaterally into the DG of the dorsal hippocampi

using the following coordinates: (from bregma) anterior = −2 mm, lateral = 1.5 mm, (from skull surface) height = −2.1 mm. A 2-µl volume was injected stereotaxically over 10 min (injection speed: 0.20 µl/min) using a 5-µl 26s-gauge Hamilton syringe. To limit reflux along the injection track, the needle was maintained *in situ* for 10 min, slowly pulled out halfway and kept in position for an additional 5 min. The skin was closed using silk suture. Each mouse was injected subcutaneously with analgesics. Mice were singly housed and monitored during recovery.

Protein Isolation. Mouse hippocampi were isolated from fresh mouse brain tissue of either 3, 12, or 24 month old mice after transcardial perfusion with cold PBS (n=3 replicates per group; n=3 mice per replicate). Protein was isolated from the hippocampus with TRIzol Reagent (Thermo Fisher Scientific), according to manufacturer's instructions. Frozen protein pellets were resuspended in 50mM ammonium bicarbonate containing 6M guanidine hydrochloride, 6X Phosphatase Inhibitor Cocktails II and III (Sigma-Aldrich), and 80mM PUGNAc (Tocris Bioscience, Avonmouth, UK). Protein concentrations were estimated with bicinchoninic acid (BCA) protein assay (ThermoFisher Scientific, Rockford, IL). The protein lysate (1 mg from each sample) was reduced for 1 hour at 56ºC with 2.5 mM Tris(2-carboxyethyl)phosphine hydrochloride and subsequently carbamidomethylated using 5 mM iodoacetamide for 45 min at room temperature in the dark. Lysates were diluted to 1M guanidine hydrochloride with 50 mM ammonium bicarbonate, pH 8.0, and equal amounts of each sample were digested overnight at 37°C with sequencing grade trypsin (ThermoFisher Scientific) at an enzyme to substrate ratio of 1:50 (w/w). Following digestion, samples were acidified with formic acid (FA) (Sigma-Aldrich), desalted using a 360-mg C18 Sep-Pak SPE cartridge (Waters), and dried to completeness using a SpeedVac concentrator (Thermo Electron).

TMT labeling. Tryptic peptides were labeled with TMT-10plex according to the manufacturer's protocol. The TMT labeling was as follows: 3month-1:TMT127C, 3month-2:TMT127N, 3month-

3:TMT128C, 12month-1:TMT128N, 12month-2:TMT129C, 12month-3:TMT129N, 24month-1:TMT130C, 24month-2:TMT130N, 24month-3: TMT-131C. Labeling efficiency was checked on Thermo Scientific Q Exactive Plus Orbitrap. TMT labeled peptides were mixed together, desalted using a 360-mg C18 Sep-Pak SPE cartridge, and dried to completeness using a SpeedVac concentrator before glycopeptide enrichment.

Lectin Weak Affinity Chromatography. Glycopeptides were enriched as described previously (42, 43). Briefly, desalted-TMT-labeled peptides were resuspended in 500 µL LWAC buffer (100 mM Tris pH 7.5, 150 mM NaCl, 10 mM MgCl2, 10 mM CaCl2, 5% acetonitrile) and 100 µL were run over a 2.0 x 250mm POROS-WGA column at 100 µL/min under isocratic conditions with LWAC buffer and eluted with a 100 µL injection of 40mM GlcNAc. Glycopeptides were collected inline on a C18 column (Phenomenex, Torrance, CA). Enriched glycopeptides from 5 initial rounds of LWAC were eluted with 50% acetonitrile, 0.1% FA in a single 500 µL fraction, dried, and LWAC enrichment was repeated for a total of 3 enrichment steps.

Glycopeptides were separated on a 1.0 × 100 mm Gemini 3µ C18 column (Phenomenex, Torrance, CA). Peptides were loaded onto the column in 20 mM NH_4OCH_3, pH 10 and subjected to a gradient from 1% to 21% 20mM NH_4OCH_3, pH10 in 50% acetonitrile over 1.1 mL, up to 62% 20mM NH_4OCH_3, pH10 in 50% acetonitrile over 5.4 mL with a flow rate of 80 µL/min while collecting 31 fractions.

Mass Spectrometry Analysis. Glycopeptides were analyzed on an Orbitrap Fusion Lumos (Thermo Scientific, San Jose, CA) equipped with a NanoAcquity UPLC (Waters, Milford, MA). Peptides were fractionated on a 50cm x 75 µm ID 2µm C18 EASY-Spray column using a linear gradient from 3.5-30% solvent B over 185 min. Precursor ions were measured from 375 to 1500 m/z in the Orbitrap analyzer (resolution: 120,000; AGC: 4.0e5). Each precursor ion (charged 2-

7+) was isolated in the quadrupole (selection window: 1.6 m/z for EThcD, 0.7 m/z for HCD; dynamic exclusion window: 30 s; MIPS Peptide filter enabled) and underwent two ms2 fragmentation methods. Ions were fragmented by EThcD (Maximum Injection Time: 250 ms, Supplemental Activation Collision Energy: 25%) and measured in the Orbitrap (resolution: 30,000; AGC; 5.0e4) for peptide identification. The same selected precursor was also fragmented by HCD (Maximum Injection Time: 86 ms; HCD Collision Energy: 50%) and measured in the Orbitrap (resolution: 50,000; AGC; 5.0e4; Scan Range: 100-400 m/z) for TMT reporter ion intensity measurement. The scan cycle was 18 scans.

Peaklists for EThcD were extracted using Proteome Discoverer 2.2. EThcD peaklists were filtered with MS-Filter and only spectra containing a 204.0867 m/z peak corresponding to the HexNAc oxonium ion were used for database searching. EThcD data was searched against the SwissProt *Mus musculus* database (downloaded September 6, 2016) (and concatenated with a randomized sequence for each entry) using Protein Prospector (v5.23.0). Cleavage specificity was set as tryptic, allowing for 2 missed cleavages. Carbamidomethylation of Cys and TMT10plex on lysine and the peptide N-terminus were set as constant modifications. The required mass accuracy was 10 ppm for precursor ions and 30 ppm for fragment ions. Two modifications per peptide were permitted. Unambiguous PTMs were determined using a minimum SLIP score of six, which corresponds to a 5% local false localization rate. Modified peptides were identified with a protein and peptide false discovery rate of 1%. O-GlcNAc and O-GalNAc modifications were differentiated based on known protein subcellular localization and HexNAc oxonium ion fragment ratios (44).

TMT Mass Spectrometry Data Analysis. Data was filtered to only include O-GlcNAcylated peptides unique to a single protein. Quantitation of TMT data was performed by calculating ratios of reporter ion peak intensities between conditions along with variance for each ratio, and median

normalized. Reporter ion peak intensities were obtained from HCD spectra corresponding to peptides identified from EThcD spectra. Peptide abundances were normalized by the median of ratio distributions. The age-dependent changes in O-GlcNAcylation were determined using a normalized median Log_2 12mo/3mo ratio of at least 1.0, corresponding to a 2.0 fold change with age. Raw data files available under MassIVE submission MSV000084825. All annotated O-GlcNAc-peptide spectra available at MS-Viewer (45) search key qcchi2to8l.

RNA Isolation. mRNA of NSCs was isolated by lysis with TRIzol Reagent (Thermo Fisher Scientific), separation with chloroform (0.2mL per mL TRIzol), and precipitated with isopropyl alcohol according to manufacturer's instructions.

NSC Library Construction and RNA-sequencing. After RNA isolation, RNA-Seq libraries were constructed using the Smart-Seq2 protocol from (46), with modifications. Briefly, 1ng high quality RNA was reverse transcribed using SuperScript II (Life Technologies, 18064-014) with a poly-dT anchored oligonucleotide primer, and a template switching oligonucleotide primer that generated homotypic PCR primer binding sites. The cDNA underwent 10 rounds of PCR amplification using KAPA HiFi Hotstart (Kapa Biosystems, KK2601), followed by Ampure bead (Agencourt) cleanup. The quality of the amplified cDNA was tested using qPCR for GAPDH and nucleic acid quantitation. 1ng of high-quality amplified cDNA was fragmented with the Tn5 transposase from the Illumina Nextera kit (FC-131-1096) to a median size of ~500bp. The fragmented library was amplified with indexed Nextera adapters (FC-131-1002) using 12 rounds of PCR. Final libraries were purified with Ampure beads and quantified using a qPCR Library Quantification Kit (Kapa Biosystems, KK4824). Libraries were pooled for sequencing on an Illumina HiSeq 2500 (paired reads 2x100bp).

Bioinformatic analysis of NSC RNA-sequencing data. Alignment of RNA sequencing reads to the mouse mm10 transcriptome was performed using STAR v2.7.3a (47) following ENCODE standard options, read counts were generated using RSEM v1.3.1, and differential expression analysis was performed in R v3.6.1 using the DESeq2 package v1.38.0 (48). [Detailed pipeline v2.0.1 and options available on https://github.com/emc2cube/Bioinformatics/]. Significance was determined using a corrected p-value<0.05 and a $\log_2$ fold change>0.5. Gene Ontology and ChEA/ENCODE transcription factor enrichment analysis was performed with Enrichr (https://amp.pharm.mssm.edu/Enrichr/). Heatmaps were generated using iDEP (http://bioinformatics.sdstate.edu/idep/). All data available under GEO submission GSE143388.

Data and statistical analysis. Graphed data are expressed as mean ± SEM. Statistical analysis was performed with Prism 6.0 software (GraphPad Software). Unless otherwise noted, means between two groups were compared with two-tailed, unpaired Student's t-test. Novel object recognition data were compared with a one sample t-test against 50% (expected preference). Comparisons of means from multiple groups with each other or against one control group were analyzed with one-way ANOVA and Tukey's post-hoc test. All histology and behavior experiments conducted were done in a randomized and blinded fashion. For each experiment, the overall size of the experimental groups corresponded to distinct animals or cultures. Unique samples were not measured repeatedly within the same characterization of a given cohort.

ACKNOWLEDGEMENTS

We thank Dr. Barbara Panning for insightful comments. Computing for this project was performed on the Sherlock cluster. We would like to thank Stanford University and the Stanford Research Computing Center for providing computational resources and support that contributed to these research results. This work was funded by HHMI (J.C.M, A.L.B), NIH NIGMS 8P41GM103481 (J.C.M, A.L.B), Dr. Miriam and Sheldon G. Adelson Medical Research Foundation (J.C.M, A.L.B), NIH Ruth L. Krischstein NRSA predoctoral fellowship (E.G.W, F31-AG050415), NIA (R01 AG055797, RF1 AG062357) and gift from Marc and Lynne Benioff (S.A.V).

REFERENCES

1. K. M. Christian, H. Song, G. L. Ming, Functions and dysfunctions of adult hippocampal neurogenesis. *Annual Review of Neuroscience* **37**, 243–262 (2014).

2. J. T. Goncalves, S. T. Schafer, F. H. Gage, Adult Neurogenesis in the Hippocampus: From Stem Cells to Behavior. *Cell* **167**, 897–914 (2016).

3. J. M. Encinas, *et al.*, Division-coupled astrocytic differentiation and age-related depletion of neural stem cells in the adult hippocampus. *Cell stem cell* **8**, 566–579 (2011).

4. B. Steiner, *et al.*, Differential regulation of gliogenesis in the context of adult hippocampal neurogenesis in mice. *Glia* **46**, 41–52 (2004).

5. M. A. Bonaguidi, *et al.*, In vivo clonal analysis reveals self-renewing and multipotent adult neural stem cell characteristics. *Cell* **145**, 1142–1155 (2011).

6. S. Bonzano, *et al.*, Neuron-Astroglia Cell Fate Decision in the Adult Mouse Hippocampal Neurogenic Niche Is Cell-Intrinsically Controlled by COUP-TFI In Vivo. *Cell reports* **24**, 329–341 (2018).

7. S. Lugert, *et al.*, Quiescent and active hippocampal neural stem cells with distinct morphologies respond selectively to physiological and pathological stimuli and aging. *Cell stem cell* **6**, 445–456 (2010).

8. H. G. Kuhn, H. Dickinson-Anson, F. H. Gage, Neurogenesis in the dentate gyrus of the adult rat: age-related decrease of neuronal progenitor proliferation. *The Journal of neuroscience : the official journal of the Society for Neuroscience* **16**, 2027–2033 (1996).

9. S. A. Villeda, *et al.*, The ageing systemic milieu negatively regulates neurogenesis and cognitive function. *Nature* **477**, 90–94 (2011).

10. G. Gontier, *et al.*, Tet2 Rescues Age-Related Regenerative Decline and Enhances Cognitive Function in the Adult Mouse Brain. *Cell Rep* **22**, 1974–1981 (2018).

11. H. G. Kuhn, T. Toda, F. H. Gage, Adult Hippocampal Neurogenesis: A Coming-of-Age Story. *The Journal of neuroscience : the official journal of the Society for Neuroscience* **38**, 10401–10410 (2018).

12. S. F. Sorrells, *et al.*, Human hippocampal neurogenesis drops sharply in children to undetectable levels in adults. *Nature* **555**, 377–381 (2018).

13. E. P. Moreno-Jimenez, *et al.*, Adult hippocampal neurogenesis is abundant in neurologically healthy subjects and drops sharply in patients with Alzheimer's disease. *Nature medicine* **25**, 554–560 (2019).

14. M. K. Tobin, *et al.*, Human Hippocampal Neurogenesis Persists in Aged Adults and Alzheimer's Disease Patients. *Cell stem cell* **24**, 974-982.e3 (2019).

15. A. C. Wang, E. H. Jensen, J. E. Rexach, H. V. Vinters, L. C. Hsieh-Wilson, Loss of O-GlcNAc glycosylation in forebrain excitatory neurons induces neurodegeneration. *Proceedings of the National Academy of Sciences of the United States of America* **113**, 15120–15125 (2016).

16. O. Lagerlof, O-GlcNAc cycling in the developing, adult and geriatric brain. *Journal of Bioenergetics and Biomembranes* **50**, 241–261 (2018).

17. E. G. Wheatley, *et al.*, Neuronal O-GlcNAcylation Improves Cognitive Function in the Aged Mouse Brain. *Current biology : CB* **29**, 3359-3369.e4 (2019).

18. Y. Zhu, X. Shan, S. A. Yuzwa, D. J. Vocadlo, The emerging link between O-GlcNAc and Alzheimer disease. *The Journal of biological chemistry* **289**, 34472–34481 (2014).

19. S. Wang, *et al.*, Quantitative proteomics identifies altered O-GlcNAcylation of structural, synaptic and memory-associated proteins in Alzheimer's disease. *The Journal of pathology* **243**, 78–88 (2017).

20. P. M. Levine, *et al.*, alpha-Synuclein O-GlcNAcylation alters aggregation and toxicity, revealing certain residues as potential inhibitors of Parkinson's disease. *Proceedings of the National Academy of Sciences of the United States of America* **116**, 1511–1519 (2019).

21. D. C. Love, *et al.*, Dynamic O-GlcNAc cycling at promoters of Caenorhabditis elegans genes regulating longevity, stress, and immunity. *Proceedings of the National Academy of Sciences of the United States of America* **107**, 7413–7418 (2010).

22. M. M. Rahman, *et al.*, Intracellular protein glycosylation modulates insulin mediated lifespan in C.elegans. *Aging* **2**, 678–690 (2010).

23. H. Jang, *et al.*, O-GlcNAc regulates pluripotency and reprogramming by directly acting on core components of the pluripotency network. *Cell stem cell* **11**, 62–74 (2012).

24. N. O'Donnell, N. E. Zachara, G. W. Hart, J. D. Marth, Ogt-dependent X-chromosome-linked protein glycosylation is a requisite modification in somatic cell function and embryo viability. *Molecular and cellular biology* **24**, 1680–1690 (2004).

25. S. Parween, *et al.*, Higher O-GlcNAc Levels Are Associated with Defects in Progenitor Proliferation and Premature Neuronal Differentiation during in-Vitro Human Embryonic Cortical Neurogenesis. *Frontiers in cellular neuroscience* **11**, 415 (2017).

26. S. O.-V. Stichelen, P. Wang, M. Comly, D. C. Love, J. A. Hanover, Nutrient-driven O-linked N-acetylglucosamine (O-GlcNAc) cycling impacts neurodevelopmental timing and metabolism. *The Journal of biological chemistry* **292**, 6076–6085 (2017).

27. H. van Praag, T. Shubert, C. Zhao, F. H. Gage, Exercise enhances learning and hippocampal neurogenesis in aged mice. *The Journal of neuroscience : the official journal of the Society for Neuroscience* **25**, 8680–8685 (2005).

28. F. He, *et al.*, A positive autoregulatory loop of Jak-STAT signaling controls the onset of astrogliogenesis. *Nature neuroscience* **8**, 616–625 (2005).

29. N. Tiwari, *et al.*, Stage-Specific Transcription Factors Drive Astrogliogenesis by Remodeling Gene Regulatory Landscapes. *Cell stem cell* **23**, 557-571.e8 (2018).

30. X. Li, *et al.*, Myeloid-derived cullin 3 promotes STAT3 phosphorylation by inhibiting OGT expression and protects against intestinal inflammation. *The Journal of experimental medicine* **214**, 1093–1109 (2017).

31. R. L. Carpenter, H. W. Lo, STAT3 Target Genes Relevant to Human Cancers. *Cancers* **6**, 897–925 (2014).

32. G. Kalamakis, *et al.*, Quiescence Modulates Stem Cell Maintenance and Regenerative Capacity in the Aging Brain. *Cell* **176**, 1407-1419.e14 (2019).

33. S. Beccari, J. Valero, M. Maletic-Savatic, A. Sierra, A simulation model of neuroprogenitor proliferation dynamics predicts age-related loss of hippocampal neurogenesis but not astrogenesis. *Sci Rep* **7**, 1–13 (2017).

34. F. Ziebell, S. Dehler, A. Martin-Villalba, A. Marciniak-Czochra, Revealing age-related changes of adult hippocampal neurogenesis using mathematical models. *Development* **145** (2018).

35. M. T. Tierney, *et al.*, STAT3 signaling controls satellite cell expansion and skeletal muscle repair. *Nature medicine* **20**, 1182–1186 (2014).

36. N. Reichenbach, *et al.*, Inhibition of Stat3-mediated astrogliosis ameliorates pathology in an Alzheimer's disease model. *EMBO molecular medicine* **11**, 10.15252/emmm.201809665 (2019).

37. A. M. Horowitz, *et al.*, Blood factors transfer beneficial effects of exercise on neurogenesis and cognition to the aged brain. *Science* **369**, 167–173 (2020).

38. S. H. Choi, *et al.*, Combined adult neurogenesis and BDNF mimic exercise effects on cognition in an Alzheimer's mouse model. *Science (New York, N.Y.)* **361**, 10.1126/science.aan8821 (2018).

39. L. K. Smith, *et al.*, beta2-microglobulin is a systemic pro-aging factor that impairs cognitive function and neurogenesis. *Nat Med* **21**, 932–937 (2015).

40. H. Babu, *et al.*, A protocol for isolation and enriched monolayer cultivation of neural precursor cells from mouse dentate gyrus. *Frontiers in Neuroscience* **5**, 1–10 (2011).

41. D. B. Dubal, *et al.*, Life extension factor klotho prevents mortality and enhances cognition in hAPP transgenic mice. *The Journal of neuroscience : the official journal of the Society for Neuroscience* **35**, 2358–2371 (2015).

42. J. C. Trinidad, *et al.*, Global identification and characterization of both O-GlcNAcylation and phosphorylation at the murine synapse. *Molecular & cellular proteomics : MCP* **11**, 215–229 (2012).

43. S. Kim, *et al.*, Schwann Cell O-GlcNAc Glycosylation Is Required for Myelin Maintenance and Axon Integrity. *The Journal of neuroscience : the official journal of the Society for Neuroscience* **36**, 9633–9646 (2016).

44. A. Halim, *et al.*, Assignment of saccharide identities through analysis of oxonium ion fragmentation profiles in LC-MS/MS of glycopeptides. *Journal of proteome research* **13**, 6024–6032 (2014).

45. P. R. Baker, R. J. Chalkley, MS-viewer: a web-based spectral viewer for proteomics results. *Molecular & cellular proteomics : MCP* **13**, 1392–1396 (2014).

46. J. J. Trombetta, *et al.*, Preparation of single-cell RNA-Seq libraries for next generation sequencing. *Current Protocols in Molecular Biology* **2014**, 4.22.1-4.22.17 (2014).

47. A. Dobin, *et al.*, STAR: ultrafast universal RNA-seq aligner. *Bioinformatics (Oxford, England)* **29**, 15–21 (2013).

48. M. I. Love, W. Huber, S. Anders, Moderated estimation of fold change and dispersion for RNA-seq data with DESeq2. *Genome biology* **15**, 550–8 (2014).

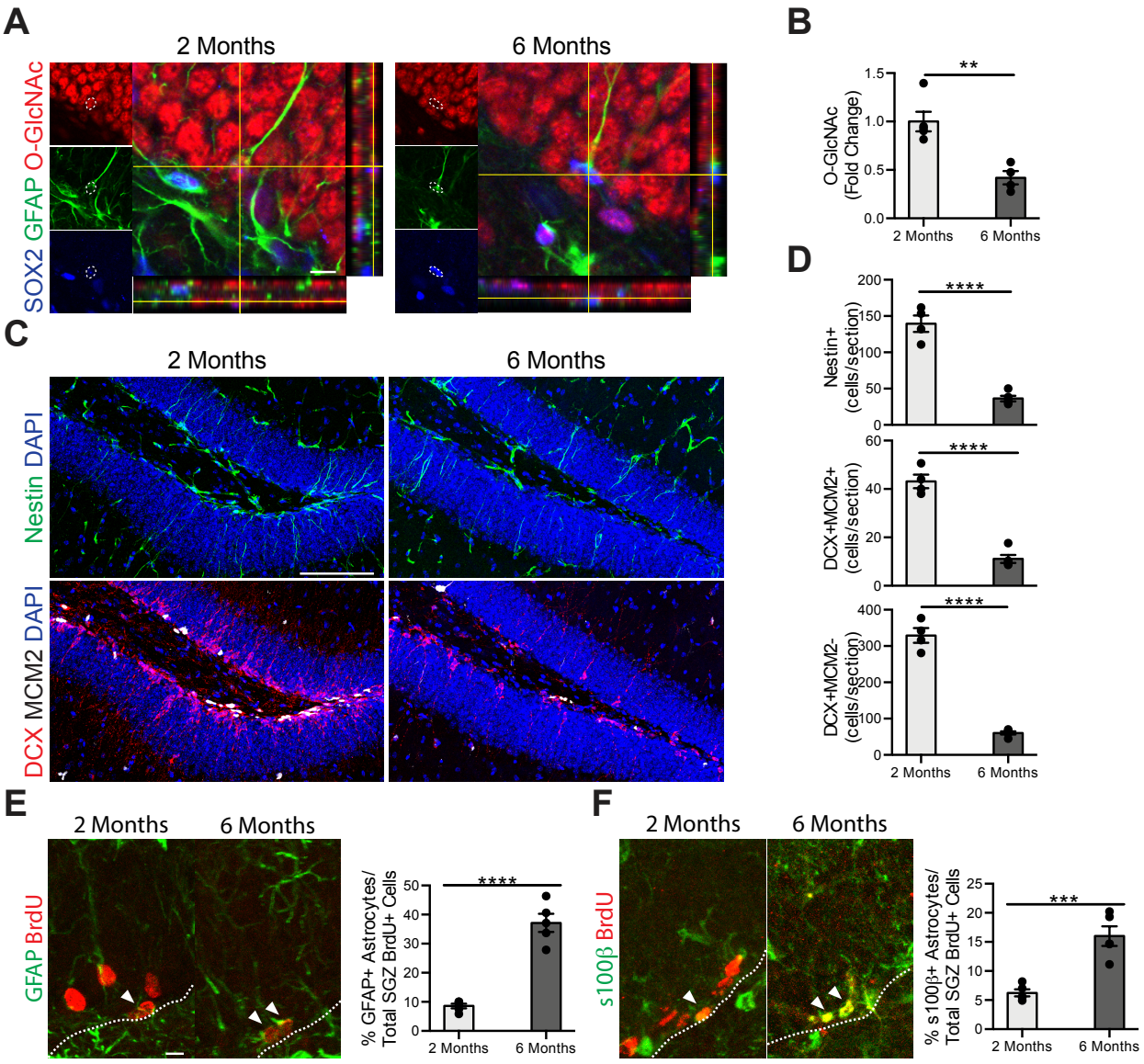
A
2 Months
6 Months
SOX2 GFAP O-GlcNAc
B
O-GlcNAc (Fold Change)
**
2 Months
6 Months
C
2 Months
6 Months
Nestin DAPI
DCX MCM2 DAPI
D
Nestin+ (cells/section)
****
DCX+MCM2+ (cells/section)
****
DCX+MCM2- (cells/section)
****
2 Months
6 Months
E
2 Months
6 Months
GFAP BrdU
% GFAP+ Astrocytes/ Total SGZ BrdU+ Cells
****
2 Months
6 Months
F
2 Months
6 Months
s100β BrdU
% s100β+ Astrocytes/ Total SGZ BrdU+ Cells
***
2 Months
6 Months

Figure 1.1. Age-related decreased NSC O-GlcNAc levels is coincident with a decline in neurogenesis and an increase in gliogenesis in the mature hippocampus.
(**A**) Representative single z-planes and orthogonal projections of a confocal image z-stack of 2- or 6-month old mouse hippocampus, labeled with anti-Sox2, anti-GFAP, anti-O-GlcNAc, and DAPI. Scale bar, 10μm. (**B**) Quantification of the fold change of the average O-GlcNAc intensity normalized to area measured in each GFAP+/Sox2+ neural stem cell (NSC) across all z-stacks per animal (n=4 animals per group). (**C**) Representative maximum intensity projections of a confocal image z-stack of 2- or 6-month old mouse hippocampus, labeled with DAPI and anti-Nestin (top) or DAPI, anti-Doublecortin (DCX), and anti-Mcm2 (bottom). Scale bar, 100μm. (**D**) Quantification of Nestin+ radial NSCs (top), DCX+/MCM2+ proliferating neuroblasts (middle) and DCX+/MCM2- immature neurons (bottom) in 2- or 6-month old mice (n=4-5 animals per group). (**E**) Representative maximum intensity projections of a confocal image z-stack of 2- or 6-month old mouse hippocampus, labeled with anti-GFAP and anti-BrdU. Mice were given 6 daily i.p. injections of BrdU (50mg/kg) 30 days before euthanasia. Quantification of the percentage of GFAP+/BrdU+ astrocytes out of total BrdU+ cells in the subgranulzar zone (SGZ) of the dentate gyrus (n=4-5 animals per group; scale bar, 10μm; white dashed line, SGZ). (**F**) Representative maximum intensity projections of a confocal image z-stack of 2- or 6-month old mouse hippocampus, labeled with anti-s100ß and anti-BrdU (left). Mice were treated as in *(E)*. Quantification of the percentage of s100ß+/BrdU+ astrocytes out of total BrdU+ cells in the SGZ of the dentate gyrus (n=4-5 animals per group; scale bar, 10μm; white dashed line SGZ). Data are represented as mean ± SEM; **p<0.01, ***p<0.001, ****p<0.0001; t test.

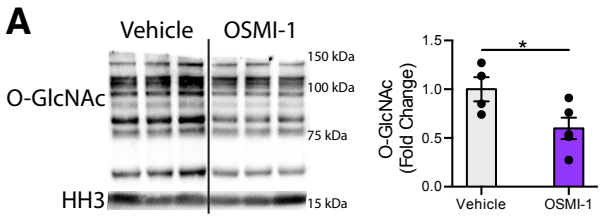

Figure 1.2. Pharmacological inhibition of Ogt by OSMI-1 treatment reduces O-GlcNAc levels in NSCs *in vitro.*

(**A**) O-GlcNAc levels were assessed by Western blot in primary hippocampal neural stem cells following 24-hour vehicle or OSMI-1 treatment. Data are represented as mean ± SEM; *p<0.05; t test; n=4-5 per group.

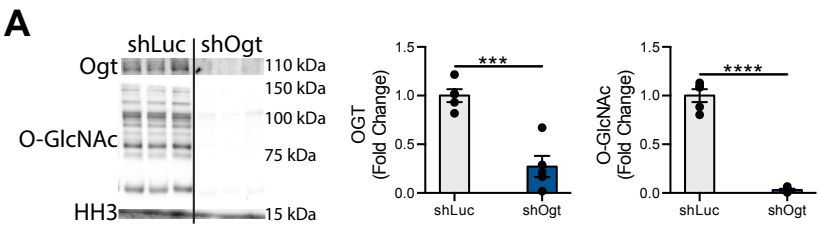

Figure 1.3. Abrogation of Ogt reduces O-GlcNAc levels in NSCs *in vitro*
(**A**) O-GlcNAc and Ogt levels were assessed by Western blot in primary hippocampal neural stem cells following infection with shLuc or shOgt. Data are represented as mean ± SEM; *p<0.05; t test; n=4-5 per group.

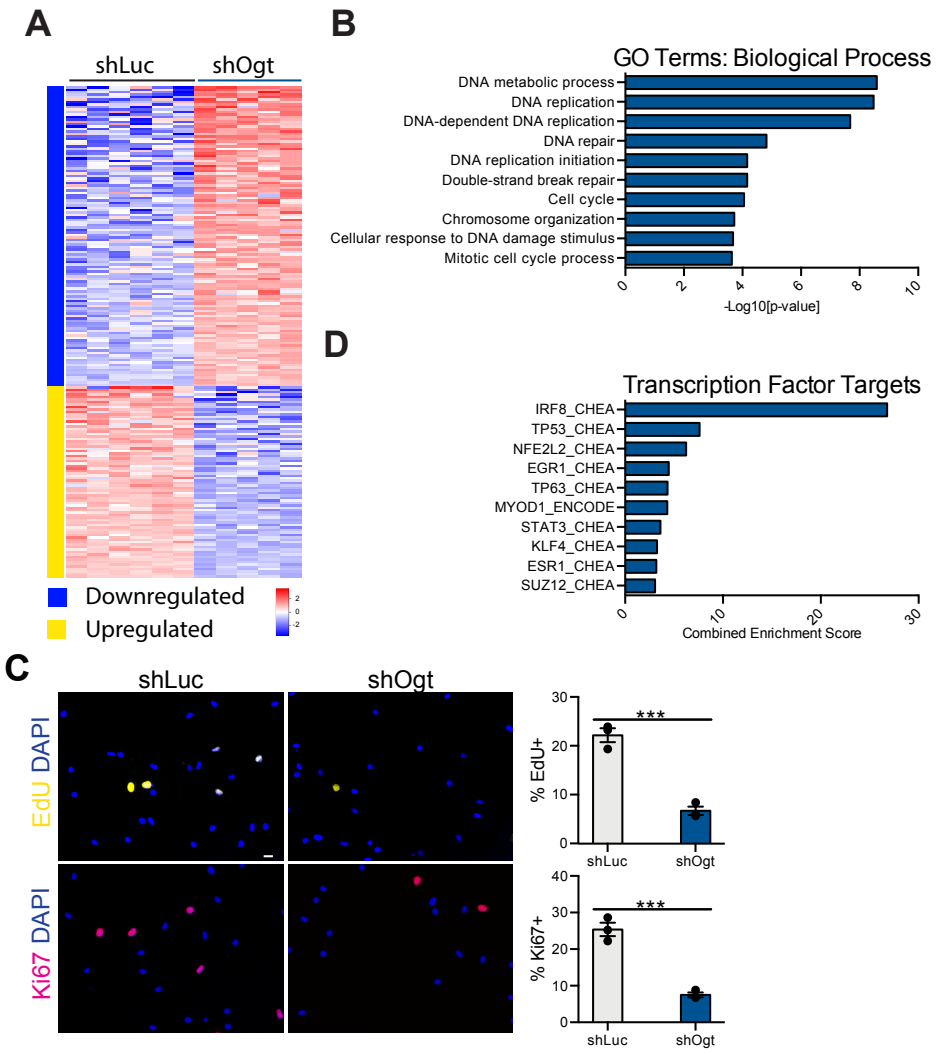

Figure 1.4. Abrogation of Ogt impairs NSC proliferation *in vitro*.
(**A**) Heatmap of significantly differentially expressed genes with fold change>2 and p<0.05 in primary hippocampal neural stem cells (NSCs) following 72-hour shOgt infection compared to vehicle shLuc control *in vitro*. (**B**) Biological Process Gene Ontology terms associated with genes downregulated following shOgt infection. (**C**) Representative field and quantification of primary mouse hippocampal NSCs following 72 hours of shLuc (left) or shOgt (right) treatment, labeled with DAPI and an 8-hour EdU-pulse (top), or DAPI and anti-Ki67 (bottom) (n=3 per group; scale bar, 10μm). (**D**) Quantification of enriched transcription factor targets as identified by ChEA or ENCODE based on upregulated genes after shOgt treatment compared to shLuc control. Data are represented as mean ± SEM; ***p<0.001; t test; n=3 per group. Scale bar, 10μm.

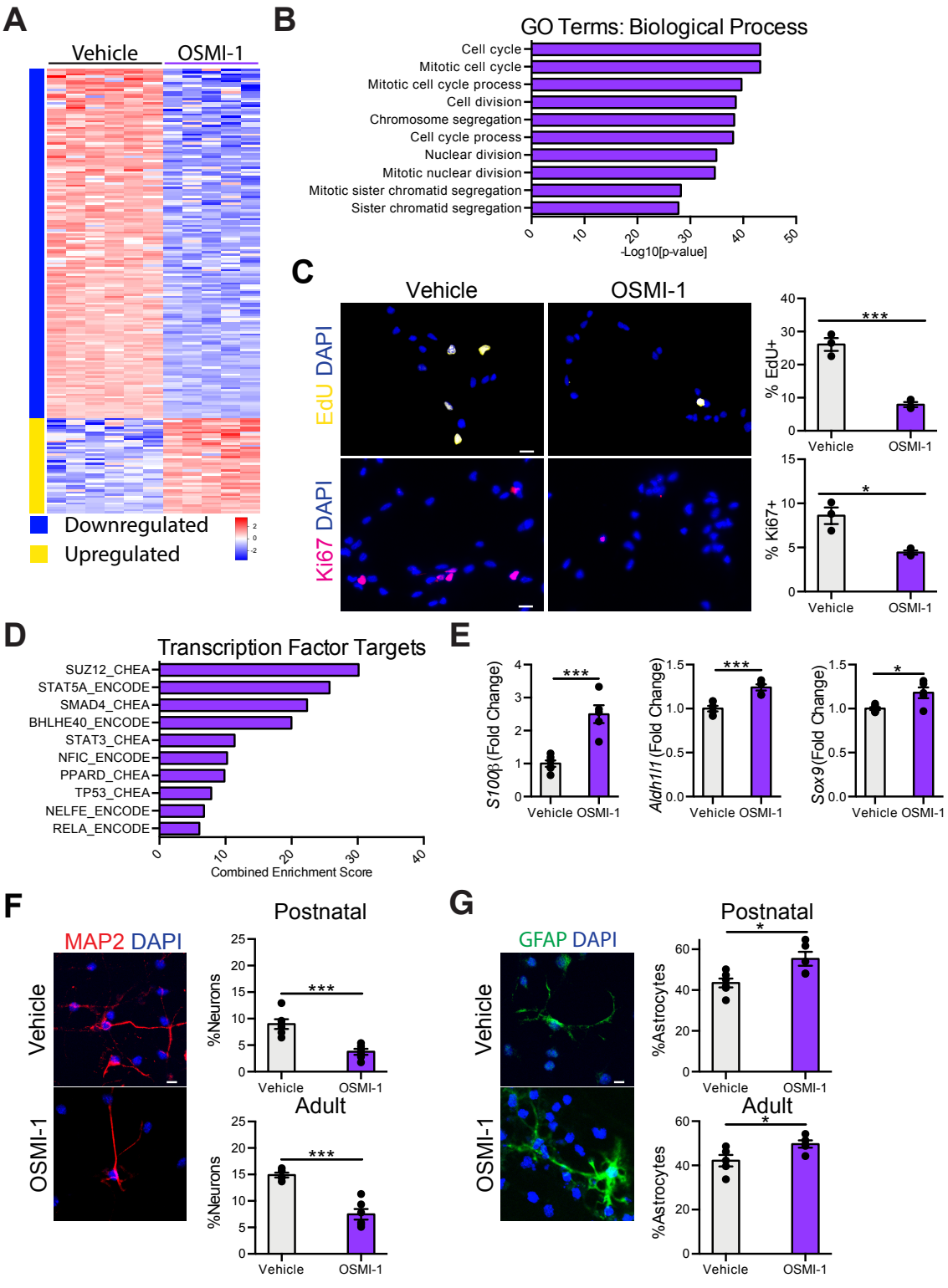
A
Vehicle
OSMI-1
Downregulated
Upregulated
B
GO Terms: Biological Process
Cell cycle
Mitotic cell cycle
Mitotic cell cycle process
Cell division
Chromosome segregation
Cell cycle process
Nuclear division
Mitotic nuclear division
Mitotic sister chromatid segregation
Sister chromatid segregation
-Log10[p-value]
C
Vehicle
OSMI-1
EdU DAPI
Ki67 DAPI
% EdU+
% Ki67+
D
Transcription Factor Targets
SUZ12_CHEA
STAT5A_ENCODE
SMAD4_CHEA
BHLHE40_ENCODE
STAT3_CHEA
NFIC_ENCODE
PPARD_CHEA
TP53_CHEA
NELFE_ENCODE
RELA_ENCODE
Combined Enrichment Score
E
S100β (Fold Change)
Aldh1l1 (Fold Change)
Sox9 (Fold Change)
F
MAP2 DAPI
Postnatal
Adult
%Neurons
G
GFAP DAPI
%Astrocytes

Figure 1.5. Decreased NSC O-GlcNAcylation promotes a neuron to glia fate switch *in vitro*. (**A**) Heatmap of significantly differentially expressed genes with fold change>2 and p<0.05 in primary hippocampal neural stem cells (NSCs) following 24-hour 12.5μM OSMI-1 treatment compared to vehicle control *in vitro*. (**B**) Biological Process Gene Ontology terms associated with genes downregulated following OSMI-1 treatment. (**C**) Representative field and quantification of primary mouse hippocampal NSCs following 24 hours of vehicle (left) or OSMI (right) treatment, labeled with DAPI and an 8-hour EdU-pulse (top), or DAPI and anti-Ki67 (bottom) (n=3 per group; scale bar, 10μm). (**D**) Quantification of enriched transcription factor targets as identified by ChEA or ENCODE based on upregulated genes after 24-hour OSMI-1 treatment compared to vehicle control. (**E**) Fold change expression (FPKM) of astrocyte-associated genes: *S100ß*, *Aldh1l1*, and *Sox9* in primary hippocampal NSCs following OSMI-1 treatment *in vitro* (n=5-6 per group). (**F**) Differentiation was induced in vehicle or OSMI-1 treated primary postnatal (P1) and adult (2-month-old) hippocampal NSCs by withdrawing growth factors 7 days prior to fixation. Cells were labeled with DAPI and anti-MAP2. MAP2+ neurons were quantified as a percentage of total DAPI+ cells (n=6 replicates per group; scale bar, 10μm). (**G**) Primary postnatal and adult hippocampal NSCs were treated as in *(F)*. Cells were labeled with DAPI and anti-GFAP. GFAP+ astrocytes were quantified as a percentage of total DAPI+ cells (n=6 per group; scale bar, 10μm). Data are represented as mean ± SEM; *p<0.05, ***p<0.001; t test.

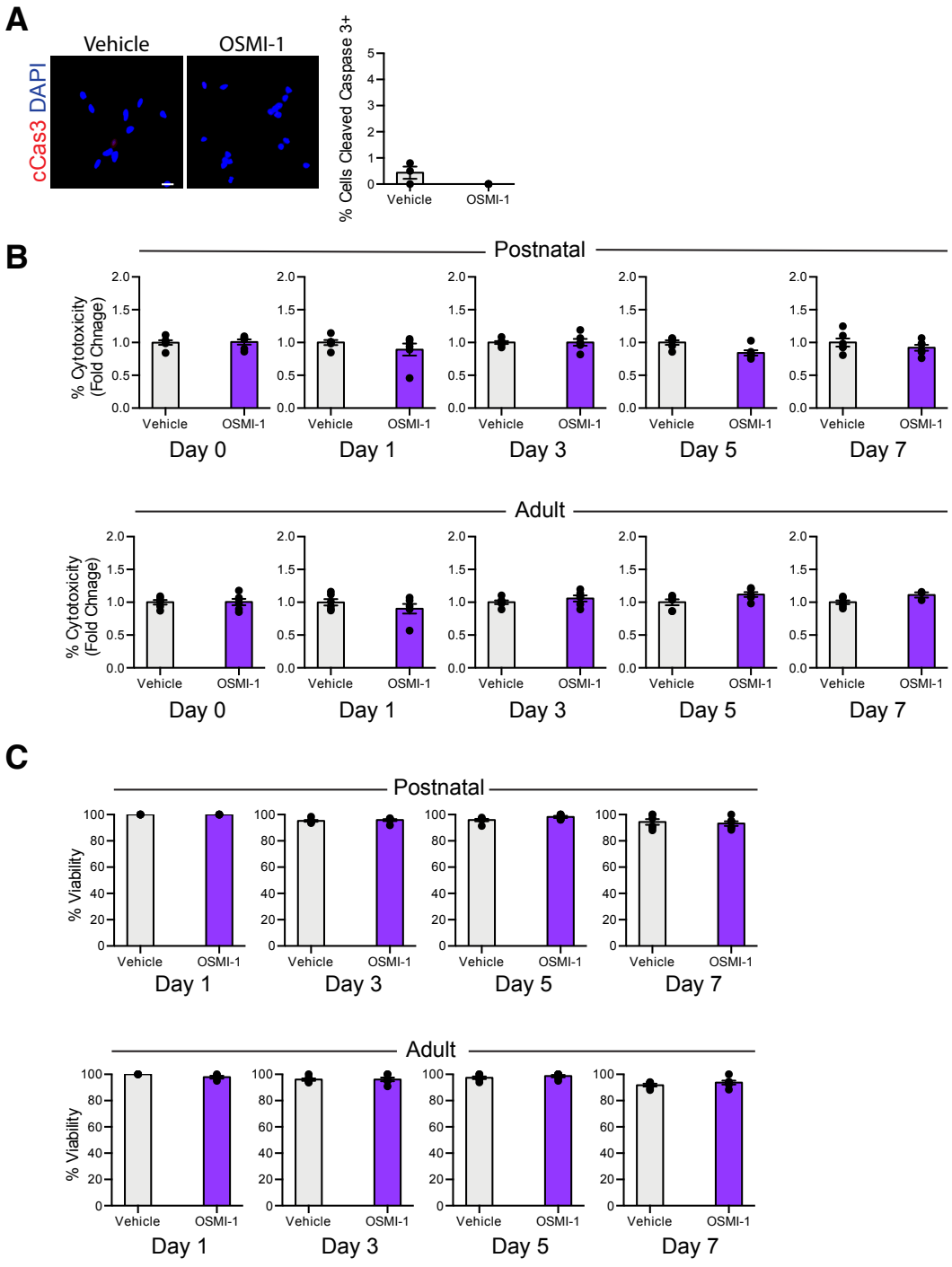
A
Vehicle
OSMI-1
cCas3 DAPI
% Cells Cleaved Caspase 3+
Vehicle
OSMI-1
B
Postnatal
% Cytotoxicity (Fold Chnage)
Day 0
Day 1
Day 3
Day 5
Day 7
Adult
C
Postnatal
% Viability
Day 1
Day 3
Day 5
Day 7
Adult

Figure 1.6. Pharmacological inhibition of Ogt by OSMI-1 treatment does not increase NSC cell death or cytotoxicity.
(**A**) Primary hippocampal neural stem cells (NSCs) were treated with OSMI-1 or vehicle for 24 hours. Cell death was assessed by immunostaining for Cleaved Caspase 3 (n=3 per group; scale bar, 10μm). (**B**) Primary postnatal and adult hippocampal NSCs were treated with OSMI-1 or vehicle and differentiation was induced by withdrawing growth factors. Cytotoxicity was assessed by lactate dehydrogenase activity at 0, 1, 3, 5, and 7 days post growth factor withdrawal (n=6 replicates per group). (**C**) Primary postnatal and adult hippocampal NSCs were treated with OSMI-1 or vehicle and differentiation was induced by withdrawing growth factors. Cell viability was assessed by trypan blue exclusion at 1, 3, 5, and 7 days post growth factor withdrawal (n=6 replicates per group). Data are represented as mean ± SEM; ns; t test.

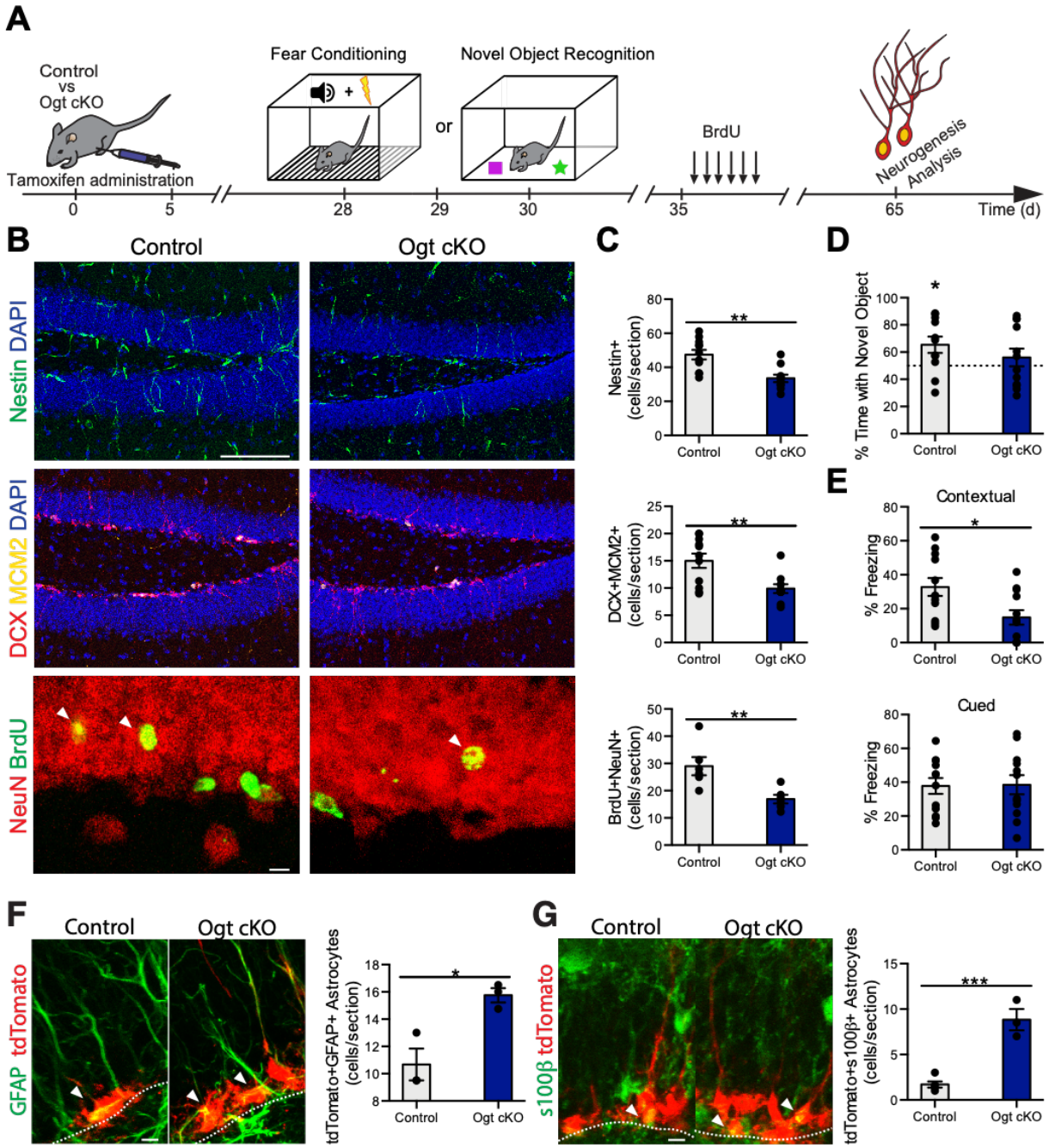
A
Control
vs
Ogt cKO
Tamoxifen administration
Fear Conditioning
or
Novel Object Recognition
BrdU
Neurogenesis
Analysis
0
5
28
29
30
35
65
Time (d)
B
Control
Ogt cKO
Nestin DAPI
DCX MCM2 DAPI
NeuN BrdU
C
Nestin+
(cells/section)
DCX+MCM2+
(cells/section)
BrdU+NeuN+
(cells/section)
Control
Ogt cKO
D
% Time with Novel Object
E
Contextual
Cued
% Freezing
F
GFAP tdTomato
tdTomato+GFAP+ Astrocytes
(cells/section)
G
s100β tdTomato
tdTomato+s100β+ Astrocytes
(cells/section)

Figure 1.7. Decreased NSC O-GlcNAcylation impairs adult neurogenesis and cognitive function while increasing gliogenesis in the young hippocampus.
(**A**) Schematic of experimental paradigm and cognitive testing timeline. 3-month old *Ogt*$^{flox/y}$ (control) or *NestinCre-ERT*$^{2+/-}$*; Ogt*$^{flox/y}$ (Ogt cKO) littermate mice were administered 5 daily i.p. tamoxifen injections (75mg/kg). One month later, hippocampal-dependent learning and memory were assessed by novel object recognition (NOR) or contextual fear-conditioning paradigms. One week after behavioral assays, mice were administered 6 daily i.p. injections of BrdU (50mg/kg). 30 days later mice were euthanized, and tissue was analyzed. (**B**) Representative maximum intensity projections of a confocal image z-stack of control or Ogt cKO hippocampus, labeled with DAPI and anti-Nestin (top) or DAPI, anti-Doublecortin (DCX), and anti-Mcm2 (middle), or anti-NeuN and anti BrdU (bottom) (scale bar, 100μm or 10 μm). (**C**) Quantification of Nestin+ radial NSCs (top), DCX+/MCM2+ proliferating neuroblasts (middle) and NeuN+/BrdU+ newborn mature neurons (bottom) in control or Ogt cKO littermate mice (n=10–11 animals per group). (**D**) Object recognition memory was assessed in control and Ogt cKO littermate mice using the novel object recognition task. Quantification of percentage of time spent with the novel object is shown. (n=11-12 per group). (**E**) Associative fear memory was assessed in Ogt cKO and control littermate mice using contextual fear conditioning. Quantification of percentage freezing in response to cue or context 24 hours after training is shown (n=12 per group). (**F**) 3-month old *NestinCre-ERT*$^{2+/-}$*; Ai14*$^{flox/wt}$ (control) or *NestinCre-ERT*^{2}*; Ai14*$^{flox/wt}$*; Ogt*$^{flox/y}$ (Ogt cKO) littermate mice were administered 5 daily i.p. tamoxifen injections (75mg/kg). One month later, mice were euthanized, and tissue was analyzed. Representative maximum intensity projections of a confocal image z-stack of control or Ogt cKO hippocampus, labeled with endogenous TdTomato and anti-GFAP. Quantification of TdTomato+/GFAP+ astrocytes (n=3-5 per group; scale bar, 10μm; white dashed line, SGZ). (**G**) Mice were treated as in *(F)*. Representative maximum intensity projections of a confocal image z-stack of control or Ogt cKO hippocampus, labeled with endogenous TdTomato and anti-s100ß. Quantification of TdTomato+/s100ß + astrocytes (n=3-5 per group; scale bar, 10μm; white dashed line, SGZ). Data are represented as mean ± SEM; *p<0.05, **p<0.01, ***p<0.001; t test (**C**,**E**-**G**); One-sample *t* test versus 50% (**D**).

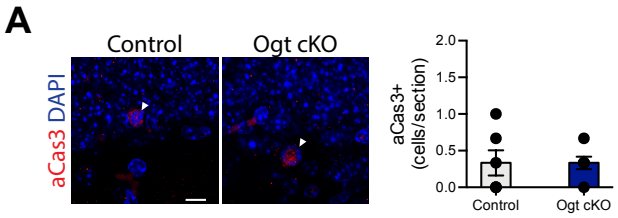

Figure 1.8. Abrogation of Ogt does not induce cell death *in vivo*.
(**A**) Representative maximum intensity projections of a confocal image z-stack of control or Ogt cKO hippocampus, labeled with DAPI and anti-cleaved caspase 3 (left). Quantification of cleaved caspase-3-positive cells in control or Ogt cKO littermate mice (n=3 per group). Data are represented as mean ± SEM; ns; t test. Scale bar, 10μm.

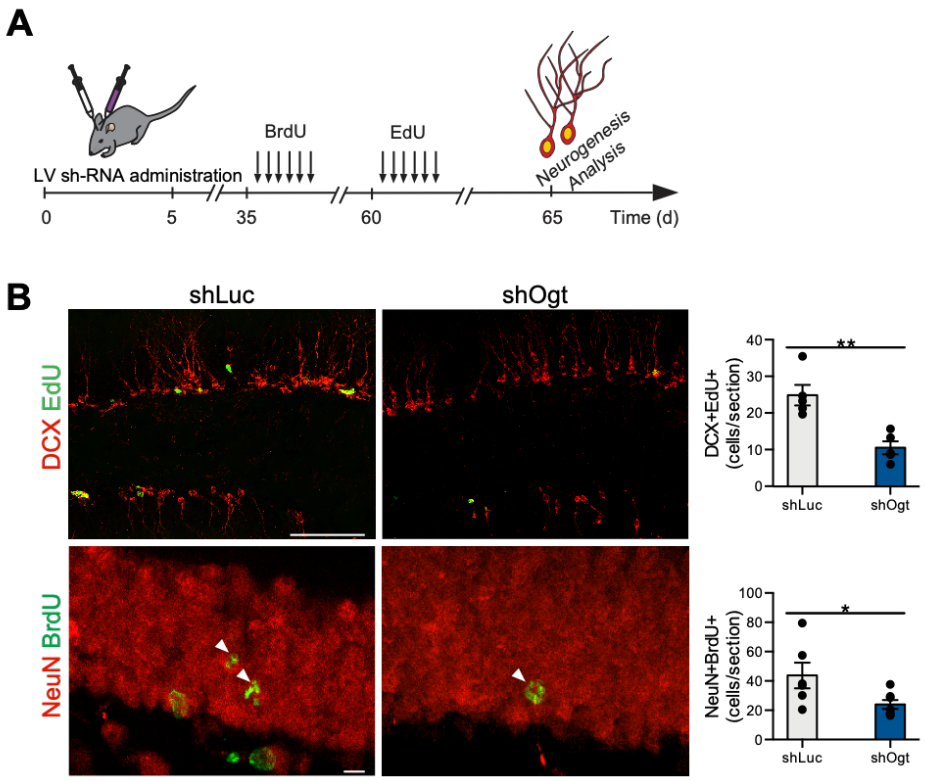

Figure 1.9. Abrogation of Ogt impairs hippocampal neurogenesis *in vivo*.
(**A**) Schematic of experimental paradigm. 3-month old mice were stereotaxically injected with lentivirus encoding shLuc or shOgt into the dentate gryrus of contralateral hippocampi. One month later, mice were given 6 daily i.p. injections of BrdU (50mg/kg). One month later, mice were given 6 daily i.p. injections of EdU (50mg/kg). 24 hours after the final EdU injection, mice were sacrified. (**B**) Representative maximum intensity projections of a confocal image z-stack of shLuc or shOgt hippocampus, labeled with anti-Doublecortin (DCX) and EdU (top) or or anti-NeuN and anti BrdU (bottom). Quantification of DCX+/EdU+ neuroblasts and NeuN+/BrdU+ newborn mature neurons (n=5-6 per group). Data are represented as mean ± SEM; *p<0.05, **p<0.01; t test; scale bar, 100μm (top) 10μm (bottom).

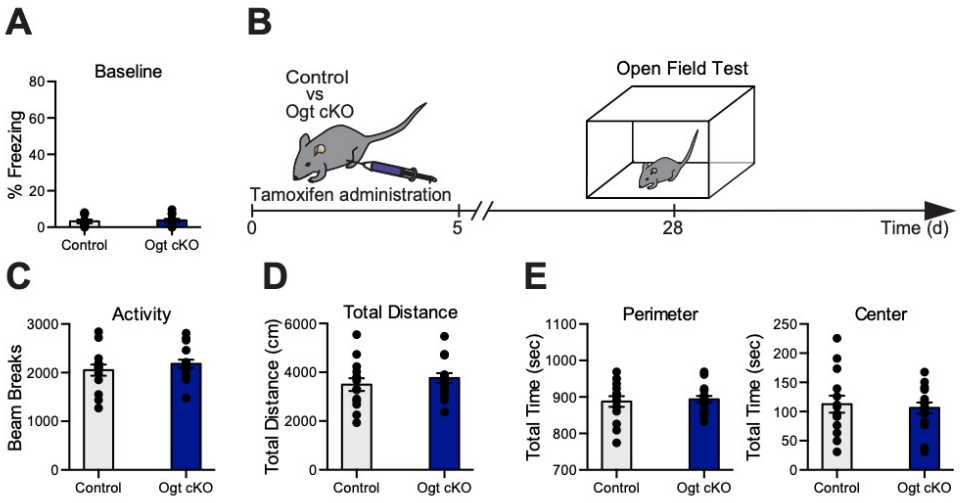

Figure 1.10. Loss of adult NSC Ogt does not affect motor function or anxiety.
(**A**) Baseline freezing was evaluated prior to training stimulus in the fear conditioning paradigm. (**B**) Schematic of cognitive testing timeline. 3-month old *Ogt*$^{flox/y}$ (control) or *NestinCre-ERT*$^{2+/-}$*; Ogt*$^{flox/y}$ (Ogt cKO) littermate mice were administered 5 daily i.p. tamoxifen injections (75mg/kg). One month later, anxiety and motor function were assessed by the open field test (OFT). (**C**) Quantification of activity as number of beam breaks during OFT. (**D**) Quanitifcation of total distance traveled during OFT. (**E**) Quantification of time spent in the perimeter and center of the chamber during OFT. Data are represented as mean ± SEM; ns; t test; n=12-16 per group.

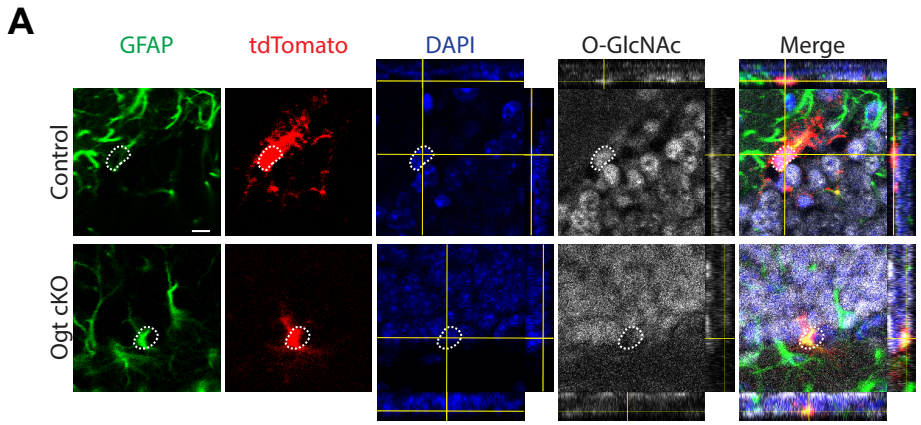

Figure 1.11. NSC-specific ablation of Ogt reduces astrocyte O-GlcNAc levels *in vivo*. (**A**) Representative single z-plane images and corresponding orthogonal views of tdTomato+ astrocytes in the DG of Ogt cKO mice and littermate controls labeled with anti-GFAP, anti-O-GlcNAc and DAPI. Scale bar, 10μm.

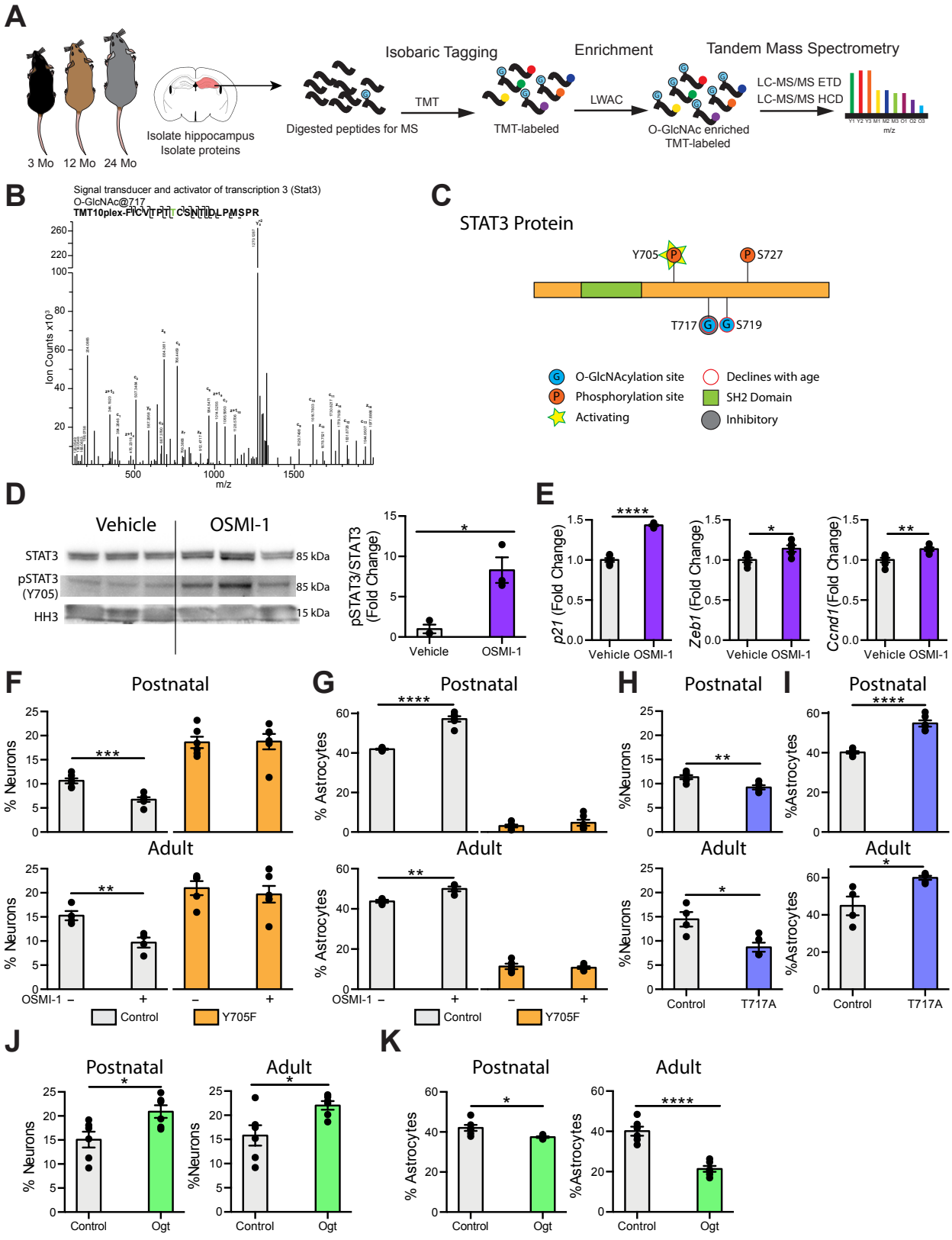
A
3 Mo
12 Mo
24 Mo
Isolate hippocampus
Isolate proteins
Digested peptides for MS
Isobaric Tagging
TMT
TMT-labeled
Enrichment
LWAC
O-GlcNAc enriched
TMT-labeled
Tandem Mass Spectrometry
LC-MS/MS ETD
LC-MS/MS HCD
B
Signal transducer and activator of transcription 3 (Stat3)
O-GlcNAc@717
TMT10plex-FICVTPTCSNTIDLPMSPR
Ion Counts x10³
m/z
C
STAT3 Protein
Y705
S727
T717
S719
O-GlcNAcylation site
Phosphorylation site
Activating
Declines with age
SH2 Domain
Inhibitory
D
Vehicle
OSMI-1
STAT3
pSTAT3 (Y705)
HH3
85 kDa
85 kDa
15 kDa
pSTAT3/STAT3 (Fold Change)
Vehicle
OSMI-1
E
p21 (Fold Change)
Zeb1 (Fold Change)
Ccnd1 (Fold Change)
Vehicle OSMI-1
F
Postnatal
Adult
% Neurons
OSMI-1
Control
Y705F
G
Postnatal
Adult
% Astrocytes
OSMI-1
Control
Y705F
H
Postnatal
Adult
%Neurons
Control
T717A
I
Postnatal
Adult
%Astrocytes
Control
T717A
J
Postnatal
Adult
% Neurons
%Neurons
Control
Ogt
K
Postnatal
Adult
% Astrocytes
%Astrocytes
Control
Ogt

Figure 1.12. STAT3 O-GlcNAcylation at T717 is reduced in the aging hippocampus and mimicking this decline in NSC promotes a gliogenic fate switch.
(A) Schematic of proteomic workflow. The hippocampus was isolated from 3-, 12-, or 24-month old mice. Hippocampi were pooled to obtain sufficient protein (n=5 animals per pool). Proteins were isolated from tissue and digested with trypsin before undergoing isobaric tagging. Tagged peptides were enriched for O-GlcNAcylation with lectin weak affinity chromatography (LWAC) and analyzed via electron transfer dissociation mass spectrometry (ETD-MS). (**B**) Representative spectra of hippocampal STAT3 O-GlcNAcylation at T717. (**C**) Diagram of O-GlcNAc sites detected by mass spectrometry in *(A)* (T717, S719), and previously identified phosphorylation sites (Y705, S727) on STAT3. (**D**) STAT3 phosphorylation at Y705 and STAT3 expression in primary hippocampal neural stem cells (NSCs) following 24-hour vehicle or OSMI-1 treatment (n=3 per group). (**E**) Expression of STAT3 target genes in primary hippocampal NSCs treated as in *(D)* was evaluated using RNAseq. (**F**) Primary hippocampal postnatal and adult NSCs were infected with a lentiviral construct expressing a non-phosphorylatable STAT3 (Y705F) or wildtype STAT3 (Control). Differentiation was induced in vehicle or OSMI-1 treated NSCs by withdrawing growth factors 7 days prior to fixation. Cells were labeled with DAPI and anti-MAP2. MAP2+ neurons were quantified as a percentage of total DAPI+ cells (n=6 replicates per group). (**G**) Primary postnatal and adult hippocampal NSCs were infected, treated, and differentiated as in *(F)*. Cells were labeled with DAPI and anti-GFAP. GFAP+ astrocytes were quantified as a percentage of total DAPI+ cells (n=6 replicates per group). (**H**) Primary postnatal and adult hippocampal NSCs were infected with a lentiviral construct expressing an O-GlcNAcylation-deficient STAT3 (T717A) or wildtype STAT3 (Control). Differentiation was induced by withdrawing growth factors 7 days prior to fixation. Cells were labeled with DAPI and anti-MAP2. MAP2+ neurons were quantified as a percentage of total DAPI+ cells (n=6 replicates per group). (**I**) Primary postnatal and adult hippocampal NSCs were infected, treated, and differentiated as in *(H)*. Cells were labeled with DAPI and anti-GFAP. GFAP+ astrocytes were quantified as a percentage of total DAPI+ cells (n=6 replicates per group). (**J**) Primary postnatal and adult hippocampal NSCs were infected with a lentiviral construct expressing Ogt or GFP under the Nestin promoter. Differentiation was by induced withdrawing growth factors 7 days prior to fixation. Cells were labeled with DAPI and anti-MAP2. MAP2+ neurons were quantified as a percentage of total DAPI+ cells (n=6 replicates per group). (**K**) Primary postnatal and adult hippocampal NSCs were infected, treated, and differentiated as in *(J)*. Cells were labeled with DAPI and anti-GFAP. GFAP+ astrocytes were quantified as a percentage of total DAPI+ cells (n=6 replicates per group). Data are represented as mean ± SEM; *p<0.05, **p<0.01, ***p<0.001, ****p<0.0001; t test.

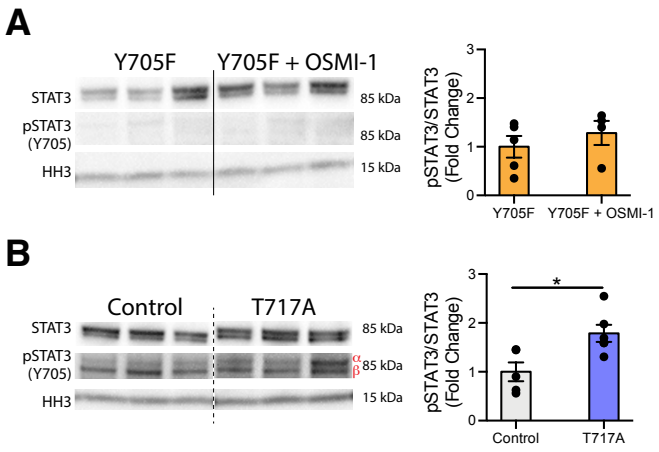

Figure 1.13. Lentiviral-mediated expression of STAT3 point mutants alters STAT3 phosphorylation in NSCs.
(**A**) Primary hippocampal neural stem cells (NSCs) were infected with a lentiviral construct expressing a non-phosphorylatable STAT3 (Y705F). 3 days after infection, NSCs were treated with OSMI-1 or a vehicle control for 24 hours. STAT3 phosphorylation at Y705 and STAT3 expression were quantified following treatment (n=4-5 per group) (**B**) Primary hippocampal NSCs were infected with a lentiviral construct expressing an O-GlcNAcylation-deficient STAT3 (T717A) or wildtype STAT3 (Control). 3 days after infection, phosphorylation of the STAT3 a isoform at Y705 and STAT3 expression were quantified following treatment (n=4-5 per group). Data are represented as mean ± SEM; *p<0.05; t test.

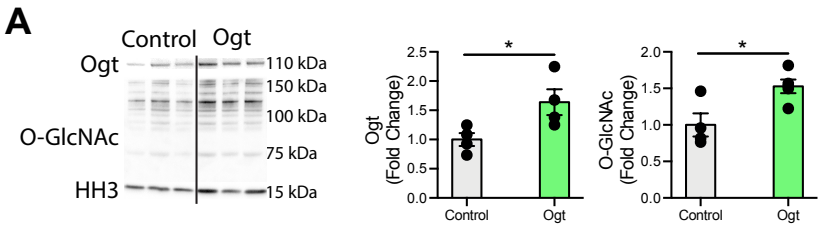

Figure 1.14. Lentiviral-mediated overexpression of Ogt increases O-GlcNAc levels in NSCs *in vitro*.
(**A**) O-GlcNAc and Ogt levels were assessed by Western blot in primary hippocampal neural stem cells following infection with a lentiviral construct overexpressing GFP or Ogt. Data are represented as mean ± SEM; *p<0.05; t test; n=4-5 per group.

CHAPTER 2:

Mitochondrial Ogt Increases with Age in The Hippocampus and Contributes to Regenerative Decline

Charles W. White III[1,2], Gregor Bieri[1], and Saul A. Villeda[1,2,3,4,#]

7. Department of Anatomy, University of California San Francisco, San Francisco, California 94143, USA
8. Developmental and Stem Cell Biology Graduate Program, University of California San Francisco, San Francisco, California 94143, USA
9. Department of Physical Therapy and Rehabilitation Science, University of California San Francisco, San Francisco, California 94143, USA
10. The Eli and Edythe Broad Center for Regeneration Medicine and Stem Cell Research, San Francisco, California 94143, USA

AUTHOR CONTRIBUTIONS

C.W.W. and S.A.V. developed concept and designed experiments. C.W.W. collected and analyzed data. C.W.W performed all experiments. G.B. generated and validated viral constructs. C.W.W and S.A.V wrote the manuscript. S.A.V supervised all aspects of this project. All authors had the opportunity to discuss results and comment on manuscript.

ABSTRACT

Mitochondrial function plays a key role in diverse biological processes including aging and stem cell regulation. Mitochondrial health has been shown to decline with age, and drive phenotypes associated with aging and neurodegenerative disease in the brain, including loss of neurogenesis and depletion of the neural stem cell (NSC) pool. While the role of mitochondria is clear, the molecular processes underlying this age-associated functional decline remain to be elucidated. We have previously implicated the post-translational modification O-linked N-Acetylglucosamine (O-GlcNAc) in age-related cognitive and regenerative decline. Interestingly, the enzyme which catalyzes the addition of this modification, O-GlcNAc transferase has a mitochondrial-specific isoform (mOGT) which is relatively unexplored. Here we report that mOGT levels increase with age in the hippocampus. Moreover, using lentiviral approaches, we demonstrate that altering mOGT expression in NSCs is sufficient to promote self-renewal and neuronal differentiation programs. Our data suggest that age-related changes in mOGT contribute to the age-related loss of neurogenesis and position mitochondrial O-GlcNAcylation as an important regulator of mitochondrial function in the brain.

INTRODUCTION

The hippocampus is an important brain region, responsible for higher order cognitive processes that include learning, memory (1, 2) and mood regulation (3). These cognitive functions are regulated in part by adult hippocampal neurogenesis (3–5), the process by which neural stem cells (NSCs) self-renew and differentiate into new neurons in the adult brain. With age, however, there is a significant decline in the regenerative capacity of the adult mammalian hippocampus. While the persistence of adult hippocampal neurogenesis in humans remains controversial (6), a precipitous decline in NSC number with age has been described in both mice and humans (7–11). Moreover, recent studies observe adult hippocampal neurogenesis throughout human life, and note a correlation between neurogenesis and disease severity in Alzheimer's disease patients (12, 13). It is clear that NSCs are an essential source of regenerative capacity in the aging brain, however the mechanisms underlying age-related decline in the NSC pool remain to be fully elucidated.

Changes in the dynamic post-translational modification, O-linked N-Acetylglucosamine (O-GlcNAc), are becoming increasingly appreciated as regulators of brain aging and NSC function. Notably, O-GlcNAc and the enzymes that catalyze its addition and removal, O-GlcNAc transferase (Ogt) and O-GlcNAcase (Oga) have been implicated in aging (14–16), neurodegenerative disease (14, 17–19), and lifespan extension (20, 21). In the brain, we have identified age-related decreases in hippocampal O-GlcNAc and Ogt levels, and demonstrated their role in driving age-related neuronal dysfunction and cognitive decline (16). In NSCs specifically, we have also reported an age-related decline in O-GlcNAc levels and established the role of O-GlcNAc in regulating adult hippocampal NSC function via modulation of STAT3 signaling (22). Notwithstanding, work from our lab and others relies primarily on broad manipulations of O-GlcNAc levels, often without addressing the contribution of specific Ogt isoforms. In mice, 3 distinct Ogt isoforms have been identified (23): a full-length isoform (ncOGT), as well as a shorter (sOGT), and mitochondrial-localized (mOGT) isoform (24). Previous work has focused mainly on

the role of ncOGT, while relatively little is known about sOGT and mOGT. Interestingly, while increased O-GlcNAcylation of mitochondrial proteins has been associated with impaired mitochondrial health (25, 26), reducing mOGT levels has been shown to promote oxidative phosphorylation and cell survival *in vitro* (27). The role of mOGT in regulating NSC function, however, has yet to be explored.

Mitochondrial function has recently been established as a major regulator of neuronal differentiation. Across several species, including mouse, NSCs have been shown to rely primarily on anaerobic glycolysis for energy production, but increasingly rely on mitochondrial oxidative phosphorylation during neuronal differentiation (28–31), ultimately becoming highly dependent on oxidative phosphorylation as mature neurons (32).This metabolic switch is necessary for NSC function, as NSCs with dysfunctional mitochondria exhibit impaired neuronal differentiation and self-renewal capacity, as well as a bias towards gliogenesis (33–35) previously associated with aged NSCs (22, 36, 37). Physiologically, an age-related decline in mitochondrial health has been reported in a multitude of tissues, including the brain (38), and the pharmacological enhancement of mitochondrial function has been shown to ameliorate the age-related decline in mammalian hippocampal neurogenesis (39). Given the demonstrated importance of mitochondrial metabolism in regulating adult NSC function, it is crucial to understand how this process is regulated.

Here we identify an age-related increase in hippocampal mOGT concurrent with the decline in adult hippocampal neurogenesis. Functionally, we utilize a lentiviral approach to demonstrate the role of mOGT in regulating metabolic and NSC function. Finally, we demonstrate that mitigating the age-related increase in mOGT is sufficient to increase NSC number and enhance neurogenesis *in vivo*.

RESULTS

Mitochondrial Ogt increases with age *in vivo* and promotes aberrant neuronal differentiation *in vitro.*

We, and others, have previously demonstrated that a precipitous decline in NSC number occurs in the dentate gyrus between young adult (2-3 months) and mature (6 months) mice (9, 22, 40). Given the involvement of O-GlcNAcylation in both age-related changes and stem cell function, we assessed how the levels of mitochondrial Ogt (mOGT) change during this same period. Using quantitative PCR (qPCR) analysis, we observed a significant increase in mOGT transcript levels in the hippocampus between 3 and 6 months of age (**Figure 2.1A**), suggesting an increase in mitochondrial O-GlcNAcylation.

To gain insight into how elevated mitochondrial O-GlcNAcylation might affect NSC function, we first generated a lentiviral construct overexpressing either mOGT (mOGT-OE) or a control (GFP-OE) under the ubiquitously expressed CMV promoter. To validate that the recombinant mOGT was localizing to the mitochondria, we created a GFP-tagged version ($mOGT^{GFP}$-OE) and evaluated its localization via immunohistochemistry in HEK 293T cells (**Figure 2.1B**). We observed colocalization with mitochondria, indicating proper localization of the recombinant mOGT. Next, we validated the expression of the mOGT-OE construct in primary hippocampal NSCs using qPCR and observed a significant increase in mOGT transcript levels following infection (**Figure 2.1C**), indicating successful overexpression of mOGT**.** Given previous reports suggesting a role of mitochondrial O-GlcNAcylation in regulating mitochondrial function, we assessed ATP production in treated NSCs. We found no differences in baseline ATP production (**Figure 2.1D**), however, after treatment with Oligomycin, a potent inhibitor of oxidative phosphorylation, we observed significantly reduced ATP content in mOGT-OE compared to control cells (**Figure 2.1E**). These data suggest an aberrant increased reliance on oxidative phosphorylation following mOGT overexpression, indicative of a more neuronally differentiated phenotype. Given these observations, we next assessed whether increased levels of mOGT

affected the self-renewal capacity of NSCs. We evaluated neurosphere formation under self-renewal conditions and observed a significant decrease in neurosphere number in NSCs overexpressing mOGT (**Figure 2.1F**), indicating impaired self-renewal. Next, we examined whether increasing mOGT levels altered NSC differentiation *in vitro*. We treated primary NSCs with the lentiviral constructs and cultured under differentiation conditions for 7 days. We evaluated neuronal differentiation by immunohistochemistry and observed a significant increase in the number of MAP2+ neurons formed by mOGT overexpressing cells (**Figure 2.1G**). Taken together, these data suggest an increase in oxidative phosphorylation and neuronal differentiation at the expense of self-renewal in NSCs with elevated mOGT.

Reducing mOGT levels decreases neuronal differentiation and enhances NSC self-renewal *in vitro*.

To investigate the effects of mitigating the age-related increase in mOGT levels, we generated a lentiviral construct encoding a short hairpin RNA (shRNA) targeted toward either mOGT (sh-mOGT) or a scrambled (sh-Scramble) control. We confirmed that expression of this shRNA transcript was sufficient to significantly reduce mOGT levels in NSCs *in vitro* (**Figure 2.2A**). Next, we wanted to understand the effects of reducing mOGT on mitochondrial function. We assessed baseline ATP levels in NSCs following infection and saw no difference (**Figure 2.2B**). We then treated the infected NSCs with Oligomycin and saw an increase in ATP levels in the sh-mOGT infected cells (**Figure 2.2C**), indicating decreased reliance on oxidative phosphorylation for ATP generation. To investigate the functional consequences of reduced mOGT expression, we first assessed self-renewal capacity following sh-mOGT infection. We observed a significant increase in neurosphere number following sh-mOGT treatment (**Figure 2.2D**), suggesting increased self-renewal. We next assessed the effects on neuronal differentiation and observed a significant decrease in neuronal differentiation following sh-mOGT expression compared to a control (**Figure**

2.2E). Taken together, these data suggest that reducing mOGT expression promotes NSC self-renewal *in vitro*.

Mitigating the age-related increase in mOGT levels is sufficient to enhance neurogenesis *in vivo*.

To understand the effects of mitigating the age-related increase in mOGT expression *in vivo*, we performed unilateral stereotaxic injections of the sh-mOGT or sh-Scramble lentiviral constructs into the dentate gyrus of contralateral hippocampi in young (3 month) mice. We aged the mice for 8 weeks and assessed short-term proliferation by a 1-week 5-Ethynyl-2´-deoxyuridine (EdU) incorporation paradigm before euthanasia. First, we examined NSC number, and saw that the dentate gyrus treated with sh-mOGT displayed an increase in Sox2+/GFAP+ NSC number, compared to the contralateral control (**Figure 2.2F**), consistent with our *in vitro* data. Additionally, sh-mOGT treated mice also had increased numbers of Doublecortin (DCX)/EdU-positive neuroblasts (**Figure 2.2G**), suggesting increased neurogenesis. Taken together, these data demonstrate that reducing mOGT levels *in vivo* is sufficient to enhance adult hippocampal neurogenesis.

DISCUSSION

Cumulatively, our data indicate that an age-related increase in hippocampal mOGT levels is sufficient to increase neuronal differentiation at the expense of self-renewal in NSCs, ultimately contributing to the depletion of the stem cell pool with age. While mitochondrial function and changes in O-GlcNAcylation have individually been implicated as regulators of aging and NSC function, the interplay between the two has not been well studied. Here, for the first time, we observe a link between these cellular processes in the context of adult hippocampal neurogenesis and demonstrate the role of O-GlcNAc as a novel regulator of NSC metabolism and neurogenesis.

Mitochondrial function has long been appreciated as a major regulator of both aging and stem cell function. The age-related decline in mitochondrial function and its resulting impact on several cell types including NSCs has been well-documented, yet the mechanisms promoting this functional decline are understudied. Our data identify O-GlcNAc as potential mediator of mitochondrial function in NSCs. While we have previously shown O-GlcNAc is a major regulator of both aging and adult hippocampal neurogenesis, others have observed changes in O-GlcNAc alongside mitochondrial dysfunction in contexts including neurodegenerative disease, diabetes, and ageing. Notwithstanding, the role of O-GlcNAc in regulating metabolic processes is poorly understood. The presence of a mitochondrial-specific OGT isoform suggests, and the present study confirms, that O-GlcNAcylation plays an active role in regulating cellular metabolism by influencing mitochondrial function.

Our work highlights the need to understand the effects of O-GlcNAc at a more specific level. For example, while this study suggests that mitochondrial O-GlcNAc increases with age and promotes neuronal differentiation, our previous work suggests that total NSC O-GlcNAc decreases with age, leading to enhanced gliogenesis. Moreover, we have explored the dynamic O-GlcNAcome of the aging brain, but due to technical limitations, have not yet explored the O-GlcNAcylated landscape of NSCs specifically. Even without this information, it is evident that O-GlcNAc plays a key regulatory role in adult hippocampal neurogenesis. Ultimately, our data position O-GlcNAc as a novel regulator of metabolic and cellular function, and set the stage for future studies, unencumbered by current technical limitations, to identify cell type- and compartment-specific O-GlcNAc modifications for therapeutic and mechanistic study.

METHOD DETAILS

Animal Models. All mouse handling and use was in accordance with institutional and ethical guidelines approved by the University of California San Francisco IACUC. All mice were C57BL/6J young mice (Jackson Laboratory). All studies were done in male mice. The numbers of mice used to result in statistically significant differences were calculated using standard power calculations with $\alpha = 0.05$ and a power of 0.8. We used an online tool (http://www.stat.uiowa.edu/~rlenth/Power/index.html) to calculate power and samples size based on experience with the respective tests, variability of the assays and inter-individual differences within groups. Mice were housed under specific pathogen-free conditions under a 12h light-dark cycle. All experiments were randomized and blinded by an independent researcher. Researchers remained blinded throughout histological, molecular, and behavioral assessments. Groups were un-blinded at the end of each experiment upon statistical analysis.

RNA Isolation and qRT-PCR. mRNA of NSCs and mRNA from hippocampal tissue was isolated by lysis with TRIzol Reagent (Thermo Fisher Scientific), separation with chloroform (0.2 mL per mL TRIzol), and precipitated with isopropyl alcohol. High Capacity cDNA Reverse Transcription Kit (Life Technologies) was used for reverse transcription of mRNA into cDNA and qRT-PCR was carried out using Power SYBR Green PCR Master Mix (Life Technologies) in a CFX384 Real Time System (Bio-Rad). Primers were: mOGT forward 5'-CCTAAGGCATGTTATTTGAAAGCA-3', mOGT Reverse 5'- TGAGTAGGACACAGACGAAGA-3', GAPDH forward 5'-GCATCCTGCACCACCAACTG-3', GAPDH reverse 5'-ACGCCACAGCTTTCCAGAGG-3'.

Viral Plasmids and Viruses. We generated overexpression lentivirus encoding a CMV promoter to drive expression of mOGT (mOGT-OE), mOGT-hrGFP fusion ($mOGT^{GFP}$-OE), or hrGFP (GFP-OE). Construct quality was tested by qPCR and sequencing. We generated

lentiviruses (LVs) encoding shRNA targeting mOGT or luciferase using a lentiviral shRNA expression system (pGreenPuro shRNA, System Biosciences) according to the manufacturer's instructions. The targeted sequences were cloned into the pGreenPuro vector (mOGT, 5′-GAGGAGTCTGGCATTACTGTT -3′; Luciferase, 5'- GCCATTCTATCCTCTAGAGGA -3'). Plasmid quality was tested by sequencing. In addition, Preparation of non-replicative lentiviral particles was performed using the UCSF Viracore, and titered to $1.0x10^9$ viral particles/ml.

Analysis of Colocalization in HEK 293T Cells. HEK 293T grown on coverslips were transfected with $mOGT^{GFP}$-OE or GFP-OE constructs using Lipofectamine 3000 (Thermo Fisher) according to manufacturer instructions. 48 hours after transfection, cells were treated with MitoTracker (Thermo Fisher) according to manufacturer protocol. 1 hour later, cells were washed with PBS and fixed with 4% PFA. Cells were mounted using ProLong Gold Antifade Reagent with DAPI (Thermo Fisher) and imaged using a Zeiss LSM 800 with a 100x objective.

Isolation of Primary Neural Stem Cells from the Postnatal Mouse Hippocampus. Primary neural stem cell isolation and culture were preformed following previously published techniques (41). Hippocampi were dissected from male postnatal day 1 (P1) Wildtype C57/BL6 mice and pooled for NSC isolation. After removing superficial blood vessels, hippocampi were mechanically dissociated by fine mincing and enzymatically digested for 30 minutes at 37ºC in DMEM media containing 2.5U/ml Papain (Worthington Biochemicals), 1U/ml Dispase II (Boeringher Mannheim), and 250U/ml DNase I (Worthington Biochemicals). NSCs were purified using a 65% Percoll gradient and cultured (Neurobasal A medium supplemented with 2% B27 without Vitamin A, 1% Glutamax, 1% Penicillin Streptomycin, 10ng/ml EGF, 10ng/ml bFGF) as a monolayer on poly-D-lysine (PDL) and laminin-coated plates at a density of 10^5 cells/cm^2.

Infections of Primary NSCs. Primary NSCs were plated at a density of 10^4 cells/cm^2 on PDL and laminin coated plates. 48 hours after plating, lentivirus was added to the culture at a ratio of 10 viral particles per cell. 48 hours later media was changed, and all assays began 24 hours after media change.

ATP Assay. Primary NSCs were infected as previously described and subsequently were plated at a density of 10^3 cells/well in a 96 well plate and maintained under self-renewal conditions. 48 hours after plating cells were treated with Oligomycin at a final concentration of 5μM or an equal volume of DMSO control. 18 hours after treatment, ATP content was measured using a Luminescent ATP Detection Assay Kit (Abcam) according to manufacturer instructions. Luminescence was measured in a Cytation5 (BioRad).

Neurosphere Assay. Primary NSCs were infected as previously described. At the start of the assay, cells were dissociated and plated at a concentration of 10^3 cells/well in an uncoated 24 well plate. Cells were cultured in suspension under self-renewal conditions for 48 hours before being analyzed for number by brightfield microscopy.

NSC Differentiation Assay. NSCs were seeded in 500μL growth medium and treated with lentivirus as previously described. 72h after treatment, media was replaced with differentiation medium (Neurobasal A medium supplemented with 2% B27 without Vitamin A, 1% Glutamax, 1% Penicillin Streptomycin). Cells were maintained in differentiation medium for 7 days, with half the media replaced every other day. Cells were fixed with 4% PFA as previously described. Cells were washed 3 times with PBS after fixation, blocked in 3% donkey serum, and incubated in primary antibody at 4ºC for 16h. staining was revealed using fluorescence conjugated secondary Alexa antibodies (1:500; s). MAP2- or GFAP-positive cells were counted per field of

view at three randomly determined locations per coverslip. *In vitro* experiments were conducted in triplicates for each condition and repeated to ensure reproducibility.

Stereotaxic injections. Animals were placed in a stereotaxic frame and anesthetized with 2% isoflurane (2 liters/min oxygen flow rate) delivered through an anesthesia nose cone. Ophthalmic eye ointment was applied to the cornea to prevent desiccation during surgery. The area around the incision was trimmed. Solutions were injected bilaterally into the DG of the dorsal hippocampi using the following coordinates: (from bregma) anterior = −2 mm, lateral = 1.5 mm, (from skull surface) height = −2.1 mm. A 2-µl volume was injected stereotaxically over 10 min (injection speed: 0.20 µl/min) using a 5-µl 26s-gauge Hamilton syringe. To limit reflux along the injection track, the needle was maintained *in situ* for 10 min, slowly pulled out halfway and kept in position for an additional 5 min. The skin was closed using silk suture. Each mouse was injected subcutaneously with analgesics. Mice were singly housed and monitored during recovery.

EdU administration and Quantification. For short-term proliferation studies, mice were intraperitoneally injected with EdU (50mg/kg body weight, Sigma-Aldrich) daily for six days prior to euthanasia. To estimate the total number of EdU-positive cells in the brain, we performed fluorescence staining for BrdU on 3-6 hemibrain sections per mouse (40µm thick, 360µm apart). To quantify neuronal differentiation and maturation of dividing cells, EdU-positive cells across 3-6 sections per mouse were analyzed by confocal microscopy for co-expression with DCX.

Immunohistochemistry. Tissue processing and immunohistochemistry was performed on free floating sections following standard published techniques (42). Briefly, mice were anesthetized with a ketamine (100mg/kg)-xylazine (10mg/kg) cocktail (Patterson Veterinary, Henry Schein) and transcardially perfused with cold PBS. Brains were removed, fixed in phosphate-buffered

4% paraformaldehyde, pH 7.4, at 4°C for 48h followed by cryoprotection in 30% sucrose, and coronally sectioned at 40µm with a cryomicrotome (Leica SM2010 R). Sections were washed three times in tris-buffered saline with 0.1% Tween 20 (TBST) and incubated in 3% normal donkey serum (Thermo Fisher Scientific) for 1h. After overnight incubation in primary antibody: Goat anti-Doublecortin (C-18) [1:7500], Goat anti-Sox2 (Y-17) [1:200], Rabbit anti-GFAP[1:1000], Mouse anti-MAP2[1:500], at 4°C, staining was revealed using fluorescence conjugated secondary Alexa antibodies (Donkey anti-Rabbit: Alexa-488 conjugated secondary antibody, Donkey anti-Rabbit: Alexa-555 conjugated secondary antibody, Donkey anti-Goat: Alexa-555 conjugated secondary antibody, Donkey anti-Mouse: Alexa-488 conjugated secondary antibody, Donkey anti-Mouse: Alexa-555 conjugated secondary antibody, Donkey anti-Mouse: Alexa-647 conjugated secondary antibody [1:500]). To visualize EdU-positive cells, the Click-iT EdU Kit (Thermo Fisher) was used according to manufacturer instructions. To estimate the total number of immunopositive cells per DG, confocal stacks of coronal sections of the DG (3-6 sections per mouse, 40µm thick, 360µm apart) were acquired on a Zeiss LSM 800.

Data and statistical analysis. Graphed data are expressed as mean ± SEM. Statistical analysis was performed with Prism 6.0 software (GraphPad Software). Unless otherwise noted, means between two groups were compared with two-tailed, unpaired Student's t-test. Novel object recognition data were compared with a one sample t-test against 50% (expected preference). Comparisons of means from multiple groups with each other or against one control group were analyzed with one-way ANOVA and Tukey's post-hoc test. All histology and behavior experiments conducted were done in a randomized and blinded fashion. For each experiment, the overall size of the experimental groups corresponded to distinct animals or cultures. Unique samples were not measured repeatedly within the same characterization of a given cohort.

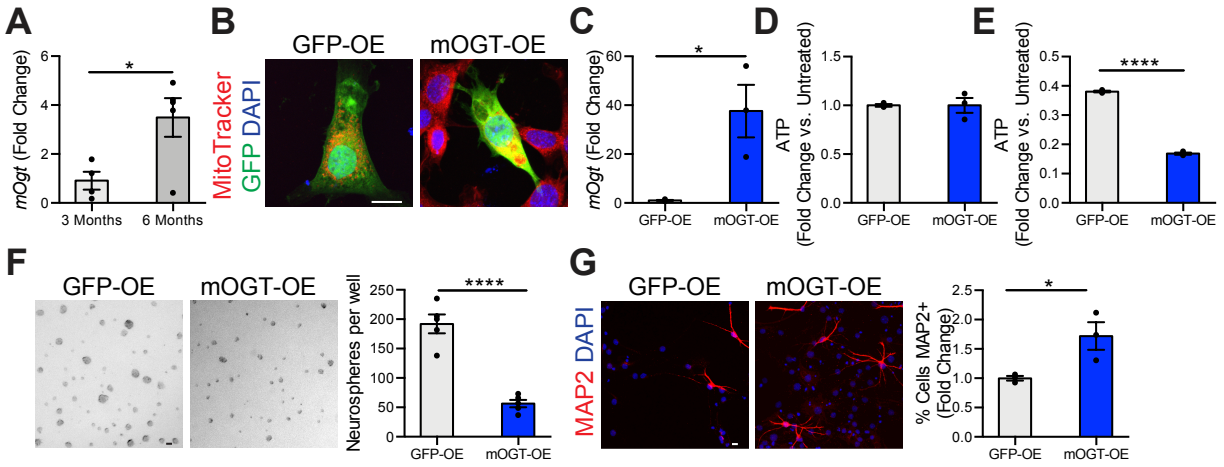

Figure 2.1. Mimicking the age-related mOGT promotes neuronal differentiation at the expense of NSC self-renewal *in vitro.*

(**A**) Quantification of *mOgt* expression by qPCR in the hippocampus at young (3 month) and mature (6 month) ages in mice (n=4-5 per group). (**B**) Representative images of HEK293T cells transfected with GFP-OE or mOGT^{GFP}-OE and treated with MitoTracker (scale bar, 10μm). (**C**) Quantification of *mOgt* expression by qPCR following infection of primary hippocampal NSCs with GFP-OE or mOGT-OE (n=3 per group). (**D**) Quantification of baseline ATP production normalized to untreated in infected primary hippocampal NSCs *in vitro* (n=3 per group). (**E**) Quantification of ATP production normalized to untreated following oligomycin treatment in infected primary hippocampal NSCs *in vitro* (n=3 per group). (**F**) Representative field and quantification of neurospheres following infection in primary hippocampal NSCs (scale bar, 10μm; n=5 per group). (**G**) Representative field and quantification of MAP2-positive cells following 7 days of differentiation under GFP-OE or mOGT-OE infection (scale bar, 10μm; n=3 per group). Data are represented as mean ± SEM; *p<0.05, ****p<0.0001, ns; t test.

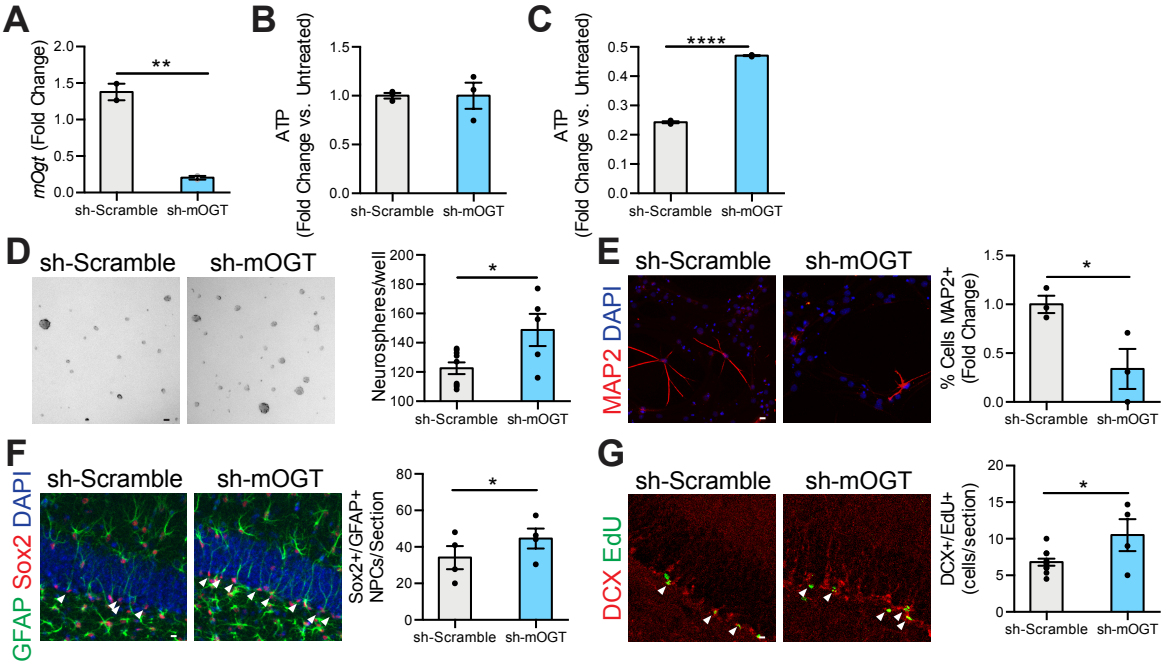

Figure 2.2. Reducing mOGT levels promotes NSC self-renewal *in vitro* and preserves the stem cell pool *in vivo.*

(**A**) Quantification of *mOgt* expression by qPCR following infection of primary hippocampal NSCs with sh-Scramble or sh-mOGT (n=3 per group). (**B**) Quantification of baseline ATP production normalized to untreated in infected primary hippocampal NSCs *in vitro* (n=3 per group). (**C**) Quantification of ATP production normalized to untreated following oligomycin treatment in infected primary hippocampal NSCs *in vitro* (n=3 per group). (**D**) Representative field and quantification of neurospheres following infection in primary hippocampal NSCs (scale bar, 10μm; n=5-9 per group). (**E**) Representative field and quantification of MAP2-positive cells following 7 days of differentiation under sh-Scramble or sh-mOGT infection (scale bar, 10μm; n=3 per group). (**F**) Representative field and quantification of GFAP+/Sox2+ NSCs (arrowheads) following contralateral stereotaxic injection of sh-Scramble and sh-mOGT (scale bar, 10μm; n=5 per group). (**G**) Representative field and quantification of DCX+/EdU+ neuroblasts and immature neurons (arrowheads) following contralateral stereotaxic injection of sh-Scramble and sh-mOGT (scale bar, 10μm; n=4-10 per group). Data are represented as mean ± SEM; *p<0.05, **p<0.01, ****p<0.0001, ns; t test.

REFERENCES

1. B. Milner, Disorders of learning and memory after temporal lobe lesions in man. *Clin. Neurosurg.* **19**, 421–446 (1972).

2. L. R. Squire, The neuropsychology of human memory. *Annu. Rev. Neurosci.* **5**, 241–273 (1982).

3. A. Sahay, R. Hen, Hippocampal neurogenesis and depression. *Novartis Found. Symp.* **289**, 152–160; discussion 160-164, 193–195 (2008).

4. Y. Kitabatake, K. A. Sailor, G. Ming, H. Song, Adult neurogenesis and hippocampal memory function: new cells, more plasticity, new memories? *Neurosurg. Clin. N. Am.* **18**, 105–113, x (2007).

5. W. Deng, J. B. Aimone, F. H. Gage, New neurons and new memories: how does adult hippocampal neurogenesis affect learning and memory? *Nat. Rev. Neurosci.* **11**, 339–350 (2010).

6. S. F. Sorrells, *et al.*, Human hippocampal neurogenesis drops sharply in children to undetectable levels in adults. *Nature* **555**, 377–381 (2018).

7. S. Lugert, *et al.*, Quiescent and active hippocampal neural stem cells with distinct morphologies respond selectively to physiological and pathological stimuli and aging. *Cell Stem Cell* **6**, 445–456 (2010).

8. H. G. Kuhn, H. Dickinson-Anson, F. H. Gage, Neurogenesis in the dentate gyrus of the adult rat: age-related decrease of neuronal progenitor proliferation. *J. Neurosci. Off. J. Soc. Neurosci.* **16**, 2027–2033 (1996).

9. G. Gontier, *et al.*, Tet2 Rescues Age-Related Regenerative Decline and Enhances Cognitive Function in the Adult Mouse Brain. *Cell Rep.* **22**, 1974–1981 (2018).

10. H. G. Kuhn, T. Toda, F. H. Gage, Adult Hippocampal Neurogenesis: A Coming-of-Age Story. *J. Neurosci. Off. J. Soc. Neurosci.* **38**, 10401–10410 (2018).

11. S. A. Villeda, *et al.*, The ageing systemic milieu negatively regulates neurogenesis and cognitive function. *Nature* **477**, 90–94 (2011).

12. E. P. Moreno-Jimenez, *et al.*, Adult hippocampal neurogenesis is abundant in neurologically healthy subjects and drops sharply in patients with Alzheimer's disease. *Nat. Med.* **25**, 554–560 (2019).

13. M. K. Tobin, *et al.*, Human Hippocampal Neurogenesis Persists in Aged Adults and Alzheimer's Disease Patients. *Cell Stem Cell* **24**, 974-982.e3 (2019).

14. A. C. Wang, E. H. Jensen, J. E. Rexach, H. V. Vinters, L. C. Hsieh-Wilson, Loss of O-GlcNAc glycosylation in forebrain excitatory neurons induces neurodegeneration. *Proc. Natl. Acad. Sci. U. S. A.* **113**, 15120–15125 (2016).

15. O. Lagerlof, O-GlcNAc cycling in the developing, adult and geriatric brain. *J. Bioenerg. Biomembr.* **50**, 241–261 (2018).

16. E. G. Wheatley, *et al.*, Neuronal O-GlcNAcylation Improves Cognitive Function in the Aged Mouse Brain. *Curr. Biol. CB* **29**, 3359-3369.e4 (2019).

17. S. Wang, *et al.*, Quantitative proteomics identifies altered O-GlcNAcylation of structural, synaptic and memory-associated proteins in Alzheimer's disease. *J. Pathol.* **243**, 78–88 (2017).

18. Y. Zhu, X. Shan, S. A. Yuzwa, D. J. Vocadlo, The emerging link between O-GlcNAc and Alzheimer disease. *J. Biol. Chem.* **289**, 34472–34481 (2014).

19. P. M. Levine, *et al.*, alpha-Synuclein O-GlcNAcylation alters aggregation and toxicity, revealing certain residues as potential inhibitors of Parkinson's disease. *Proc. Natl. Acad. Sci. U. S. A.* **116**, 1511–1519 (2019).

20. D. C. Love, *et al.*, Dynamic O-GlcNAc cycling at promoters of Caenorhabditis elegans genes regulating longevity, stress, and immunity. *Proc. Natl. Acad. Sci. U. S. A.* **107**, 7413–7418 (2010).

21. M. M. Rahman, *et al.*, Intracellular protein glycosylation modulates insulin mediated lifespan in C.elegans. *Aging* **2**, 678–690 (2010).

22. C. W. White, *et al.*, Age-related loss of neural stem cell O-GlcNAc promotes a glial fate switch through STAT3 activation. *Proc. Natl. Acad. Sci.* (2020) https:/doi.org/10.1073/pnas.2007439117 (August 27, 2020).

23. J. A. Hanover, *et al.*, Mitochondrial and nucleocytoplasmic isoforms of O-linked GlcNAc transferase encoded by a single mammalian gene. *Arch. Biochem. Biophys.* **409**, 287–297 (2003).

24. D. C. Love, *et al.*, Mitochondrial and nucleocytoplasmic targeting of O-linked GlcNAc transferase. *J. Cell Sci.* **116**, 647–654 (2003).

25. E. P. Tan, *et al.*, Altering O-linked β-N-acetylglucosamine cycling disrupts mitochondrial function. *J. Biol. Chem.* **289**, 14719–14730 (2014).

26. E. P. Tan, *et al.*, Sustained O-GlcNAcylation reprograms mitochondrial function to regulate energy metabolism. *J. Biol. Chem.* **292**, 14940–14962 (2017).

27. J. L. Sacoman, R. Y. Dagda, A. R. Burnham-Marusich, R. K. Dagda, P. M. Berninsone, Mitochondrial *O* -GlcNAc Transferase (mOGT) Regulates Mitochondrial Structure, Function, and Survival in HeLa Cells. *J. Biol. Chem.* **292**, 4499–4518 (2017).

28. C. C. F. Homem, *et al.*, Ecdysone and mediator change energy metabolism to terminate proliferation in Drosophila neural stem cells. *Cell* **158**, 874–888 (2014).

29. M. Agathocleous, *et al.*, Metabolic differentiation in the embryonic retina. *Nat. Cell Biol.* **14**, 859–864 (2012).

30. X. Zheng, *et al.*, Metabolic reprogramming during neuronal differentiation from aerobic glycolysis to neuronal oxidative phosphorylation. *eLife* **5** (2016).

31. M. Khacho, *et al.*, Mitochondrial Dynamics Impacts Stem Cell Identity and Fate Decisions by Regulating a Nuclear Transcriptional Program. *Cell Stem Cell* **19**, 232–247 (2016).

32. C. N. Hall, M. C. Klein-Flügge, C. Howarth, D. Attwell, Oxidative phosphorylation, not glycolysis, powers presynaptic and postsynaptic mechanisms underlying brain information processing. *J. Neurosci. Off. J. Soc. Neurosci.* **32**, 8940–8951 (2012).

33. D. Cabello-Rivera, H. Sarmiento-Soto, J. López-Barneo, A. M. Muñoz-Cabello, Mitochondrial Complex I Function Is Essential for Neural Stem/Progenitor Cells Proliferation and Differentiation. *Front. Neurosci.* **13** (2019).

34. M. Khacho, *et al.*, Mitochondrial dysfunction underlies cognitive defects as a result of neural stem cell depletion and impaired neurogenesis. *Hum. Mol. Genet.* **26**, 3327–3341 (2017).

35. B. Díaz-Castro, *et al.*, Resistance of glia-like central and peripheral neural stem cells to genetically induced mitochondrial dysfunction--differential effects on neurogenesis. *EMBO Rep.* **16**, 1511–1519 (2015).

36. J. M. Encinas, *et al.*, Division-coupled astrocytic differentiation and age-related depletion of neural stem cells in the adult hippocampus. *Cell Stem Cell* **8**, 566–579 (2011).

37. H. van Praag, T. Shubert, C. Zhao, F. H. Gage, Exercise enhances learning and hippocampal neurogenesis in aged mice. *J. Neurosci. Off. J. Soc. Neurosci.* **25**, 8680–8685 (2005).

38. N. Sun, R. J. Youle, T. Finkel, The Mitochondrial Basis of Aging. *Mol. Cell* **61**, 654–666 (2016).

39. R. Beckervordersandforth, *et al.*, Role of Mitochondrial Metabolism in the Control of Early Lineage Progression and Aging Phenotypes in Adult Hippocampal Neurogenesis. *Neuron* **93**, 560-573.e6 (2017).

40. T.-T. Yang, *et al.*, Aging and Exercise Affect Hippocampal Neurogenesis via Different Mechanisms. *PloS One* **10**, e0132152 (2015).

41. H. Babu, *et al.*, A protocol for isolation and enriched monolayer cultivation of neural precursor cells from mouse dentate gyrus. *Front. Neurosci.* **5**, 1–10 (2011).

42. L. K. Smith, *et al.*, beta2-microglobulin is a systemic pro-aging factor that impairs cognitive function and neurogenesis. *Nat. Med.* **21**, 932–937 (2015).

CHAPTER 3:

Reducing O-GlcNAcase Does Not Alter Adult Hippocampal Neural Stem Cell Function and Cognition

Charles W. White III[1,2], Gregor Bieri[1], Julien Couthouis[3], and Saul A. Villeda[1,2,4,5]

11. Department of Anatomy, University of California San Francisco, San Francisco, California 94143, USA
12. Developmental and Stem Cell Biology Graduate Program, University of California San Francisco, San Francisco, California 94143, USA
13. Department of Genetics, Stanford University School of Medicine, Stanford, California 94305, USA
14. Department of Physical Therapy and Rehabilitation Science, University of California San Francisco, San Francisco, California 94143, USA
15. The Eli and Edythe Broad Center for Regeneration Medicine and Stem Cell Research, San Francisco, California 94143, USA

AUTHOR CONTRIBUTIONS

C.W.W. and S.A.V. developed concept and designed experiments. C.W.W. collected and analyzed data. C.W.W performed all experiments. G.B. generated and validated viral constructs. G.B. and J.C. analyzed RNA-sequencing studies. C.W.W and S.A.V wrote the manuscript. S.A.V supervised all aspects of this project. All authors had the opportunity to discuss results and comment on manuscript.

ABSTRACT

The post-translational modification, O-linked N-Acetylglucosamine (O-GlcNAc) is a major regulator of aging, neurodegenerative disease, and neural stem cell (NSC) function. While mimicking the age-related decline in O-GlcNAc transferase (Ogt) has been shown to induce premature aging phenotypes such as impaired cognition and loss of neurogenesis, ameliorating this decline has been shown to rejuvenate cognitive phenotypes and promote neuronal differentiation. Notwithstanding, the possibility of replicating these beneficial effects by inhibiting or reducing O-GlcNAcase (OGA) has yet to be explored. Here we report that inhibiting or reducing OGA does not affect NSC function *in vitro* or *in vivo*. Moreover, using a novel, cell-type specific, temporally controlled, conditional genetic knockout of OGA, we demonstrate the partial loss of OGA does not affect adult hippocampal neurogenesis or associated cognitive processes in mature animals. Our data suggest that reducing OGA may not be functionally equivalent to increasing Ogt levels, and highlights the need for more in-depth analysis of site-specific modifications in future O-GlcNAc focused studies.

INTRODUCTION

The mammalian hippocampus is a primary source of regenerative capacity in the adult brain (1, 2), and is responsible for higher order cognitive processes including learning, memory (3, 4) and mood regulation (5). With age, there is a marked decrease in both neurogenesis (6–10) - the process by which new neurons are generated - and synaptic plasticity (11–14), ultimately resulting in impaired cognitive function. The post-translational modification, O-GlcNAc, and the enzymes that catalyze the addition and removal of this dynamic modification, O-GlcNAc Transferase (Ogt) and O-GlcNAcase (OGA), respectively, have recently been established as major regulators of the aging process. Our lab and others have identified changes in O-GlcNAc underlying lifespan extension (15, 16), as well as brain aging (17–20) and neurodegenerative disease (17, 21–23). Moreover, we have reported an age-related decline in hippocampal Ogt and O-GlcNAc levels and shown that increasing O-GlcNAc levels through overexpression of Ogt is sufficient to restore cognitive function in aged mice (19). Additionally, we have shown that O-GlcNAc plays a major role in regulating neural stem cell function as loss of Ogt is sufficient to impair neurogenesis and promote gliogenesis (20). Notwithstanding, much of this work has focused primarily on understanding the role of O-GlcNAc through modulation of Ogt, leaving the contribution of OGA relatively unexplored.

As Ogt and OGA are traditionally considered to be the “writer” and “eraser” of O-GlcNAc, respectively (24), the reduction of one may be expected to replicate the effect of increasing the other. For example, we have shown that loss of Ogt in adult NSCs impairs proliferation and neuronal differentiation, whereas increasing Ogt levels promotes neuronal differentiation (20). Moreover, others have demonstrated that the loss of OGA in the embryonic brain leads to enhanced proliferation and an accumulation of neural progenitors and immature neurons in the olfactory bulb (25). Alternatively, loss of either enzyme can produce the same or completely disparate effects. During embryonic development, complete loss of either enzyme results in pre- or peri-natal lethality *in vivo* (26, 27). Within embryonic stem cells, loss of Ogt is lethal (27), while

loss of OGA leads to a primed pluripotency state marked by transcriptional deregulation (25). Interestingly, while we have demonstrated that increasing Ogt levels is sufficient to enhance cognitive function in aged animals (19), others have shown that loss or pharmacological inhibition of OGA impairs cognitive function (28, 29), suggesting that O-GlcNAc levels are not the sole determinant of this effect. Given our recent work establishing the role of O-GlcNAc in regulating the aging brain, it is essential to understand how alterations of OGA affect this process.

In this study, we explore the role of OGA in regulating adult hippocampal neurogenesis and associated cognitive function. *In vitro*, we demonstrate that neither pharmacological inhibition, nor lentiviral-mediated knockdown of OGA is sufficient to alter proliferation of NSCs. *In vivo*, we demonstrate that pharmacological inhibition of OGA is not sufficient to enhance cognitive function in aged mice or restore neurogenesis in mature mice. Finally, using a temporally controlled genetic knockout model, we demonstrate that loss of OGA in adult NSCs does not affect cognition or neurogenesis, but may play a role in non-neuronal differentiation of NSCs.

RESULTS

Elevated O-GlcNAc levels do not alter neural stem cell proliferation or differentiation *in vitro.*

To gain insight into how elevated O-GlcNAcylation might affect adult NSC function, we employed a pharmacological and lentiviral-mediated approach. First, we treated primary adult hippocampal NSCs with Thiamet-G (ThG), a widely used and potent inhibitor of OGA. We evaluated O-GlcNAc levels in ThG treated NSCs 48 hours after treatment and observed a significant increase in O-GlcNAc levels by Western blot (**Figure 3.1A**). As a complementary approach, we used a previously validated (19) lentiviral construct encoding a short hairpin RNA (shRNA) targeted toward either OGA (shOGA) or Luciferase (shLuc) as a control. Next, we evaluated how increased O-GlcNAc levels affected NSC function *in vitro*. First, we analyzed proliferation via immunohistochemistry following ThG (**Figure 3.1B**) or shOGA treatment (**Figure 3.1C**). We

observed no change in the percentage of EdU+ or Ki67+ proliferating NSCs in either condition. To ensure ThG was not causing significant cytotoxicity, we analyzed cleaved caspase-3+ apoptosing cells and found no difference between ThG and vehicle treated NSCs. These results indicate that increasing O-GlcNAc levels through inhibition or knockdown of OGA is insufficient to affect NSC proliferation *in vitro*.

Increased O-GlcNAcylation alters NSC metabolic gene expression *in vitro.*

Given the significant increase of O-GlcNAcylation, but absence of a proliferation- or differentiation-related phenotype, we next assessed how gene expression was altered following knockdown of OGA. We treated primary hippocampal NSCs with shOGA and analyzed their expression 72 hours after infection by RNA-sequencing. We observed relatively minor changes in gene expression, with 129 genes downregulated and 60 genes upregulated (**Figure 3.2A**). To understand how these genes may affect cellular function, we performed Kyoto Encyclopedia of Genes and Genomes (KEGG) Pathway analysis on the significantly differentially expressed genes. We observed a decrease in expression of genes in pathways related to glycolytic process, such as Pyruvate Metabolism and Cysteine and Methionine Metabolism (**Figure 3.2B**), alongside a corresponding increase in pathways related to Oxidative Phosphorylation (**Figure 3.2B**). These data suggest that increasing O-GlcNAcylation promotes oxidative rather than glycolytic metabolism in NSCs.

Pharmacological inhibition of OGA increases hippocampal O-GlcNAc levels but not neurogenesis *in vivo.*

We have previously described the decline in adult hippocampal NSC O-GlcNAc levels between young (2 month) and mature (6 month) mice. To explore the possibility of ameliorating this decline via pharmacological inhibition of OGA, we treated mature mice with 3mg/kg ThG daily for 7 days via intraperitoneal (i.p.) injection. We also assessed short-term proliferation by a 4-day EdU

incorporation paradigm before euthanasia. We first determined whether our systemic treatment paradigm was sufficient to affect O-GlcNAc levels in the hippocampus. We analyzed hippocampal O-GlcNAc levels by Western blot and observed a significant increase in ThG compared to vehicle treated mice (**Figure 3.3A**). Next, to confirm that O-GlcNAc was elevated specifically within the granule cell layer (GCL) where the NSCs reside, we analyzed tissue via 3,3'-Diaminobenzidine (DAB) staining for O-GlcNAc. We observed a significant increase in O-GlcNAc staining intensity in the GCL of the hippocampus (**Figure 3.3B**), indicating that this paradigm is sufficient to increase hippocampal GCL O-GlcNAc levels. Next, we assessed whether this increase in O-GlcNAc was sufficient to ameliorate the previously reported age-related decline in hippocampal neurogenesis. We performed immunohistochemical analysis for Doublecortin (DCX)/EdU-positive neuroblasts and observed no difference in cell number (**Figure 3.3C**). Taken together, these data indicate that while i.p. delivery of ThG is sufficient to increase GCL O-GlcNAcylation, it does not increase adult neurogenesis.

Increasing NSC-specific O-GlcNAc does not affect adult hippocampal neurogenesis or cognitive function *in vivo*.

To further understand the relationship between O-GlcNAcylation and adult neurogenesis *in vivo*, we asked whether ameliorating the age-related decline in NSC O-GlcNAcylation while maintaining a functional O-GlcNAcylation system would restore neurogenesis. To assess the role of increasing O-GlcNAc in a temporally defined and cell type-specific manner in the adult brain, we generated heterozygous $Oga^{flox/wt}$ mice carrying an inducible *NestinCre-ERT*^{2} gene, in which one copy of the *Oga* gene is excised specifically in adult NSCs (OGA hetKO) upon tamoxifen administration. Young (4 months) mice were administered tamoxifen and changes in neurogenesis were assessed in mature OGA hetKO and littermate control ($Oga^{flox/wt}$) mice by immunohistochemical analysis (**Figure 3.4A**). Partial loss of OGA expression in adult NSCs did not alter the number of DCX/EdU-positive neuroblasts (**Figure 3.4B**). We also evaluated neuronal

differentiation and survival using a long-term 5-bromo-2'-deoxyuridine (BrdU) incorporation paradigm, in which mature differentiated neurons express both BrdU and the neuronal marker NeuN. We observed no change in the number of BrdU/NeuN-positive newly differentiated neurons (**Figure 3.4C**). Interestingly, we observed a significant decrease in the numbers of both DCX-negative/EdU-positive (**Figure 3.4B**) and NeuN-negative/BrdU-positive (**Figure 3.4C**) cells in OGA hetKO animals, indicating that while increasing NSC O-GlcNAc was insufficient to affect neuroblast or newborn neuron numbers, the generation of other NSC-derived populations was impaired.

Next, to determine whether increasing NSC O-GlcNAcylation affected cognitive processes associated with adult neurogenesis, we assessed general health and anxiety using the open field test, hippocampal-dependent object recognition using novel object recognition (NOR), and hippocampal-dependent associative fear memory using the contextual fear conditioning paradigms (**Figure 3.4A**). In the open field test, we observed no differences in overall activity (**Figure 3.4D**), total distance traveled (**Figure 3.4E**), or time spent in the periphery or center of the open field (**Figure 3.4F**), indicative of normal motor and anxiety functions. In the hippocampal-dependent NOR task, OGA hetKO animals exhibited no significant difference in object preference compared to control littermates (**Figure 3.4G**). Finally, during the fear conditioning task, no difference was observed in baseline freezing, contextual freezing, or amygdala-dependent cued freezing between OGA hetKO animals and controls (**Figure 3.4H**,**I**). Taken together, this data suggests that increasing NSC O-GlcNAcylation is insufficient to enhance neurogenesis or cognition in mature mice.

DISCUSSION

Cumulatively, our data indicate that increasing O-GlcNAcylation via modulation of OGA alone is insufficient to affect cognition or adult hippocampal neurogenesis. While we and others have previously described the rejuvenating and neuroprotective effects of increased O-GlcNAcylation

through elevated Ogt expression, a question remains as to whether reducing OGA levels is functionally equivalent to increasing Ogt expression. Our data provide evidence that reducing OGA is relatively inconsequential for neurogenesis and cognition in mature mice, in contrast to our previous work identifying Ogt as a key regulator of adult neurogenesis (20).

The functional role of O-GlcNAc has long been debated. Many potential mechanisms have been proposed including acting as a competitive inhibitor of phosphorylation, playing a role in epigenetic histone code, and even serving as an intracellular source of sugar storage (30), yet evidence for and against each of these conclusions continues to accumulate. An alternative explanation is that much like certain signaling pathways play disparate roles in various tissues, O-GlcNAcylation may function differently depending on its substrate and binding partners. In this case, it is essential to complement studies of broad Ogt and OGA manipulations with mass spectrometry evaluating changes in site-specific O-GlcNAc modifications and probes into their functional consequences. While the former work has been successful in linking O-GlcNAcylation to conditions such as aging (17–19) and neurodegenerative disease (17, 21–23), the latter has expanded our understanding of how O-GlcNAc modulates the function of crucial proteins such as Stat3 (20) and Sox2 (31). Our study further highlights the necessity of understanding site-specific O-GlcNAc modifications as we present non-opposing roles for Ogt and OGA in NSC function.

Therapeutically, restoring regenerative potential in the brain by enhancing NSC function is a promising strategy, given the association between regenerative capacity and disease progression in Alzheimer's disease (32), as well as the established neurogenesis-dependent benefits of exercise (33). We have previously demonstrated a critical role of Ogt in regulating age-related neurogenic decline and promoting neuronal differentiation (20), positioning O-GlcNAc as a potential therapeutic target for restoring NSC function. While O-GlcNAc is an attractive target given its role in many disease states and non-redundant cycling enzymes, our combined work on O-GlcNAc in NSC function highlights the importance of understanding the molecular changes

resulting from altered O-GlcNAc levels and demonstrates the utility of modulating O-GlcNAc in identifying site-specific targets for future therapeutics.

METHOD DETAILS

Animal Models. All mouse handling and use was in accordance with institutional and ethical guidelines approved by the University of California San Francisco IACUC. The following mouse lines were used: C57BL/6J young mice (Jackson Laboratory), B6.129-Ogt^{tm1Gwh}/J (The Jackson Laboratory line 004860), and C57BL/6-Tg(Nes-cre/ERT2)KEisc/J (Jackson Laboratory line 016261). All studies were done in male mice. The numbers of mice used to result in statistically significant differences were calculated using standard power calculations with $\alpha = 0.05$ and a power of 0.8. We used an online tool (http://www.stat.uiowa.edu/~rlenth/Power/index.html) to calculate power and samples size based on experience with the respective tests, variability of the assays and inter-individual differences within groups. Mice were housed under specific pathogen-free conditions under a 12h light-dark cycle. All experiments were randomized and blinded by an independent researcher. Researchers remained blinded throughout histological, molecular, and behavioral assessments. Groups were un-blinded at the end of each experiment upon statistical analysis.

Immunohistochemistry. Tissue processing and immunohistochemistry was performed on free-floating sections following standard published techniques (34). Briefly, mice were anesthetized with a ketamine (100mg/kg)-xylazine (10mg/kg) cocktail (Patterson Veterinary, Henry Schein) and transcardially perfused with cold PBS. Brains were removed, fixed in phosphate-buffered 4% paraformaldehyde, pH 7.4, at 4°C for 48h followed by cryoprotection in 30% sucrose, and coronally sectioned at 40µm with a cryomicrotome (Leica SM2010 R). Sections were washed three times in tris-buffered saline with 0.1% Tween 20 (TBST) and incubated in 3% normal donkey serum (Thermo Fisher Scientific) for 1h. After overnight incubation in primary, Goat anti-Doublecortin (C-18) [1:7500], Rabbit anti-GFAP[1:1000], Mouse anti-NeuN (clone A60) [1:1000], Rat anti-BrdU [BU1/75 (ICR1)] [1:1000], Mouse anti-Ki67 (clone B56) [1:500], Mouse anti-MAP2[1:500]) at 4°C, staining was revealed using fluorescence conjugated secondary Alexa

antibodies (Donkey anti-Rabbit: Alexa-488 conjugated secondary antibody, Donkey anti-Rabbit: Alexa-555 conjugated secondary antibody, Donkey anti-Rat: Alexa-488 conjugated secondary antibody, Donkey anti-Goat: Alexa-555 conjugated secondary antibody, Donkey anti-Mouse: Alexa-488 conjugated secondary antibody, Donkey anti-Mouse: Alexa-555 conjugated secondary antibody, Donkey anti-Mouse: Alexa-647 conjugated secondary antibody [1:500]). Antigen retrieval for BrdU labeling required incubation in 3M HCl at 37°C for 30min before incubation with primary antibody. To estimate the total number of immunopositive cells per DG, confocal stacks of coronal sections of the DG (3-6 sections per mouse, 40µm thick, 360µm apart) were acquired on a Zeiss LSM 800.

Isolation of Primary Neural Stem Cells from the Postnatal Mouse Hippocampus. Primary neural stem cell isolation and culture were preformed following previously published techniques (35). Hippocampi were dissected from male postnatal day 1 (P1) Wildtype C57/BL6 mice and pooled for NSC isolation. After removing superficial blood vessels, hippocampi were mechanically dissociated by fine mincing and enzymatically digested for 30 minutes at 37ºC in DMEM media containing 2.5U/ml Papain (Worthington Biochemicals), 1U/ml Dispase II (Boeringher Mannheim), and 250U/ml DNase I (Worthington Biochemicals). NSCs were purified using a 65% Percoll gradient and cultured (Neurobasal A medium supplemented with 2% B27 without Vitamin A, 1% Glutamax, 1% Penicillin Streptomycin, 10ng/ml EGF, 10ng/ml bFGF) as a monolayer on poly-D-lysine and laminin-coated plates at a density of 10^5 cells/cm^2.

Viral Plasmids and Viruses. We generated lentiviruses (LVs) encoding shRNAs targeting Oga or luciferase using a lentiviral shRNA expression system (pGreenPuro shRNA, System Biosciences) according to the manufacturer's instructions. The targeted sequences were cloned into the pGreenPuro vector (OGA, 5′-AAGTATACCAAGCCAAATGGT-3′; Luciferase, 5’-

GCCATTCTATCCTCTAGAGGA-3'). Plasmid quality was tested with western blot analysis and sequencing.

NSC Proliferation Assay. NSCs were seeded in 500 µL growth medium (Neurobasal A medium supplemented with 2% B27 without Vitamin A, 1% Glutamax, 1% Penicillin Streptomycin, 10ng/ml EGF, 10ng/ml bFGF) at a density of 10,000 cells/well on PDL/laminin-coated glass coverslips in a 24-well tissue culture plate. 24h later, cells were treated with either DMSO or 50µM Thiarmet-G (Sigma-Aldrich). 16h later, cells were treated with 20µM EdU for 8h prior to fixing with 4% PFA. Acute knockdown of OGA was induced by treating plated NSCs with shRNA-encoding lentiviruses (10 viral particles per cell) for three days prior to EdU treatment as described. Cells were washed 3 times with PBS after fixation, blocked in 3% donkey serum, and incubated in primary antibody at 4ºC for 16h. After 3 washes with PBS, EdU incorporation was revealed using a Click-iT EdU Alexa Fluor Imaging Kit (Thermo Fisher Scientific) and nuclei were counterstained with Hoechst 33342 (1:10000; Thermo Fisher Scientific). EdU-positive cells were counted per field of view at three randomly determined locations per coverslip. *In vitro* experiments were conducted in triplicates for each condition and repeated to ensure reproducibility.

NSC Differentiation Assay. NSCs were seeded in 500µL growth medium and treated with Thiamet-G or shOGA as previously described. 24h (Thiamet-G) or 72h (knockdown) after treatment, media was replaced with differentiation medium (Neurobasal A medium supplemented with 2% B27 without Vitamin A, 1% Glutamax, 1% Penicillin Streptomycin). Cells were maintained in differentiation medium for 7 days, with half the media replaced every other day. Cells were fixed with 4% PFA as previously described. Cells were washed 3 times with PBS after fixation, blocked in 3% donkey serum, and incubated in primary antibody at 4ºC for 16h. staining was revealed using fluorescence conjugated secondary Alexa antibodies (1:500; see Key Resource Table). MAP2- or GFAP-positive cells were counted per field of view at three randomly determined

locations per coverslip. *In vitro* experiments were conducted in triplicates for each condition and repeated to ensure reproducibility.

Western Blot Analysis. Primary NSCs were lysed in RIPA lysis buffer (500 mM Tris, pH 7.4, 150 mM NaCl, 0.5% Na deoxycholate, 1% NP40, 0.1% SDS, complete protease inhibitors; Roche, Halt Phosphatase Inhibitor Cocktail; Thermo Fisher, and PUGNAc; Sigma-Aldrich). Protein lysates were mixed with 4x NuPage LDS loading buffer (Invitrogen) and loaded on a 4-12% SDS polyacrylamide gradient gel (Invitrogen) and subsequently transferred onto a nitrocellulose membrane. The blots were blocked in 5% milk in Tris-Buffered Saline with Tween (TBST) and incubated with primary antibody at 4°C for 16h. Horseradish peroxidase-conjugated secondary antibodies and an ECL kit (GE Healthcare/BioRad) were used to detect protein signals. Blots were imaged with a ChemiDoc (BioRad) and quantified using ImageJ software (Version 1.8.0_91). Actin or HH3 bands were used for normalization.

DAB Staining. Tissue was processed as previously described. Free floating coronal sections were incubated overnight with Mouse anti-O-GlcNAc (RL2) [1:500] primary antibody, and staining was revealed using biotinylated secondary antibody and the ABC kit (Vector) with Diaminobenzidine (DAB, Sigma-Aldrich). Sections were mounted in phosphate buffer on superfrost plus microscope slides (ThermoFisher), allowed to dry overnight, briefly soaked in Citrasolv and cover slipped with Entellan. Staining signal intensity in the granule cell layer of the DG was quantified with Fiji (Version 2.0).

PCR Genotyping. OGA floxed and Nestin-CreERT2 alleles were genotyped from skin biopsies using PCR. Primers specific for the beta-globin gene were included in the reaction as a control. OGA floxed forward primer: CATCTCTCCAGCCCCACAAACTG. OGA floxed reverse primer: GACGAAGCAGGAGGGGAGAGCAC. Primer Cre forward: CACCCTGTTACGTATAGCCG.

Primer Cre reverse: GAGTCATCCTTAGCGCCGTA. Beta-globin forward primer: CCAATCTGCTCACACAGGATAGAGAGGGCAGG. Beta-globin reverse primer: CCTTGAGGCTGTCCAAGTGATTCAGGCCATCG.

Tamoxifen injections. Animals were injected via intraperitoneal injection with 75mg/kg of tamoxifen or vehicle once every 24 hours for a total of 5 injections per animal. Animals were monitored after recovery and four weeks allowed to pass after the final injection before any analyses were performed.

BrdU administration and Quantification. For short-term proliferation studies, mice were intraperitoneally injected with EdU (50mg/kg body weight, Sigma-Aldrich) daily for six days prior to euthanasia. For study of newborn neuron survival, mice were injected with BrdU (50mg/kg) for six days and animals were euthanized 28 days after administration. To estimate the total number of BrdU-positive cells in the brain, we performed fluorescence staining for BrdU on 3-6 hemibrain sections per mouse (40μm thick, 360μm apart). The number of BrdU-positive cells in the granule cell and subgranular cell layer of the DG were counted. To quantify neuronal fate and maturation of dividing cells, BrdU-positive cells across 3-6 sections per mouse were analyzed by confocal microscopy for co-expression with NeuN.

Contextual Fear Conditioning. Paradigm follows previously published techniques (10). Mice learned to associate the environmental context (fear conditioning chamber) with an aversive stimulus (mild foot shock; unconditioned stimulus, US) enabling testing for hippocampal-dependent contextual fear conditioning. The mild foot shock was paired with a light and tone cue (conditioned stimulus, CS) in order to also assess amygdala- dependent cued fear conditioning. Conditioned fear was displayed as freezing behavior. Specific training parameters are as follows: tone duration is 30 seconds; level is 70dB, 2kHz; shock duration is 2 seconds; intensity is 0.6mA.

On day 1 each mouse was placed in a fear-conditioning chamber and allowed to explore for 2 minutes before delivery of a 30-second tone (70dB) ending with a 2-second foot shock (0.6mA). Two minutes later, a second CS-US pair was delivered. On day 2 each mouse was first place in the fear- conditioning chamber containing the same exact context, but with no administration of a CS or foot shock. Freezing was analyzed for 1-3 minutes. One hour later, the mice were placed in a new context containing a different odor, cleaning solution, floor texture, chamber walls and shape. Animals were allowed to explore for 2 minutes before being re-exposed to the CS. Freezing was analyzed for 1-3 minutes. Freezing was measured using a FreezeScan video tracking system and software (Clever Sys, Inc). All behavior is performed double blinded.

Novel Object Recognition. The novel object recognition task was adapted from a previously described protocol (36). During the habituation phase (day 1), mice could freely explore an empty arena for 10 minutes. During the training phase (day 2), two identical objects were placed in the habituated arena, and mice could explore the objects for 5 minutes. For the testing phase (day 3), one object was replaced with a novel object, and mice could explore the objects for 5 minutes. Time spent exploring each object was quantified using the Smart Video Tracking Software (Panlab; Harvard Apparatus). Two different sets of objects are used. To control for any inherent object preference, half of the mice are exposed to object A as their novel object and half to object B. To control for any potential object-independent location preference, the location of the novel object relative to the trained object is also varied. The objects were chosen based on their ability to capture the animal's interest, independent of genetic background or age. To determine percent time with novel object, we calculate (Time with novel object)/(Time with Trained Object + Time with Novel Object) * 100. In this preference index, 100% indicates full preference for the novel object, and 0% indicates full preference for the trained object. A mouse with a value of 50% would have spent equal time exploring both objects. Mice that did not explore both objects during the training phase were excluded from analysis.

Open Field. Mice were placed in the center of an open 40cm x 40cm square chamber (Kinder Scientific) with no cues or stimuli and allowed to move freely for 10 minutes. Infrared photobeam breaks were recorded and movement metrics analyzed by MotorMonitor software (Kinder Scientific).

RNA Isolation. mRNA of NSCs was isolated by lysis with TRIzol Reagent (Thermo Fisher Scientific), separation with chloroform (0.2mL per mL TRIzol) and precipitated with isopropyl alcohol according to manufacturer's instructions.

NSC Library Construction and RNA-sequencing. After RNA isolation, RNA-Seq libraries were constructed using the Smart-Seq2 protocol from (37), with modifications. Briefly, 1ng high quality RNA was reverse transcribed using SuperScript II (Life Technologies, 18064-014) with a poly-dT anchored oligonucleotide primer, and a template switching oligonucleotide primer that generated homotypic PCR primer binding sites. The cDNA underwent 10 rounds of PCR amplification using KAPA HiFi Hotstart (Kapa Biosystems, KK2601), followed by Ampure bead (Agencourt) cleanup. The quality of the amplified cDNA was tested using qPCR for GAPDH and nucleic acid quantitation. 1ng of high-quality amplified cDNA was fragmented with the Tn5 transposase from the Illumina Nextera kit (FC-131-1096) to a median size of ~500bp. The fragmented library was amplified with indexed Nextera adapters (FC-131-1002) using 12 rounds of PCR. Final libraries were purified with Ampure beads and quantified using a qPCR Library Quantification Kit (Kapa Biosystems, KK4824). Libraries were pooled for sequencing on an Illumina HiSeq 2500 (paired reads 2x100bp).

Bioinformatic analysis of NSC RNA-sequencing data. Alignment of RNA sequencing reads to the mouse mm10 transcriptome was performed using STAR v2.7.3a (38) following ENCODE

standard options, read counts were generated using RSEM v1.3.1, and differential expression analysis was performed in R v3.6.1 using the DESeq2 package v1.38.0 (39). [Detailed pipeline v2.0.1 and options available on https://github.com/emc2cube/Bioinformatics/]. Significance was determined using a corrected p-value<0.05 and a $\log_2$ fold change>0.5. Gene Ontology and ChEA/ENCODE transcription factor enrichment analysis was performed with Enrichr (https://amp.pharm.mssm.edu/Enrichr/). Heatmaps were generated using iDEP (http://bioinformatics.sdstate.edu/idep/). All data available under GEO submission GSE143388.

Data and statistical analysis. Graphed data are expressed as mean ± SEM. Statistical analysis was performed with Prism 6.0 software (GraphPad Software). Unless otherwise noted, means between two groups were compared with two-tailed, unpaired Student's t-test. Novel object recognition data were compared with a one sample t-test against 50% (expected preference). Comparisons of means from multiple groups with each other or against one control group were analyzed with one-way ANOVA and Tukey's post-hoc test. All histology and behavior experiments conducted were done in a randomized and blinded fashion. For each experiment, the overall size of the experimental groups corresponded to distinct animals or cultures. Unique samples were not measured repeatedly within the same characterization of a given cohort.

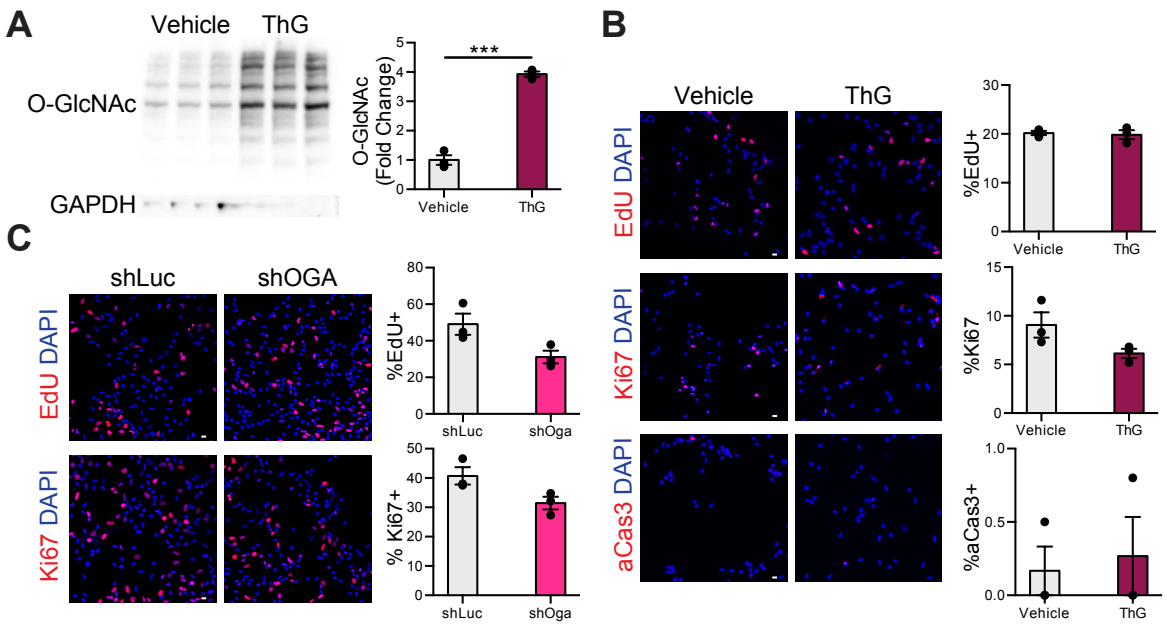

Figure 3.1. NSC proliferation is unaffected by pharmacological inhibition or knockdown of OGA *in vitro*.
(**A**) Representative Western blot and quantification of O-GlcNAc levels in primary hippocampal neural stem cells (NSCs) following ThG treatment (n=3 per group). (**B**) Representative images and quantification of EdU+ proliferating, Ki67+ actively cycling, or cleaved caspase 3+ apoptosing primary hippocampal NSCs following ThG treatment (scale bar, 10μm; n=3 per group). (**C**) Representative images and quantification of EdU+ proliferating and Ki67+ actively cycling, primary hippocampal NSCs following shOGA infecftion (scale bar, 10μm; n=3 per group). All data are represented as mean ± SEM; ***p<0.001, ns; t test.

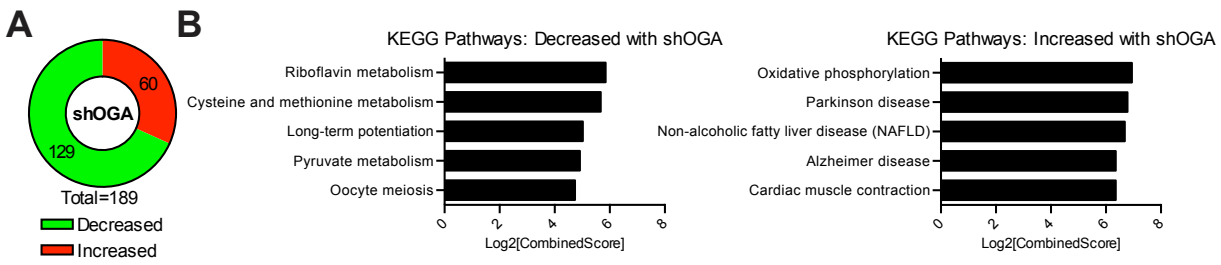

Figure 3.2. Knockdown of OGA alters metabolic pathways in primary NSCs *in vitro*. (**A**) 129 genes were decreased, and 60 genes were increased in primary NSCs following shOGA treatment *in vitro*. (**B**) Quantification of enriched pathways as identified by KEGG based on downregulated genes after shOGA infection. (**C**) Quantification of enriched pathways as identified by KEGG based on upregulated genes after shOGA infection.

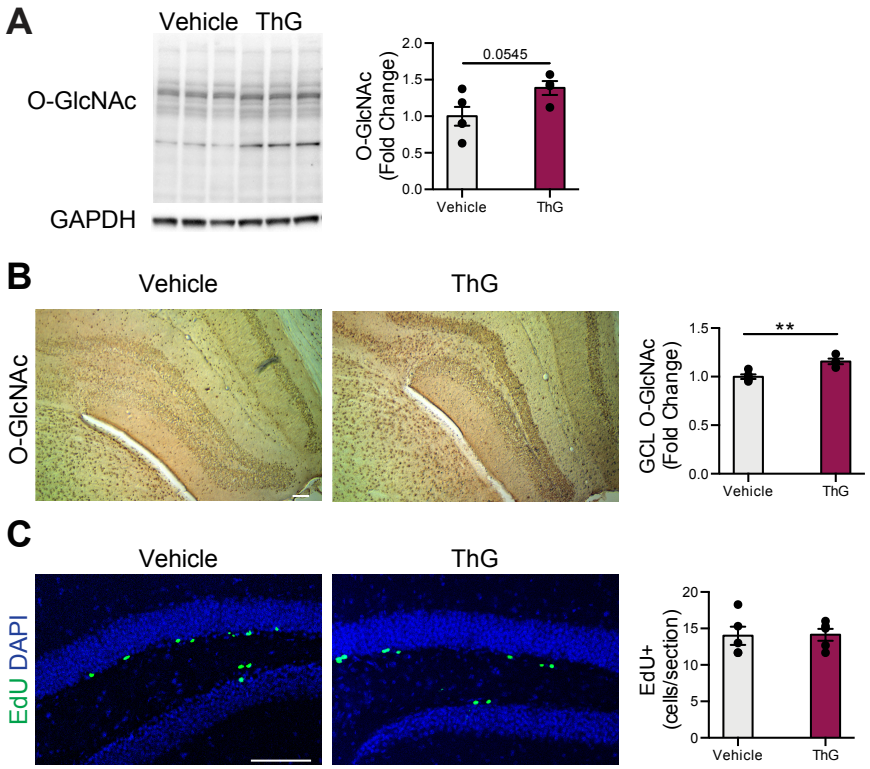

Figure 3.3. Acute pharmacological inhibition of OGA does not alter neurogenesis *in vivo*. (**A**) Representative Western blot and quantification of O-GlcNAc levels in hippocampal tissue following 7 days of 3mg/kg ThG treatment via i.p. injection (n=3-4). (**B**) Representative image of DAB staining for O-GlcNAc in the hippocampus following ThG treatment (left) and quantification of staining intensity in the GCL of the DG (right) (scale bar, 100μm; n=4-5 per group). (**C**) Representative images and quantification of DCX+/EdU+ cells in the DG following ThG treatment (scale bar, 100μm; n=5 per group). All data are represented as mean ± SEM; ns; t test.

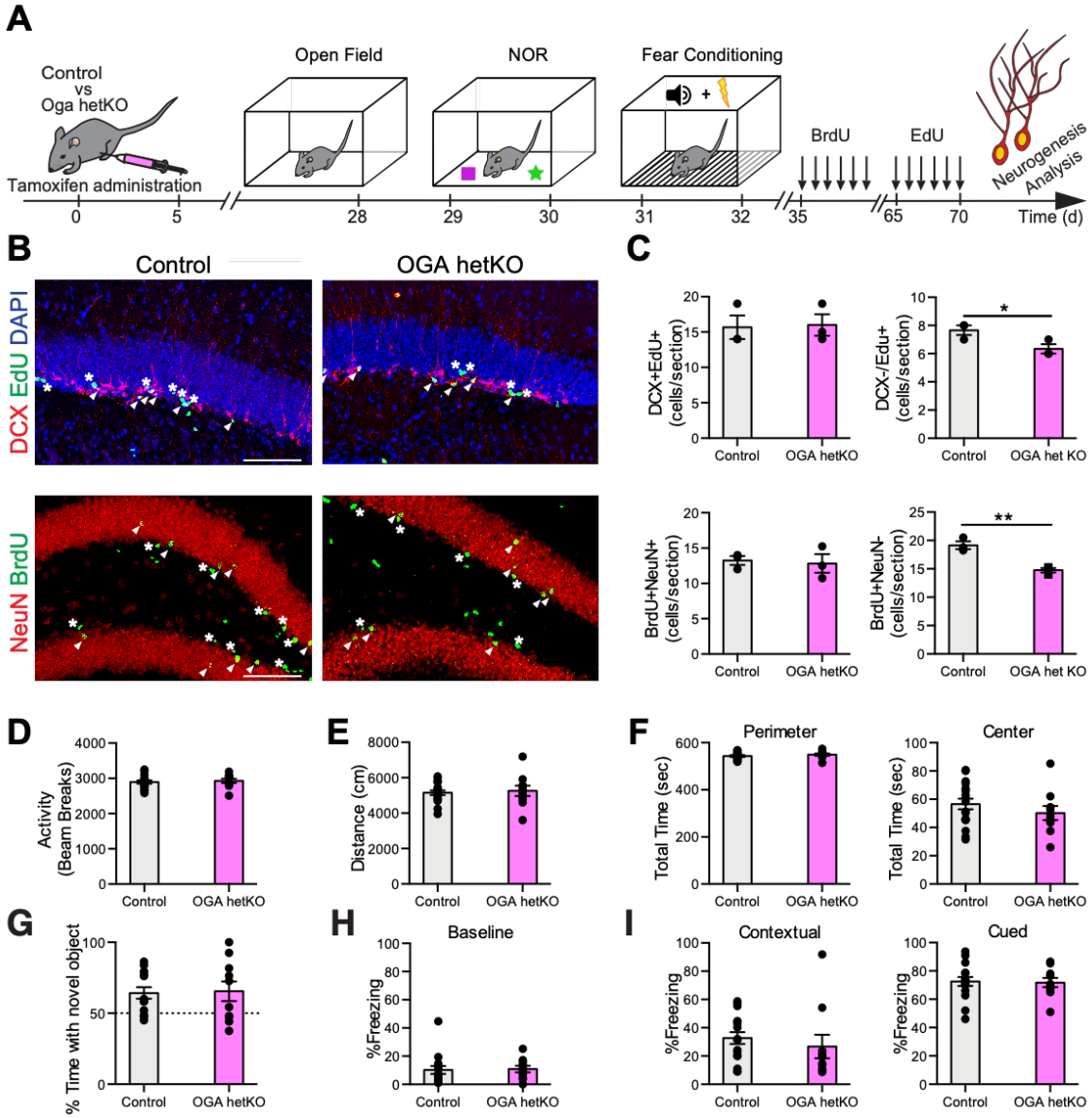
A
Control
vs
Oga hetKO
Tamoxifen administration
0
5
Open Field
28
NOR
29
30
Fear Conditioning
31
32
BrdU
35
EdU
65
70
Neurogenesis
Analysis
Time (d)
B
Control
OGA hetKO
DCX EdU DAPI
NeuN BrdU
C
DCX+EdU+
(cells/section)
Control
OGA hetKO
DCX-/Edu+
(cells/section)
OGA het KO
*
BrdU+NeuN+
(cells/section)
BrdU+NeuN-
(cells/section)
**
D
Activity
(Beam Breaks)
E
Distance (cm)
F
Perimeter
Total Time (sec)
Center
G
% Time with novel object
H
Baseline
%Freezing
I
Contextual
Cued

Figure 3.4. Heterozygous loss of NSC-specific OGA does not alter neurogenesis or associated cognitive function in mature mice.
(**A**) Schematic of experimental paradigm and cognitive testing timeline. Anxiety and motor function were assessed with the Open Field test. Hippocampal-dependent learning and memory were assessed by novel object recognition (NOR) or contextual fear-conditioning paradigms. (**B**) Representative images of the DG stained for DCX and EdU (top) or NeuN and BrdU (bottom) (scale bar, 100μm; arrowhead, DCX+/EdU+ or NeuN+/EdU+; asterisk DCX-/EdU+ or NeuN-/EdU+). (**C**) Quantification of DCX+/EdU+ and DCX-/EdU+ cells (top) and quantification of NeuN+/BrdU+ and NeuN-BrdU+ cells (bottom) (n=3 per group). (**D**-**F**) Quantification of activity (**D**), total distance traveled (**E**), and total time spent in the center or periphery (**F**) during Open Field testing (n=10-16 per group). (**G**) Quantification of percentage time spent with the novel object during NOR (n=10-14 per group). (**H**-**I**) Quantification of percentage freezing at baseline (**H**) and in response to context or cue (**I**) in the fear conditioning task (n=10-16 per group). All data are represented as mean ± SEM; *p<0.05, **p<0.01, ns; t test (**C**-**F**, **H**-**I**), One-sample *t* test versus 50% (**G**).

REFERENCES

1. F. H. Gage, G. Kempermann, T. D. Palmer, D. A. Peterson, J. Ray, Multipotent progenitor cells in the adult dentate gyrus. *J. Neurobiol.* **36**, 249–266 (1998).

2. H. van Praag, *et al.*, Functional neurogenesis in the adult hippocampus. *Nature* **415**, 1030–1034 (2002).

3. B. Milner, Disorders of learning and memory after temporal lobe lesions in man. *Clin. Neurosurg.* **19**, 421–446 (1972).

4. L. R. Squire, The neuropsychology of human memory. *Annu. Rev. Neurosci.* **5**, 241–273 (1982).

5. A. Sahay, R. Hen, Hippocampal neurogenesis and depression. *Novartis Found. Symp.* **289**, 152–160; discussion 160-164, 193–195 (2008).

6. S. Lugert, *et al.*, Quiescent and active hippocampal neural stem cells with distinct morphologies respond selectively to physiological and pathological stimuli and aging. *Cell Stem Cell* **6**, 445–456 (2010).

7. H. G. Kuhn, H. Dickinson-Anson, F. H. Gage, Neurogenesis in the dentate gyrus of the adult rat: age-related decrease of neuronal progenitor proliferation. *J. Neurosci. Off. J. Soc. Neurosci.* **16**, 2027–2033 (1996).

8. H. G. Kuhn, T. Toda, F. H. Gage, Adult Hippocampal Neurogenesis: A Coming-of-Age Story. *J. Neurosci. Off. J. Soc. Neurosci.* **38**, 10401–10410 (2018).

9. S. A. Villeda, *et al.*, The ageing systemic milieu negatively regulates neurogenesis and cognitive function. *Nature* **477**, 90–94 (2011).

10. G. Gontier, *et al.*, Tet2 Rescues Age-Related Regenerative Decline and Enhances Cognitive Function in the Adult Mouse Brain. *Cell Rep.* **22**, 1974–1981 (2018).

11. T. Hedden, J. D. E. Gabrieli, Insights into the ageing mind: a view from cognitive neuroscience. *Nat. Rev. Neurosci.* **5**, 87–96 (2004).

12. M. P. Mattson, T. Magnus, Ageing and neuronal vulnerability. *Nat. Rev. Neurosci.* **7**, 278–294 (2006).

13. J. R. Andrews-Hanna, *et al.*, Disruption of Large-Scale Brain Systems in Advanced Aging. *Neuron* **56**, 924–935 (2007).

14. N. A. Bishop, T. Lu, B. A. Yankner, Neural mechanisms of ageing and cognitive decline. *Nature* **464**, 529–535 (2010).

15. D. C. Love, *et al.*, Dynamic O-GlcNAc cycling at promoters of Caenorhabditis elegans genes regulating longevity, stress, and immunity. *Proc. Natl. Acad. Sci. U. S. A.* **107**, 7413–7418 (2010).

16. M. M. Rahman, *et al.*, Intracellular protein glycosylation modulates insulin mediated lifespan in C.elegans. *Aging* **2**, 678–690 (2010).

17. A. C. Wang, E. H. Jensen, J. E. Rexach, H. V. Vinters, L. C. Hsieh-Wilson, Loss of O-GlcNAc glycosylation in forebrain excitatory neurons induces neurodegeneration. *Proc. Natl. Acad. Sci. U. S. A.* **113**, 15120–15125 (2016).

18. O. Lagerlof, O-GlcNAc cycling in the developing, adult and geriatric brain. *J. Bioenerg. Biomembr.* **50**, 241–261 (2018).

19. E. G. Wheatley, *et al.*, Neuronal O-GlcNAcylation Improves Cognitive Function in the Aged Mouse Brain. *Curr. Biol. CB* **29**, 3359-3369.e4 (2019).

20. C. W. White, *et al.*, Age-related loss of neural stem cell O-GlcNAc promotes a glial fate switch through STAT3 activation. *Proc. Natl. Acad. Sci.* (2020) https:/doi.org/10.1073/pnas.2007439117 (August 27, 2020).

21. S. Wang, *et al.*, Quantitative proteomics identifies altered O-GlcNAcylation of structural, synaptic and memory-associated proteins in Alzheimer's disease. *J. Pathol.* **243**, 78–88 (2017).

22. Y. Zhu, X. Shan, S. A. Yuzwa, D. J. Vocadlo, The emerging link between O-GlcNAc and Alzheimer disease. *J. Biol. Chem.* **289**, 34472–34481 (2014).

23. P. M. Levine, *et al.*, alpha-Synuclein O-GlcNAcylation alters aggregation and toxicity, revealing certain residues as potential inhibitors of Parkinson's disease. *Proc. Natl. Acad. Sci. U. S. A.* **116**, 1511–1519 (2019).

24. N. E. Zachara, Critical observations that shaped our understanding of the function(s) of intracellular glycosylation (O-GlcNAc). *FEBS Lett.* **592**, 3950–3975 (2018).

25. S. O.-V. Stichelen, P. Wang, M. Comly, D. C. Love, J. A. Hanover, Nutrient-driven O-linked N-acetylglucosamine (O-GlcNAc) cycling impacts neurodevelopmental timing and metabolism. *J. Biol. Chem.* **292**, 6076–6085 (2017).

26. C. Keembiyehetty, *et al.*, Conditional knock-out reveals a requirement for O-linked N-Acetylglucosaminase (O-GlcNAcase) in metabolic homeostasis. *J. Biol. Chem.* **290**, 7097–7113 (2015).

27. R. Shafi, *et al.*, The O-GlcNAc transferase gene resides on the X chromosome and is essential for embryonic stem cell viability and mouse ontogeny. *Proc. Natl. Acad. Sci. U. S. A.* **97**, 5735–5739 (2000).

28. Y. R. Yang, *et al.*, Memory and synaptic plasticity are impaired by dysregulated hippocampal O-GlcNAcylation. *Sci. Rep.* **7**, 44921 (2017).

29. E. W. Taylor, *et al.*, O-GlcNAcylation of AMPA receptor GluA2 is associated with a novel form of long-term depression at hippocampal synapses. *J. Neurosci. Off. J. Soc. Neurosci.* **34**, 10–21 (2014).

30. X. Yang, K. Qian, Protein O-GlcNAcylation: emerging mechanisms and functions. *Nat. Rev. Mol. Cell Biol.* **18**, 452–465 (2017).

31. S. A. Myers, *et al.*, SOX2 O-GlcNAcylation alters its protein-protein interactions and genomic occupancy to modulate gene expression in pluripotent cells. *eLife* **5** (2016).

32. E. P. Moreno-Jimenez, *et al.*, Adult hippocampal neurogenesis is abundant in neurologically healthy subjects and drops sharply in patients with Alzheimer's disease. *Nat. Med.* **25**, 554–560 (2019).

33. S. H. Choi, *et al.*, Combined adult neurogenesis and BDNF mimic exercise effects on cognition in an Alzheimer's mouse model. *Science* **361**, 10.1126/science.aan8821 (2018).

34. L. K. Smith, *et al.*, beta2-microglobulin is a systemic pro-aging factor that impairs cognitive function and neurogenesis. *Nat. Med.* **21**, 932–937 (2015).

35. H. Babu, *et al.*, A protocol for isolation and enriched monolayer cultivation of neural precursor cells from mouse dentate gyrus. *Front. Neurosci.* **5**, 1–10 (2011).

36. D. B. Dubal, *et al.*, Life extension factor klotho prevents mortality and enhances cognition in hAPP transgenic mice. *J. Neurosci. Off. J. Soc. Neurosci.* **35**, 2358–2371 (2015).

37. J. J. Trombetta, *et al.*, Preparation of single-cell RNA-Seq libraries for next generation sequencing. *Curr. Protoc. Mol. Biol.* **2014**, 4.22.1-4.22.17 (2014).

38. A. Dobin, *et al.*, STAR: ultrafast universal RNA-seq aligner. *Bioinforma. Oxf. Engl.* **29**, 15–21 (2013).

39. M. I. Love, W. Huber, S. Anders, Moderated estimation of fold change and dispersion for RNA-seq data with DESeq2. *Genome Biol.* **15**, 550–8 (2014).

Publishing Agreement

It is the policy of the University to encourage open access and broad distribution of all theses, dissertations, and manuscripts. The Graduate Division will facilitate the distribution of UCSF theses, dissertations, and manuscripts to the UCSF Library for open access and distribution. UCSF will make such theses, dissertations, and manuscripts accessible to the public and will take reasonable steps to preserve these works in perpetuity.

I hereby grant the non-exclusive, perpetual right to The Regents of the University of California to reproduce, publicly display, distribute, preserve, and publish copies of my thesis, dissertation, or manuscript in any form or media, now existing or later derived, including access online for teaching, research, and public service purposes.

DocuSigned by:
Charles White
706C72D8D72D4F7...
Author Signature

9/7/2020
Date